Efficient reliability analysis of concrete structures on the basis of non-linear finite element analysis under numerical noise

Roy, Anindya

DOI
10.4233/uuid:389bbb4d-141d-425f-bc0f-b7e37918720c

Publication date
2019

Document Version
Final published version

Citation (APA)
Roy, A. (2019). *Efficient reliability analysis of concrete structures on the basis of non-linear finite element analysis under numerical noise*. [Dissertation (TU Delft), Delft University of Technology]. https://doi.org/10.4233/uuid:389bbb4d-141d-425f-bc0f-b7e37918720c

Important note
To cite this publication, please use the final published version (if applicable).
Please check the document version above.

EFFICIENT RELIABILITY ANALYSIS OF CONCRETE STRUCTURES ON THE BASIS OF NON-LINEAR FINITE ELEMENT ANALYSIS UNDER NUMERICAL NOISE

EFFICIENT RELIABILITY ANALYSIS OF CONCRETE STRUCTURES ON THE BASIS OF NON-LINEAR FINITE ELEMENT ANALYSIS UNDER NUMERICAL NOISE

Proefschrift

ter verkrijging van de graad van doctor
aan de Technische Universiteit Delft,
op gezag van de Rector Magnificus prof. dr. ir. T.H.J.J. van der Hagen,
voorzitter van het College voor Promoties,
in het openbaar te verdedigen op donderdag 11 juli 2019 om 15.00 uur

door

Anindya ROY

Masters in Applied Mechanics en Masters in Mechanical Engineering,
Indian Institute of Technology, Madras en Indian Institute of Technology, Kanpur,
geboren te Siliguri, India.

Dit proefschrift is goedgekeurd door de promotoren:

prof. dr. ir. M.A.N. Hendriks
prof. dr. ir. R.D.J.M. Steenbergen

Samenstelling promotiecommissie:

Rector Magnificus,	voorzitter
prof. dr. ir. M.A.N. Hendriks,	Technische Universiteit Delft (TU Delft) en NTNU, Norway
prof. dr. ir. R.D.J.M. Steenbergen,	TNO en Universiteit Gent (UGent)
Onafhankelijke leden:	
prof. dr. A. Der Kiureghian,	American University of Armenia (AUA) en UC Berkeley
prof. dr. ir. R. Caspeele,	Universiteit Gent (UGent)
prof. ir. A.C.W.M. Vrouwenvelder,	Toegepast Natuurwetenschappelijk Onderzoek (TNO)
prof. dr. J. Köhler,	Norwegian University of Science and Technology (NTNU)
prof. dr. ir. L. J. Sluys,	Technische Universiteit Delft (TU Delft)
prof. dr. ir. J. G. Rots,	Technische Universiteit Delft (TU Delft), reservelid

Keywords: BDARS, GDARS

Printed by: Ipskamp Printing

ISBN 978-94-028-1583-2

An electronic version of this dissertation is available at
http://repository.tudelft.nl/.

CONTENTS

SUMMARY

The analytical expressions for the ultimate load bearing capacity of the RC structures do not provide the generalized notion of ultimate load bearing capacity, which can be obtained through nonlinear finite element analysis (NLFEA). In order to obtain an accurate estimate of failure probability of a RC structure it is necessary to use NLFEA based limit state function in a reliability analysis. However, there is a relative lack of NLFEA based reliability analysis efforts in the literature. Whatever efforts there are, none of them explicitly attempts to account for the uncertainty introduced by the NLFEA model, called modeling uncertainty, in the reliability analysis. Nor has there been much effort to study the impact of the numerical noise from NLFEA on the accuracy and efficiency of the reliability algorithms. Since the run time of each NLFEA is high, for a NLFEA based reliability analysis to be practically feasible it is imperative that the reliability algorithm is efficient and capable of handling different kinds of limit state functions (with multiple failure modes, for example). Keeping this in mind two adaptive response surface based methods, directional adaptive response surface method (DARS) and adaptive Kriging Monte Carlo simulation (AK-MCS), are selected based on the preliminary literature survey, for the investigation of NLFEA based reliability analysis of RC structures. The key objective of this thesis is to study the strengths and limitations of these two algorithms for RC structures and make necessary modifications in the DARS algorithm to make it more suitable for the reliability analysis of RC structure.

A NLFEA solution strategy is formulated for RC beams and the modeling uncertainty is quantified based on 53 experimental results. Three RC beams, are selected as demonstrative cases. One of these beams fails in shear, another in bending and the last one can switch in failure modes between shear and bending. Based on these three beams it is demonstrated in this thesis that there is pronounced numerical noise in the NLFEA predicted bearing capacity whenever the beams fail is shear failure mechanism. Whereas for the bending failure mechanism the NLFEA solution strategy produces a much more smooth capacity prediction. Clear indications are found to the effect that the shear failure mechanism is more sensitive to certain choices adopted in the NLFEA solution strategy.

It is found out that the inclusion of the modeling uncertainty in the reliability analysis makes a substantial difference in the reliability estimate. This huge difference underscores the importance of accounting for the modeling uncertainty in a NLFEA based reliability analysis. Since the modeling uncertainty term is multiplied with the ultimate load bearing capacity term in the limit state function, this makes the limit state function an explicit function of the modeling uncertainty.

The verification of the performance of the DARS algorithm for the RC structures revealed that the number of exact function evaluations (NLFEA based) depends on the target coefficient of variation of failure probability, line search tolerance and the added offset to the current minimum distance of the limit state surface. The line search tol-

erance is used to find the intersection with the limit-state function for each direction. The added offset determines whether NLFEA or response surface function evaluations are used. It is demonstrated that a strict line search tolerance criterion only marginally improves the reliability index, even though the number of exact function evaluation increases significantly with stricter tolerance. A moderate value of the line search tolerance will be sufficient to efficiently obtain a very accurate reliability index. As for the influence of the added offset, it is found out that using a fixed value of the offset throughout the reliability analysis increases the number of exact limit state function evaluations. Using an adaptive offset instead of a constant offset value increased the efficiency of DARS. Just these two adjustments however could not keep the NLFEA based function evaluations low for the RC beam case which fail in shear. The pronounced numerical noise in the limit state function for this case made DARS inefficient. DARS's polynomial interpolation based uni-variate line search scheme is found to be a major source of inefficiency. Such scheme works well for well behaving, smooth limit state functions. But for highly noisy limit state functions such strategy is found to be inefficient. Instead of the interpolation based line search method Brent's uni-variate root finding algorithm is used to improve the efficiency of DARS. For the adaptive response surface a Gaussian process regression (GPR) based response surface is used instead of quadratic response surface function because such a response surface provides better initial guess for a line search. Brent's method restricts the use of interpolation as long as the bracket of the sign change around the root is wide. In narrow interval, where the effect of numerical noise is most severe, Brent's method switches to the Bisection method, which is unaffected by noise. This, combined with the initial guess provided by the GPR based response surface improved the efficiency of DARS method for noisy cases.

The AK-MCS method is examined for the RC beam cases. This method uses a learning function to find samples close to the limit state surface. It is found that the AK-MCS has no trouble in dealing with the smooth limit state function of the beam failing in bending. But for the shear dominated beam cases it is much more inefficient compared to DARS. The reason is that because of the noisy behavior of the limit state function samples which are not in the closest proximity to the actual limit state surface often get misidentified for design enrichment by the learning function. This unnecessarily increases the overall number of NLFEAs, delaying the convergence.

It is shown in this thesis that the existing DARS method is not efficient when the RC structure in consideration undergoes shear failure. This implies that the existing DARS method cannot be applied in a black box fashion for a RC structure, without first considering its possible mode of failure. But such shortcoming has been overcome with the novel improvement forwarded in this thesis, because now the line search scheme of DARS is just as efficient for shear failure cases (with limit state functions under the influence of numerical noise) as bending failure cases. This makes the improved DARS method a versatile reliability algorithm, capable of working in any case without requiring any prior knowledge of the behavior of the structure.

With the improvements forwarded in this thesis for DARS (coined as BDARS in this thesis), together with the fact that the number of exact function evaluations for DARS does not strongly depend on the number of input random variables and only a moderate value of line search tolerance suffices to obtain an accurate reliability estimate,

makes the improved DARS method particularly useful in terms of practical utility. This improved DARS method makes it possible to obtain an accurate estimate of failure probability for any type of RC structures within a feasible number of NLFEA. It is no longer necessary to be content with just semi-probabilistic safety checks, out of concerns for efficiency.

SAMENVATTING

Analytische formules voor het draagvermogen van de gewapende betonconstructies bieden niet het algemene raamwerk voor de uiteindelijke draagkracht, zoals die wel kan worden verkregen met niet-lineaire eindige-elementenanalyses (NLEEA). Om een nauwkeurige schatting van de faalkans van een gewapende betonconstructie te verkrijgen, is het noodzakelijk de op NLEEA gebaseerde grenstoestandfunctie te gebruiken in een betrouwbaarheidsanalyse. In de literatuur is er echter een relatief gebrek aan op NLEEA gebaseerde analyses van de betrouwbaarheid. Nergens wordt geprobeerd expliciet rekening te houden met de onzekerheid die het NLEEA-model, de zogenaamde modelonzekerheid, introduceert in de betrouwbaarheidsanalyse. Evenmin is er veel moeite gedaan om de impact van numerieke ruis van NLEEA op de nauwkeurigheid en efficiëntie van de betrouwbaarheidsalgoritmen te bestuderen. Omdat de looptijd van elke NLEEA hoog is, is het voor de praktische haalbaarheid van een op NLEEA gebaseerde betrouwbaarheidsanalyse nodig dat het betrouwbaarheidsalgoritme efficiënt is en in staat om verschillende soorten grenstoestandfuncties aan te kunnen (bijvoorbeeld met meerdere bezwijkmechanismen). Met dit in gedachte worden twee op adaptieve responsoppervlak gebaseerde methoden – op basis van adaptief richtingsgewijs bemonsteren (DARS) en op basis van adaptieve Kriging Monte Carlo-simulatie (AK-MCS) – geselecteerd voor het onderzoeken van op NLEEA gebaseerde betrouwbaarheidsanalyse van gewapende betonconstructies. Het belangrijkste doel van dit proefschrift is om de sterktes en beperkingen van deze twee algoritmen voor gewapende betonconstructies te bestuderen en noodzakelijke wijzigingen aan te brengen in het DARS-algoritme om het meer geschikt te maken voor de betrouwbaarheidsanalyse van gewapendbetonconstructies.

Een NLEEA-oplossingsstrategie is geformuleerd voor gewapende betonbalken en de modelonzekerheid wordt gekwantificeerd op basis van 53 experimentele resultaten. Als voorbeeld worden drie gewapende betonbalken geselecteerd. Een van deze balken bezwijkt op afschuiving, een andere op buiging en in de laatste ligt het bezwijkmechanisme tussen afschuiving en buiging in. Op basis van deze drie balken wordt in dit proefschrift een duidelijke numerieke ruis aangetoond voor het voorspelde draagvermogen op basis van NLFEA wanneer de balken falen op afschuiving, terwijl voor het bezwijkmechanisme op buiging de NLEEA-oplossingsstrategie een veel gladdere capaciteitsvoorspelling oplevert. Er zijn duidelijke aanwijzingen dat het mechanisme van afschuiving meer gevoelig is voor bepaalde keuzes in de NLEEA-oplossingsstrategie.

Geconstateerd is dat de opname van de modelonzekerheid in de betrouwbaarheidsanalyse een wezenlijk verschil maakt in de betrouwbaarheidsschatting. Dit verschil onderstreept het belang van het meenemen van de modelonzekerheid in een op NLEEA gebaseerde betrouwbaarheidsanalyse. Omdat de modelonzekerheid wordt vermenigvuldigd met de draagcapaciteit in de grenstoestandfunctie geeft dit een grenstoestandfunctie die een expliciete functie van de modelonzekerheid is.

De verificatie van de prestaties van het DARS-algoritme voor gewapendbetoncon-

structies liet zien dat het aantal exacte functie-evaluaties (gebaseerd op NLEEA) afhangt van de beoogde variatiecoëfficiënt van de faalkans, de tolerantie voor het vinden van een oplossing per zoekrichting en de offset voor de minimale afstand tot het grenstoestandoppervlak. De genoemde tolerantie wordt gebruikt om het snijpunt met de grenstoestandfunctie voor elke richting te vinden. De genoemde offset bepaalt of NLEEA- of responsfunctie-evaluaties worden gebruikt. Er wordt aangetoond dat een strikte tolerantie de betrouwbaarheidsindex slechts marginaal verbetert, terwijl het aantal exacte functie-evaluaties significant toeneemt. Een ruime waarde voor deze tolerantie zal voldoende zijn om efficiënt een nauwkeurige betrouwbaarheidsindex te verkrijgen. Wat de invloed van de toegevoegde offset betreft is gevonden dat het gebruik van een vaste waarde van de offset tijdens de betrouwbaarheidsanalyse het aantal exacte grenstoe stand functie-evaluaties verhoogt. Het gebruik van een adaptieve offset in plaats van een constante offsetwaarde verhoogde de efficiëntie van DARS. Alleen deze twee aanpassingen konden echter het aantal op NLEEA gebaseerde functie-evaluaties voor de gewapende betonbalken die falen op afschuiving niet laag houden. De numerieke ruis in de grenstoestandfunctie maakte, voor dit geval, DARS inefficiënt. De polynoominterpolatie van DARS voor het vinden van een oplossing per richting blijkt een belangrijke oorzaak van de inefficiëntie te zijn. Een dergelijk schema werkt goed voor goed gedragende, gladde grenstoestandfuncties, maar voor grenstoestandfuncties met veel numerieke ruis blijkt een dergelijke strategie inefficiënt. In plaats van de op interpolatie gebaseerde zoekmethode wordt het univariabele algoritme van Brent gebruikt om de efficiëntie van DARS te verbeteren. Voor het adaptieve responsoppervlak wordt een op Gaussiaans procesregressie (GPR) gebaseerd responsoppervlak gebruikt in plaats van de kwadratische responsoppervlakfunctie omdat een dergelijk responsoppervlak een betere initiële schatting biedt voor een oplossing per richting. De methode van Brent beperkt het gebruik van interpolatie zolang de insluiting rondom de wortel breed is. Bij een klein interval, waar het effect van numerieke ruis het grootst is, schakelt de methode van Brent over op de bisectiemethode die niet wordt beïnvloed door ruis. Dit, in combinatie met de initiële schatting van het op GPR gebaseerde responsoppervlak, verbeterde de efficiëntie van de DARS-methode voor gevallen met numerieke ruis.

De AK-MCS-methode is onderzocht voor de gewapende betonbalken. Deze methode maakt gebruik van een leerfunctie om monsters dichtbij het grensgebied te vinden. Gebleken is dat de AK-MCS geen problemen heeft bij het verwerken van de gladde grenstoestandfunctie van de balk die faalt op buiging, maar voor de door schuifkracht gedomineerde balken is het in vergelijking met DARS veel inefficiënter. De reden hiervoor is dat door de numerieke ruis van de grenstoestandfunctie functie-evaluaties die zich niet in de buurt van het werkelijke grenstoestandoppervlak bevinden vaak verkeerd worden geïdentificeerd door de leerfunctie. Dit onnodig verhoogt het totale aantal functie-evaluaties op basis van NLEEA, waardoor de convergentie vertraagd wordt.

In dit proefschrift wordt aangetoond dat de bestaande DARS-methode niet efficiënt is wanneer de desbetreffende gewapendbetonconstructies bezwijkt op afschuiving. Dit impliceert dat de bestaande DARS-methode niet op een blackboxmanier kan worden toegepast voor een gewapendbetonconstructie zonder eerst de mogelijke bezwijkmechanismes te bestuderen. Een dergelijke tekortkoming is echter verholpen met de nieuwe verbetering die in dit proefschrift wordt aanbevolen, omdat nu het lijnzoek-

schema van DARS net zo efficiënt is voor gevallen met bezwijken op afschuiving (met limietstatusfuncties onder invloed van numerieke ruis) als gevallen met bezwijken op buiging. Dit maakt de verbeterde DARS-methode een veelzijdig betrouwbaarheidsalgoritme dat in staat is om in elk geval te werken zonder voorafgaande kennis van het gedrag van de constructie.

De in dit proefschrift aanbevolen verbeteringen voor DARS (als BDARS in dit proefschrift gebruikt), samen met het feit dat het aantal exacte functie-evaluaties voor DARS niet sterk afhankelijk is van het aantal variabelen en dat een ruime waarde van de lijnzoektolerantie volstaat om een nauwkeurige schatting voor de betrouwbaarheid te krijgen, maken de verbeterde DARS-methode bijzonder nuttig voor de praktijk. Deze verbeterde DARS-methode maakt het mogelijk om een accurate schatting te maken van de kans op falen voor elk type gewapendbetonconstructie binnen een haalbaar aantal evaluaties op basis van NLEEA . Het is niet langer nodig om genoegen te nemen met alleen semiprobabilistische veiligheidscontroles op basis van efficiëntie.

1

INTRODUCTION

1.1. BACKGROUND: RELIABILITY OF RC STRUCTURES

REINFORCED concrete (RC) structures account for a vast majority of civil infrastructures, like bridges. Existing structures like these are expected to be loaded beyond their intended capacity due to increased traffic loads. It is then necessary to confirm whether the structures are safe operating under increased loading condition. In fact, the quantification of the chances of a structure's survival is always of paramount importance from public safety's point of view. The safety assessment of these structures is based on uncertain or incomplete information, because it is not possible to obtain full information about structural parameters like material properties, boundary conditions etc. through experiments. In such cases, a useful decision-making tool is reliability analysis, where the safety assessment is done within the framework of probability. In a reliability analysis the failure probability of a structure is quantified based on the limit state function of the structure. A limit state function of a structure is a mathematical expression which gives the measure of safe state and failure state for the structure. The failure probability of a structure is essentially the measure of the likelihood of a structure attaining the failure state, given the state of available information and predictive models.

1.1.1. IMPORTANCE OF NONLINEAR FINITE ELEMENT BASED LIMIT STATE FUNCTION

Limit state functions are defined based on the mechanical response of the structure. It is a common practice in RC literature to define the limit state function in terms of the ultimate load bearing capacity. There are several ways to determine the ultimate load bearing capacity of a RC structure. The simplest are the analytical formulas which express the ultimate bearing capacity as analytical function of the material properties of the RC structure. Such formulas, or analytical models, are derived based on assumptions and experimental observations. The analytical models can range from the most basic one to the highly sophisticated models, based on the level of assumptions and approximations involved. A discussion of this topic can be found in Muttoni & Ruiz [1]. The application

of the analytical models are limited to the kind of structures they are derived for. So for structures with complicated configuration such formulas will not hold good. Finite element analysis is a better choice in this regard, because its application is not restricted by the type and shape of the structures. Nonlinear finite element analysis (NLFEA) in particular constitutes a system level evaluation in which all structural parts interact leading to a generalization of the notion of ultimate load bearing capacity [2]. The redistribution of internal stresses owing to complex phenomena such as micro cracks in concrete cover, plastic yielding of the reinforcement bar etc. can only be accounted for in a NLFEA. So, NLFEA presents the best opportunity to determine the ultimate load bearing capacity accurately for a RC structure.

1.1.2. COMPUTATIONAL COST OF A NLFEA BASED RELIABILITY ANALYSIS

Since the probability density function of the limit state function is usually not known a priory, a reliability analysis process typically entails repeated evaluation of the limit state function in order to determine the failure probability. The number of such evaluations depends on the kind of reliability algorithm used and the geometrical nature of the limit state function. If the limit state functions are not available as a simple, explicit function of the input stochastic properties, it might require large number of limit state function evaluations to obtain the failure probability. Large number of limit state function evaluations are not a problem as long as such evaluations are not time consuming. The NLFEA involves repeated solving of linearized system of equations to determine the ultimate load bearing capacity. This means that each NLFEA can be time consuming, especially for large structures or finer mesh discretization. A computationally expensive NLFEA prohibits large number of evaluations of the NLFEA defined limit state functions. This makes the reliability analysis of RC structure with NLFEA quite challenging. Because although it is important to estimate the failure probability accurately, computational cost forces such analysis to use as less number of NLFEA as possible. Reliability algorithms which can produce an accurate failure probability estimate in limited number of NLFEAs are of paramount interest.

1.1.3. NUMERICAL NOISE ASSOCIATED WITH NLFEA AND ITS IMPACT ON RELIABILITY ANALYSIS

While there are many advantages of nonlinear finite element based reliability analysis, the use of NLFEA is also a source of numerical noise, which can pose major difficulty for the reliability method. This numerical noise can be understood as fluctuations around an expected smooth response. The reason behind such fluctuations is the discrete nature of the finite element algorithm, such as inadequate discretization, convergence criterion in the iterative solution procedure for the system of nonlinear equations, round off error etc. This numerical noise in the predicted ultimate load bearing capacity is manifested in the limit state function. The resulting limit state function will be addressed as 'noisy limit state function' in this thesis. The influence of this numerical noise in the outcome of the reliability analysis can be quite significant, in terms of accuracy and efficiency (efficiency in the sense of the total number of NLFEA). For example, Henriksen [3] have reported that the adaptive response method construction was impeded by the difficulties in producing consistent NLFEA response and it was only the bending failure

mechanism for which the author achieved a consistent (and accurate) performance of the reliability algorithm.

1.2. EXAMPLES OF RELIABILITY ANALYSIS OF RC STRUCTURES IN LITERATURE AND DIRECTIONS OF IMPROVEMENT

The reliability analysis examples in the literature for RC structure are often limited to reliability analysis based on analytical limit state functions [4–6]. Such approach is popular because the analytical model based limit state functions can undergo a large number of simulations in a reliability analysis, owing to their fast execution time. NLFEA based reliability analysis of RC structures can account for a much greater scope of complexity in the mechanical response of the RC structures. But such examples are relatively scarce in the literature due to the (possible) high run time of each NLFEA. A selected set of NLFEA based reliability analysis examples are discussed here in order to find possible directions of improvement in the existing literature.

Val *et al.* [7] used the First Order Reliability Method (FORM) in combination with NLFEA to determine the reliability of plane frame RC structures. FORM is a highly efficient method in terms of number of function calls. It employs constrained optimization methods to determine the design point and its distance from the origin in the standard normal space. The constrained optimization methods require the calculation of gradient of the limit state surface, with respect to each input random variables. But it is not always easy to compute this gradient. Depending on the material property, such a gradient may not even always exist. FORM is also known to be inaccurate for cases with a highly nonlinear limit state function. These limitations of FORM have motivated the development of other structural reliability algorithms. The simplest and the most robust way to deal with any kind of limit state functions is the Monte Carlo simulation (MCS). Biondini *et al.* [8] evaluated the reliability of a materially and geometrically nonlinear pre-stressed RC bridge by MCS with a limited number of samples. The samples were drawn close to the mean values of the input random material properties. Darmawan *et al.* [9] used MCS to investigate the spatial time dependent reliability of corroded RC bridge girder, however it is not clear how many samples they used. In civil engineering structures, it is expected that the failure probability are typically in the range $10^{-3} - 10^{-6}$. The pure randomness with which MCS draws samples in the sample space means that an accurate estimation of the failure probability of a structure would require an impractically large number of limit state evaluations. If the sampling is done around the design point then limited number of samples would suffice. It is not possible to predict the design point beforehand however. If the limited number of samples are not around the design point then the failure probability estimate can be completely wrong. Especially if there is non-linearity in the structural response then such estimates are of little use. An efficient simulation technique compared to MCS is the Latin Hypercube sampling (LHS), which is a stratified sampling technique which divides the sample space in several non-overlapping equal probability regions and draws one sample from each of these regions. Delgado *et al.* [10] applied LHS to a RC beam and concrete problem, with two random variables. Using only 30 samples the authors managed to achieve a low variation in the failure probability estimate. While LHS is an effective variance reduction technique, it

does not necessarily lead to optimal space-filling designs, which can be a shortcoming for problems with higher stochastic dimension. Another efficient simulation technique is the Subset simulation (SS). This method expresses a small failure probability as a product of larger conditional probabilities, by introducing intermediate failure events. The SS however is shown to be less efficient compared to Directional simulation [11]. Directional methods try to avoid the pure randomness in sampling by trying to determine failure probability contents along random directions in the sample space. To do so, these methods measure the distances to the limit state function along those directions in a line search procedure. But line search procedure incurs limit state function evaluations, so indiscriminate sampling of directions could still make directional methods impractically inefficient for RC structures.

Response surface based reliability algorithms are a promising prospect for the reliability analysis of RC structures. Such an approach tries to construct a surrogate function of the actual limit state function based on limited number of samples. Especially, if the samples are selected through some intelligent strategy, this method can be vastly more efficient compared to MCS. One way to reduce the number of limit state function evaluation would be to use machine learning methods, like artificial neural network (ANN) to construct the response surface. Cheng *et al.* [12] used an ANN based response surface method for reliability analysis of pre-stressed RC bridges. But such fixed response surface would still require relatively larger number of samples to train the machine learning functions to produce accurate response surface. Response surface methods are particularly accurate if the response surface is constructed around the design point in the space of random variables. Adaptive response methods are ideal in this respect. It is because these methods actively try to fit the response surface around the most vulnerable parts of the limit state function. This is accomplished by adaptively improving the response surface in successive iteration. In this process the total number of actual (NLFEA based) function evaluations are reduced. Henriksen [3] used a FORM based adaptive response surface method to perform reliability analysis of RC beams. FORM was used this approach to guide the sampling closer to the design point. This method however retained the inherent short coming of FORM to deal with multiple failure modes. A better strategy is to combine directional approach with adaptive response method, because directional methods are much more robust in dealing with variety of limit state functions. This approach, the so called directional adaptive response surface (DARS) method, was proposed by Harbitz *et al.* [13]. Waarts [14] found DARS to be the most efficient and robust reliability algorithm based on several finite element based limit state functions. It is because the adaptive response surface makes sure that the exact function evaluation takes place only close to the design point. However, numerical noise was not part of any of the examples considered by Waarts. One other example of a NLFEA based reliability analysis with DARS is by Evangeliou [15], where the procedure is demonstrated for a RC beam failing in shear. The basic premise of DARS method makes it a promising candidate for reliability analysis of RC structure. Another interesting candidate is the adaptive Kriging Monte Carlo simulation (AK-MCS) method. This method uses a machine learning technique, Gaussian process regression, to construct an adaptive response surface. Currently not many examples of the application of AK-MCS exists in RC literature, except the work of Rózsás *et al.* [16]. This specific work compared the performance of DARS with

AK-MCS. The comparison was made based on the examples of an RC deep beam and an RC continuous girder. The result was inconclusive with regards to the comparison of the efficiency for DARS and AK-MCS. Also, the effect of numerical noise on the efficiency of DARS and AK-MCS was not addressed in that work. This leaves scope for exploration.
One key element is missing in the current literature for the NLFEA based reliability analysis of RC structure. It is the study of the impact of uncertainty introduced by the NLFEA solver itself, on the reliability outcome. Finite element model of a structure is an abstraction of the physical structure with a number of assumptions, generalizations, and idealizations [17]. It entails assumptions and simplifications regarding to what extent and to what detail the structure has to be modeled, how the boundaries of the model are described, etc. In the process of abstraction from the structure to the mechanical model, and then the abstraction from the mechanical model to the finite element model, NLFEA introduces a potential for significant uncertainties in all steps from idealization of the physical problem, discretization into finite elements, numerical material modeling and selection of solution procedures. This uncertainty is termed as Modeling uncertainty in literature. It is usually quantified on the basis of comparison between experimental results and numerical predictions of the failure load. Introducing modeling uncertainty as a separate random entity in the reliability analysis incorporates the scope of uncertainty that comes from the finite element solver itself. The failure probability estimate without accounting for this modeling uncertainty can be completely wrong, so it is essential to include modeling uncertainty in the reliability analysis of RC structures.

1.3. OBJECTIVES OF THIS THESIS

The discussions in the preceding sections highlights the relative lack of NLFEA based reliability analysis efforts in the literature. Whatever efforts there are, none of them attempted to include the NLFEA modeling uncertainty in the reliability analysis. Nor has there been much effort to study the impact of the numerical noise from NLFEA on the accuracy and efficiency of the reliability algorithms. For a NLFEA based reliability analysis to be practically feasible, given its computational cost, it is imperative that the reliability algorithm is efficient and capable of handling different kinds of limit state functions (with multiple failure modes, for example). Keeping this in mind two adaptive response surface based methods, DARS and AK-MCS, are selected for the reliability analysis of RC structures, based on the preliminary literature survey. It needs to be studied under what circumstances and to what extent the numerical noise influences the performance of these algorithms. These key threads of investigations are outlined in the following steps,

- To formulate a NLFEA solution strategy for RC beams and to quantify the modeling uncertainty for the adopted NLFEA solution strategy based on experimental results. The formulation is done within the frame work of the guidelines issued by Dutch Ministry of Infrastructure and the Environment [18] in order to minimize the user factors in such modeling as much as possible.
- To investigate to what extent the noise in the NLFEA prediction of ultimate bearing capacity is related to the failure mode. This investigation is done based on three RC beam cases, the first one failing in shear, the second in shear or bending (mixed) and the last one in bending.

- To include the modeling uncertainty associated with solution strategy, along with material parameters, as an additional random variable in the reliability analysis of the beam failing in shear and study its effect on the outcome.
- To verify the DARS method for the RC beam failing in pure shear. Of particular interest is the behavior of the line search procedure in DARS method under numerical noise in the limit state function. Assessing the strength and weaknesses of DARS and exploring the possibility of its improvement is the key focus.
- To study the performance of AK-MCS method for the selected beam cases. Based on this study a comparative analysis, with respect to the RC beams, between DARS and AK-MCS is performed.

2

STRUCTURAL RELIABILITY METHODS

2.1. BASIC CONCEPTS OF STRUCTURAL RELIABILITY

THE concept of structural reliability is introduced in this chapter. Various reliability algorithms are discussed from the point of view of their relative strengths and weaknesses. The discussions of this chapter have been predominantly taken from existing literature such as Sudret *et al.* [19]. But for the sake of brevity the concepts are discussed in necessary details.

$\boldsymbol{\xi}$ denote the set of all basic random variables pertaining to the a given structure describing the randomness in geometry, material parameters and loading. For each realization of $\boldsymbol{\xi}$ the state of the structure is determined by the mechanical response of the structure, such as displacements, strains, stresses. Alternatively, ultimate load bearing capacity is also used to determine the state of the structure. Let $\mathbf{S}$ denote a vector of such effects, whose values enter in the definition of the failure of the system. These two vectors are related through the mechanical transformation,

$$\mathbf{S} = \mathbf{S}(\boldsymbol{\xi}) \tag{2.1}$$

which is defined, in all but simple situations, in an algorithmic sense, e.g. through finite element computer code. To assess the reliability of a structure, a limit state function g depending on mechanical response is defined as follows,

- $g(\mathbf{S}) > 0$, define the safe state of the structure.
- $g(\mathbf{S}) \leq 0$, define the failure state of the structure.

In a reliability context, failure state does not necessarily mean the breakdown of the structure, but the fact that certain requirements of serviceability or safety limit states have been reached or exceeded. The value of $\mathbf{S}$ satisfying $g(\mathbf{S}) = 0$ describes the limit state surface of the structure. There can be various kinds of limit state functions, like

for example, $g(\mathbf{S}) = \delta_{threshold} - \delta$, where δ can be deflection of a beam. The definition of the limit state function can also be based on maximum sustained load. If the joint probability density function of $\mathbf{S}$ is denoted by $f_{\mathbf{S}}(\mathbf{S})$, then the probability of failure of the structure can be defined as,

$$P_f = \int_{g(\mathbf{S})\leq 0} f_{\mathbf{S}}(\mathbf{S})\mathrm{d}\mathbf{S} \tag{2.2}$$

There are two practical difficulties associated with the above integral,

- The joint PDF of the response quantities, $f_{\mathbf{S}}(\mathbf{S})$ is usually not known, the available information being given in terms of the basic variables .
- The multi-fold integral 2.2 over the failure domain is not easy to compute.

One way around this problem of evaluating P_f from Eq.2.2 is by a sampling technique, called Monte Carlo simulation (MCS). In MCS a set of random samples are generated based on the probability density function $f_{\mathbf{S}}(\mathbf{S})$. Then taking each of those samples as input it is determined whether it leads to a failure state or safe state of the limit state function. The failure probability of a structure is obtained as the relative frequency of the number of times the failure state occurs. The failure probability directly follows from the number of occurrences of failure state over the total number of simulations. While MCS is conceptually simple, an accurate estimation of the failure probability of a structure typically requires a large number of simulations (i.e. limit state function evaluations). If the limit state function is not explicitly available, a costly numerical methods such as finite element method has to be used, which makes large number of simulations practically not viable. Other alternative ways need to be adopted to evaluate the failure probability in that case.
One of the alternative ways of determining the failure probability is to determine the second moment statistics of the resistance and demand variables. Suppose these are lumped into two random variables denoted by R and F respectively. The limit state function is defined by,

$$Z = R - F \tag{2.3}$$

Now,let's define an entity β which is given by,

$$\beta = \frac{\mu_Z}{\sigma_Z} \tag{2.4}$$

Here μ_Z and σ_Z are the mean and standard deviation of the safety margin Z. If R and F are jointly normal, so would be Z. The probability of failure of the system in that case would be,

$$P_f = P(Z \leq 0) = P\Big(\frac{Z-\mu_Z}{\sigma_Z} \leq -\frac{\mu_Z}{\sigma_Z}\Big) = \Phi(-\beta) \tag{2.5}$$

Here Φ is the standard normal cumulative distribution function. Let us consider now a general case where Z is actually a limit state function,

$$Z = g(\mathbf{S}) \tag{2.6}$$

If the mean $\boldsymbol{\mu}_\mathbf{S}$ and covariance matrix $\boldsymbol{\Sigma}_{\mathbf{SS}}$ are known then by Taylor expansion of Z around the mean of $\mathbf{S}$ we have,

$$Z = g(\mu_\mathbf{S}) + (\nabla_\mathbf{S} g)^T_{\mathbf{S}=\boldsymbol{\mu}_\mathbf{S}}.(\mathbf{S}-\boldsymbol{\mu}_\mathbf{S}) + O\|(\mathbf{S}-\boldsymbol{\mu}_\mathbf{S})^2\| \tag{2.7}$$

Here, $O(.)$ signifies the higher order terms. The following first order approximations are obtained,

$$\mu_Z = g(\mu_S) \tag{2.8}$$

$$\sigma_Z^2 = (\nabla_\mathbf{S} g)^T_{\mathbf{S}=\boldsymbol{\mu}_\mathbf{S}} \boldsymbol{\Sigma}_{\mathbf{SS}} (\nabla_\mathbf{S} g)_{\mathbf{S}=\boldsymbol{\mu}_\mathbf{S}} \tag{2.9}$$

With these values of μ_Z and σ_Z, the so called mean value first order second moment reliability index can be found out from the equation 2.4 [19].

$$\beta_{MVFORM} = \frac{g(\mu_S)}{\sqrt{(\nabla_\mathbf{S} g)^T_{\mathbf{S}=\boldsymbol{\mu}_\mathbf{S}} \boldsymbol{\Sigma}_{\mathbf{SS}} (\nabla_\mathbf{S} g)_{\mathbf{S}=\boldsymbol{\mu}_\mathbf{S}}}} \tag{2.10}$$

While the method outlined here for obtaining the β_{MVFORM} is convenient, there are couple of problems with this method. First one is that R and F are in general not Gaussian, so Z will not be Gaussian either, and in that case the relationship which leads to the failure probability P_f will not be valid. Besides, the β_{MVFORM} is not invariant with respect to changing the limit state function for an equivalent one. The problem of non-Gaussian input variables can be circumvented by transforming them to corresponding Gaussian variables. This also solves the problem of invariance. Second problem is the fact that expansion of Z around the mean value of S does not lead to an accurate estimate of the value of reliability index. The point of linearization should be selected as the point on the limit state surface nearest to the origin in the standard normal space. This point is called the design point. The distance to the Design point is the first order reliability index β_{MVFORM}.

2.2. TRANSFORMATION OF RANDOM VARIABLES

The estimation of failure probability P_f becomes easier if the input random variables are (Standard) Normally distributed, because in that case many structural reliability methods are available to evaluate the Design point. It is also easier to construct a response surface in the space of (input) standard normal variables. But a Gaussian distribution for input parameters is not always an available option, because physical parameters, like Young's Modulus in our case, cannot attain negative values, and with a normal distribution there is a finite probability of physical properties attaining absurd value. Log-normal distribution is best suited for where physical parameters like Young's modulus are the input stochastic quantity. But even if the input quantities are non-normally distributed, they can be transformed like the following,

$$\mathbf{Y} = \mathbf{Y}(\boldsymbol{\xi}) \tag{2.11}$$

such that **Y** is a Gaussian random vector with zero mean and unit covariance matrix, which means that Y_i are independent. The input variables $\xi_i$are correlated though. The transformation is done in two stages. In the first stage non-Normally distributed variables ξ_i are transformed in Gaussian random variables Z_i in such a manner that the correlation of the random variables ξ_i among themselves are maintained. One of the most convenient method to perform such transformation is Nataf's transformation [20]. This is a transformation process which helps transforming the input random variables $\boldsymbol{\xi}$ without altering the covariance structure $A_{\boldsymbol{\xi\xi}}$ of $\boldsymbol{\xi}$. The steps of such a transformation is outlined here.
The goal is to produce

$$Z_i = \boldsymbol{\Phi}^{-1}(F_i(\xi_i)) \tag{2.12}$$

where F_i is non-Gaussian cumulative distribution(CDF) function and $\boldsymbol{\Phi}$ is the joint CDF of Gaussian variables Z_i which is given by,

$$\varphi_n(\mathbf{Z}, \mathbf{R}_0) = \frac{1}{(2\pi)^{\frac{n}{2}}\sqrt{\det(\mathbf{R}_0)}}\exp\Big(-\frac{1}{2}\mathbf{Z}^T\mathbf{R}_0^{-1}\mathbf{Z}\Big) \tag{2.13}$$

The covariance matrix, $\mathbf{R}_0$ needs to be simulated in such a way that the corresponding (target) covariance matrix of ξ_i remain **R**. PDFs of ξ_i and Z_i are related as,

$$f_\xi(\boldsymbol{\xi}) = f_1(x_1)\cdots f_n(x_n)\frac{\varphi_n(\mathbf{Z}, \mathbf{R}_0)}{\varphi_1(z_1)\cdots\varphi_n(z_n)} \tag{2.14}$$

Here $\varphi_n(\mathbf{Z}, \mathbf{R}_0)$ is the joint PDF of the n Gaussian variables Z_i and $\varphi_n(z_n)$ is the marginal PDF of the Gaussian variable Z_n. The problem comes down to numerically solving the integral equation,

$$\rho_{ij} = \int\int_{-\infty}^{\infty}\Big(\frac{\xi_i-\mu_i}{\sigma_i}\Big)\Big(\frac{\xi_j-\mu_j}{\sigma_j}\Big)\varphi_2(z_i, z_j, \rho_{0,ij})\mathrm{d}Z_i\mathrm{d}Z_j \tag{2.15}$$

Here ρ_{ij} are the target correlation coefficients and $\rho_{0,ij}$ are correlation coefficients of Z_i we need to solve for. Once Z_i is obtained then the second stage of the transformation is needed to be done where the independent standard normal random variables Y_i are produced from Z_i by the straight forward transformation,

$$\mathbf{Z} = \mathbf{LY} \tag{2.16}$$

where **L** is the lower triangular Cholesky matrix of $\mathbf{R}_0$, or,

$$\mathbf{R}_0 = \mathbf{L}\mathbf{L}^T \tag{2.17}$$

These two stages of transformation can be combined to establish the direct relationship between Y_i and ξ_i

$$\mathbf{Y} = \mathbf{L}^{-1}.\mathrm{diag}\Big(\frac{f_i(\xi_i)}{\varphi_i(y_i)}\Big)[\boldsymbol{\xi} - \mathbf{M}] \tag{2.18}$$

M is the diagonal matrix containing the mean values of ξ_i. The equation 2.18 is significant because it establishes a functional relationship between a vector of independent

Table 2.1: The comparison of target and simulated correlation coefficients by Nataf's transformation

Correlation coefficient	Target	Simulated
ρ_{12}	0.6766	0.6767
ρ_{13}	0.2096	0.2097
ρ_{14}	0.0297	0.0296
ρ_{15}	0.0019	0.0017
ρ_{23}	0.6766	0.6767
ρ_{24}	0.2096	0.2098
ρ_{25}	0.0297	0.0297
ρ_{34}	0.6766	0.6768
ρ_{35}	0.2096	0.2098
ρ_{45}	0.6766	0.6766

standard normal variables with a vector of correlated Non-Gaussian random variables with specific correlations among themselves. The procedure of Nataf's transformation is demonstrated with an example of an one dimensional case. The correlation coefficients are described by the following equation,

$$R(x_i, x_j) = \exp\Big(-\frac{(x_i - x_j)^2}{a^2}\Big) \tag{2.19}$$

x_i suggests the co-ordinate associated with the i^{th} node. The entity a is called correlation length. Let there be five Log-normally distributed random variables with identical mean and variances. The result of target and simulated correlation coefficients of these 5 random variables are given in the Table 2.1. It should be noted however that in the case of Nataf's distribution with Log-normal marginals, there are closed form relations between the correlation coefficients in the Log-normal and normal spaces [20]. There is no need for numerical analysis, as described in the Table 2.1. The table is only shown for illustration.

2.3. STOCHASTIC FINITE ELEMENT BASED STRUCTURAL RELIABILITY METHODS

At the beginning of this chapter it has been discussed how Monte Carlo simulation (MCS) is impractical for a finite element based reliability analysis. In this section several reliability methods, alternative to MCS, will be presented from literature. Methods like Perturbation method, First order reliability method (FORM), Second order reliability method (SORM), various kinds of Response surface methods, Directional simulation (DS), Directional adaptive response surface method (DARS) and Adaptive Kriging Monte Carlo simulation method (AK-MCS) will be described briefly, in key details.

2.3.1. PERTURBATION METHOD

In the context of a finite element analysis for quasi-static linear problems, the equilibrium equation obtained after discretizing the geometry generally reads,

$$\mathbf{K}.\mathbf{U} = \mathbf{F} \tag{2.20}$$

Suppose the input parameters ξ used in constructing the stiffness matrix $\mathbf{K}$ and the load vector $\mathbf{F}$ are varying around the mean of the input. As a consequence, the three quantities appearing in the above equation will also vary around the values $\mathbf{K}_0$, $\mathbf{U}_0$, $\mathbf{F}_0$ they take for these mean values of the input parameters [19]. The Taylor series expansions of the terms appearing in Eq.(2.20) around the mean values of ξ read,

$$\mathbf{K} = \mathbf{K}_0 + \sum_{i}^{N} \mathbf{K}_i^I \xi_i + \frac{1}{2}\sum_{j}^{N}\sum_{i}^{N} \mathbf{K}_{ij}^{II}\xi_i\xi_j + o\|\boldsymbol{\xi}\|^2 \tag{2.21}$$

$$\mathbf{F} = \mathbf{F}_0 + \sum_{i}^{N} \mathbf{F}_i^I \xi_i + \frac{1}{2}\sum_{j}^{N}\sum_{i}^{N} \mathbf{F}_{ij}^{II}\xi_i\xi_j + o\|\boldsymbol{\xi}\|^2 \tag{2.22}$$

$$\mathbf{U} = \mathbf{U}_0 + \sum_{i}^{N} \mathbf{U}_i^I \xi_i + \frac{1}{2}\sum_{j}^{N}\sum_{i}^{N} \mathbf{U}_{ij}^{II}\xi_i\xi_j + o\|\boldsymbol{\xi}\|^2 \tag{2.23}$$

Here N is the number of random variables. For the first and second order derivatives the corresponding quantities evaluated at the mean values of $\boldsymbol{\xi}$ (the mean of $\boldsymbol{\xi}$ is 0) are $\mathbf{K}_i^I = \frac{\partial \mathbf{K}}{\partial \xi_i}$ and $\mathbf{K}_{ij}^{II} = \frac{\partial^2 \mathbf{K}}{\partial \xi_i \partial \xi_j}$. Collecting the coefficients the similar order coefficients on both sides of the equation, the following expressions are obtained successively,

$$\mathbf{U}_0 = \mathbf{K}_0^{-1}\mathbf{F}_0 \tag{2.24}$$

$$\mathbf{U}_i^I = \mathbf{K}_0^{-1}(\mathbf{F}_i^I - \mathbf{K}_i^I\mathbf{U}_0) \tag{2.25}$$

$$\mathbf{U}_{ij}^{II} = \mathbf{K}_0^{-1}(\mathbf{F}_{ij}^{II} - \mathbf{K}_i^I\mathbf{U}_j^I - \mathbf{K}_j^I\mathbf{U}_i^I - \mathbf{K}_{ij}^{II}\mathbf{U}_0) \tag{2.26}$$

From the Eq.(2.24), Eq.(2.25), Eq.(2.26) and Eq.(2.20) an expression for $\mathbf{U}$ in terms of a polynomial of $\boldsymbol{\xi}$ is obtained. This expression then can be used for the reliability analysis with Monte Carlo method. But the reliability obtained from such a process will be poor. To improve the reliability it is better to expand $\mathbf{K}$, $\mathbf{F}$ and $\mathbf{U}$ around their own mean, like the following [21],

$$\begin{aligned} \mathbf{K} &= \bar{\mathbf{K}} + \delta\mathbf{K} \\ \mathbf{F} &= \bar{\mathbf{F}} + \delta\mathbf{F} \\ \mathbf{U} &= \bar{\mathbf{U}} + \delta\mathbf{U} \end{aligned} \tag{2.27}$$

Instead of collecting coefficients, if the first moment is taken now, then after some rearrangement,

$$\mathbf{A}\bar{\mathbf{U}} = \bar{\mathbf{F}} - \mathrm{E}[\delta\mathbf{K}\bar{\mathbf{K}}^{-1}\bar{\mathbf{F}}] \tag{2.28}$$

where,

$$\mathbf{A} = \bar{\mathbf{K}} - \mathrm{E}[\delta\mathbf{K}\bar{\mathbf{K}}^{-1}\bar{\mathbf{K}}] \tag{2.29}$$

The covariance matrix can be found from,

$$\mathrm{cov}(\mathbf{U},\mathbf{U}^T) = \bar{\mathbf{K}}^{-1}\mathbf{C}\bar{\mathbf{K}}^{-1} \tag{2.30}$$

Using the Eq.(2.30) in Eq.(2.9) will produce the standard deviation of the limit state function (here $\mathbf{S} = \mathbf{U}$). Using this standard deviation the mean value first order second moment reliability index β_{MVFORM} can be found from the Eq.(2.10).

2.3.2. FIRST ORDER RELIABILITY METHOD

The mapping of the limit state function onto the standard normal space by using the probabilistic transformation is described by,

$$g(\mathbf{S}) = g(\mathbf{S}(\boldsymbol{\xi})) = g(\mathbf{S}(Y^{-1}(\mathbf{Y}))) = G(\mathbf{Y}) \tag{2.31}$$

With such transformation, the failure probability can be conveniently estimated from,

$$P_f = \int_{G(\mathbf{Y})\leq 0} \varphi_{\mathbf{Y}}(\mathbf{Y})\mathrm{d}\mathbf{Y} \tag{2.32}$$

Where $\varphi_{\mathbf{Y}}$ is the standard normal PDF of $\mathbf{Y}$ given by,

$$\varphi_{\mathbf{Y}}(\mathbf{Y}) = \frac{1}{(2\pi)^{\frac{n}{2}}}\exp(-\frac{1}{2}\|\mathbf{Y}\|^2) \tag{2.33}$$

This PDF has two interesting properties, namely it is rotationally symmetric and decays exponentially with the square of the norm $\|\mathbf{Y}\|$. Thus the points making significant contributions to the integral Eq.(2.32) are those with nearest distance to the origin of the standard normal space. This leads to the definition of the reliability index β,

$$\beta = \boldsymbol{\alpha}^T\mathbf{Y}^* \tag{2.34}$$

$$\mathbf{Y}^* = \mathrm{argmin}(\|\mathbf{Y}\||G(\mathbf{Y}) \leq 0) \tag{2.35}$$

The solution $\mathbf{Y}^*$ of the constrained optimization problem Eq.(2.35) is called the design point or the most likely failure point in the standard normal space. When the limit state function $G(\mathbf{Y})$ is linear in $\mathbf{Y}$, it is easy to show that,

$$P_f = \Phi(-\beta) \tag{2.36}$$

For determination of the design point, the optimization problem above can be re-formulated as,

$$\mathbf{Y}^* = \mathrm{argmin}(\frac{1}{2}\|\mathbf{Y}\|^2|G(\mathbf{Y}) \leq 0) \tag{2.37}$$

The Lagrangian of the above problem is,

$$\mathscr{L}(\mathbf{Y},\lambda) = \frac{1}{2}\|\mathbf{Y}\|^2 + \lambda G(\mathbf{Y}) \tag{2.38}$$

Assuming sufficient smoothness of the functions involved, the partial derivatives of $\mathscr{L}$ have to be zero at the solution point. Hence,

$$\mathbf{Y}^* + \lambda^* \nabla G(\mathbf{Y})|_{\mathbf{Y}=\mathbf{Y}^*} = 0 \tag{2.39}$$

$$G(\mathbf{Y}^*) = 0 \tag{2.40}$$

The Eq.(2.39) yields,

$$\lambda^* = \frac{\|\mathbf{Y}^*\|}{\|\nabla G(\mathbf{Y})|_{\mathbf{Y}=\mathbf{Y}^*}\|} \tag{2.41}$$

Putting this back into the Eq.(2.39) produces the first-order optimality conditions,

$$\mathbf{Y}^* \|\nabla G(\mathbf{Y})|_{\mathbf{Y}=\mathbf{Y}^*}\| + \|\mathbf{Y}^*\| \nabla G(\mathbf{Y})|_{\mathbf{Y}=\mathbf{Y}^*} = 0 \tag{2.42}$$

For FORM the first-order reliability index β i.e. the minimum distance from the origin of the standard normal space to the limit state surface, is numerically the most challenging task. One source of difficulty is the calculation of the gradient $\nabla G(\mathbf{Y})$. Many of the well known optimization algorithms, like sequentially quadratic programming (SQP) or gradient projection method (GPM) requires calculation of the gradient (even hessian in case of SQP). The direct differentiation method [22], [23] is used to compute the gradient, where possible. Through finite elements the gradient of the limit state surface with respect to the stochastic variables can be elegantly obtained. In a stochastic finite element problem the stiffness matrix $\mathbf{K}$, the vector of degrees of freedom $\mathbf{U}$ and load vector $\mathbf{F}$ are all functions of the input stochastic variables $\boldsymbol{\xi}$. The resulting global system of equations in that case is,

$$\mathbf{K}(\boldsymbol{\xi})\mathbf{U}(\boldsymbol{\xi}) = \mathbf{F}(\boldsymbol{\xi}) \tag{2.43}$$

In direct differentiation method the above equation is differentiated w.r.t stochastic input variable ξ_i, which yields,

$$\mathbf{K}(\boldsymbol{\xi})\frac{\partial \mathbf{U}(\boldsymbol{\xi})}{\partial \xi_i} + \frac{\partial \mathbf{K}(\boldsymbol{\xi})}{\partial \xi_i}\mathbf{U}(\boldsymbol{\xi}) = \frac{\partial \mathbf{F}(\boldsymbol{\xi})}{\partial \xi_i} \tag{2.44}$$

From this follows,

$$\frac{\partial \mathbf{U}(\boldsymbol{\xi})}{\partial \xi_i} = \mathbf{K}(\boldsymbol{\xi})^{-1}\Big[\frac{\partial \mathbf{F}(\boldsymbol{\xi})}{\partial \xi_i} - \frac{\partial \mathbf{K}(\boldsymbol{\xi})}{\partial \xi_i}\mathbf{U}(\boldsymbol{\xi})\Big] \tag{2.45}$$

If the limit state function is defined as $g(\mathbf{U}(\boldsymbol{\xi}))$ in the space of original input variables $\boldsymbol{\xi}$ and as $G(\mathbf{Y})$ in the transformed space of independent standard normal variables $\mathbf{Y}$, then the gradient $\nabla_{\mathbf{Y}} G(\mathbf{Y})$ can be obtained by chain rule,

$$\nabla_{\mathbf{Y}} G(\mathbf{Y}) = \nabla_{\mathbf{U}} g(\mathbf{U}) \nabla_{\boldsymbol{\xi}}(\mathbf{U}) \mathbf{J}_{\boldsymbol{\xi},\mathbf{Y}} \tag{2.46}$$

Here $\mathbf{J}_{\boldsymbol{\xi},\mathbf{Y}}$ is the inverse of the Jacobian $\mathbf{J}_{\mathbf{Y},\boldsymbol{\xi}}$,

$$\mathbf{J}_{\mathbf{Y},\boldsymbol{\xi}} = \mathbf{L}^{-1}\mathrm{diag}\Big(\frac{f_i(\xi_i)}{\varphi_i(Y_i)}\Big) \tag{2.47}$$

If material non linearity is considered then the resulting Finite Element formulation would be nonlinear. Direct differentiation based FORM can be still used to determine the reliability, the equations need to be adjusted on account of the non linearity. For example, in elastic nonlinear case, due to non linearity the stiffness matrix would be a direct function of the displacement vector $\mathbf{U}$, So, the set of algebraic equations would look like,

$$\mathbf{K}(\mathbf{U}(\boldsymbol{\xi}),\boldsymbol{\xi})\mathbf{U}(\boldsymbol{\xi}) = \mathbf{F}(\boldsymbol{\xi}) \tag{2.48}$$

The residual,

$$\mathbf{R}(\mathbf{U}(\boldsymbol{\xi}),\boldsymbol{\xi}) = \mathbf{K}(\mathbf{U}(\boldsymbol{\xi}),\boldsymbol{\xi})\mathbf{U}(\boldsymbol{\xi}) - \mathbf{F}(\boldsymbol{\xi}) \tag{2.49}$$

The Newton-Raphson iteration formula,

$$\mathbf{U}_{r+1}(\boldsymbol{\xi}) = \mathbf{U}_r(\boldsymbol{\xi}) - \mathbf{T}(\mathbf{U}_r(\boldsymbol{\xi}),\boldsymbol{\xi})^{-1}\mathbf{R}(\mathbf{U}_r(\boldsymbol{\xi}),\boldsymbol{\xi}) \tag{2.50}$$

where $\mathbf{T}(\mathbf{U}_r(\boldsymbol{\xi}),\boldsymbol{\xi}) = \frac{\partial \mathbf{R}_r(\mathbf{U}(\boldsymbol{\xi}),\boldsymbol{\xi})}{\partial \mathbf{U}_r(\boldsymbol{\xi})}$. Upon differentiation of Eq.(2.48) with respect to ξ_i and after some rearrangement,

$$\frac{\partial \mathbf{U}(\boldsymbol{\xi})}{\partial \xi_i} = \mathbf{T}(\mathbf{U}(\boldsymbol{\xi}),\boldsymbol{\xi})^{-1}\Big[\frac{\partial \mathbf{F}(\boldsymbol{\xi})}{\partial \xi_i} - \frac{\partial \mathbf{K}(\mathbf{U}(\boldsymbol{\xi}),\boldsymbol{\xi})}{\partial \xi_i}\mathbf{U}(\boldsymbol{\xi})\Big] \tag{2.51}$$

More details on the derivation of the gradient for nonlinear finite element analysis can be found in [24]. Calculating the gradient in this manner would require extensive intrusion into the finite element program down to the elemental level. Besides, the non-linearity in reality could be much more involved. A closed form expression for gradient will be quite difficult to obtain in that case. Also, it is difficult to generalize this method of obtaining gradient for any kind of non-linearity. Currently few finite element softwares, like OpenSees, has the provision to calculate the gradient with the direct differentiation method [25]. This limits the possibility of using different commercial FE softwares in black box fashion and exploit their specific area of expertise. One alternative to the direct differentiation method could be the Finite difference method (FDM), facilitating the computation of gradient in a non intrusive manner. However, the use of FDM can result into wrong estimate of gradient if there is numerical noise in the limit state function. There are cheaper alternative methods to update the gradient. Also, there are some optimization methods which do not require the gradient. A few widely used optimization methods are discussed here.

HLRF

Hasofer and Lind suggested an iterative algorithm, called HLRF [26], to solve Eq.(2.42). This algorithm may not always converge. This algorithm generates a sequence of points $\mathbf{Y}_i$ from the recursive rule,

$$\mathbf{Y}_{i+1} = \frac{\nabla G(\mathbf{Y}_i)^T \mathbf{Y}_i - G(\mathbf{Y}_i)}{\|\nabla G(\mathbf{Y}_i)\|} \frac{\nabla G(\mathbf{Y}_i)}{\|\nabla G(\mathbf{Y}_i)\|} \tag{2.52}$$

From Eq.(2.52) the expression for design point is obtained in a straight forward fashion,

$$\beta = \sqrt{\mathbf{Y}_{i+1}^T \mathbf{Y}_{i+1}} \tag{2.53}$$

SEQUENTIALLY QUADRATIC PROGRAMMING

In the sequentially quadratic programming [27] the objective function is formed in the following fashion,

$$\mathbf{W} = \nabla^2 \Big(-\frac{1}{2} \|\mathbf{Y}_i\|^2 \Big) + \lambda \nabla^2 G(\mathbf{Y}) \tag{2.54}$$

Where λ is the Lagrange multiplier. Now the Newton-Lagrange equation for the SQP is,

$$\begin{bmatrix} \mathbf{W} & \nabla G(\mathbf{Y}_k)^T \\ \nabla G(\mathbf{Y}_k) & \mathbf{0} \end{bmatrix} \begin{pmatrix} \mathbf{s}_k \\ \lambda_{k+1} \end{pmatrix} = \begin{pmatrix} \nabla \Big(-\frac{1}{2} \|\mathbf{Y}_k\|^2 \Big) \\ G(\mathbf{Y}_k) \end{pmatrix} \tag{2.55}$$

Here $\mathbf{s}_k$ is the search direction at k^{th} iteration step and λ_{k+1} is the Lagrange multiplier for $(k+1)^{th}$ step. For small number variables and constraint the size of the matrix is small, so it can be directly inverted to obtain $\mathbf{s}_k$ and λ_{k+1}. From this the new candidate solution at $(k+1)^{th}$ iteration can be obtained,

$$\mathbf{Y}_{i+1} = \mathbf{Y}_i + \alpha \mathbf{s}_k \tag{2.56}$$

α is the step size in the search direction.

GRADIENT PROJECTION METHOD

In the Gradient projection method [28] the projection matrix $\mathbf{P}$ is found by,

$$\mathbf{P} = \mathbf{I} - \nabla G(\mathbf{Y}_k)(\nabla G(\mathbf{Y}_k) \nabla G(\mathbf{Y}_k)^T) \nabla G(\mathbf{Y}_k)^T \tag{2.57}$$

The search direction is found by,

$$\mathbf{s}_k = -\mathbf{P} \nabla \Big(-\frac{1}{2} \|\mathbf{Y}_k\|^2 \Big) \tag{2.58}$$

But, this solution lies at the tangent space of the constraint surface, so in order to bring it on the constraint,

$$\mathbf{c} = -(\nabla G(\mathbf{Y}'_{k+1}) \nabla G(\mathbf{Y}'_{k+1})^T)^{-1} G(\mathbf{Y}'_{k+1}) \tag{2.59}$$

From Eq.(2.58) and Eq.(2.59) the solution is finally found,

$$\mathbf{Y}_{k+1\,j+1} = (\mathbf{Y}'_{k+1} - \nabla G(\mathbf{Y}'_{k+1}) \mathbf{c})_j \tag{2.60}$$

2.3.3. SECOND ORDER RELIABILITY METHOD

In Second order reliability method or (SORM), the failure probability , which is basically a multidimensional integral, is approximated by replacing the limit state surface $G(\mathbf{Y}) = 0$ with a paraboloid in the transformed normal space [29]. The steps involved in the SORM are similar to FORM to the point of obtaining the design point. Once the design point is obtained, the Jacobian matrix $\mathbf{J}$ can be computed as the following,

$$\mathbf{J} = \sum_{i=1}^{N}\sum_{i=1}^{N} Y_i^* Y_j^* \text{cof}\Big(\delta_{ij} - \frac{1}{\|\nabla G(\mathbf{Y})\|}\frac{\partial^2 G}{\partial Y_i \partial Y_j}|_{\mathbf{Y}=\mathbf{Y}^*}\Big) \tag{2.61}$$

where Y_i^* is the i^{th} component of the Design point. The δ_{ij} is called the Kronecker delta, which is such that $\delta_{ij} = 1$ if $i = j$, else $\delta_{ij} = 0$. Once the design point is found, the corrected failure probability can be found as per SORM by,

$$P_f = \Phi(-\beta)\|\mathbf{J}\|^{-\frac{1}{2}} \tag{2.62}$$

The difficulty with above method is that the Hessian matrix $\frac{\partial^2 G}{\partial Y_i \partial Y_j}$ at the Design point. For linear problems evaluation of this Hessian matrix is not difficult but for nonlinear stochastic problems Hessian matrix could be intractable. There is a SORM method that avoids computing the Hessian [30].

2.3.4. RESPONSE SURFACE METHOD

Some authors have used response surfaces (also referred to as surrogate models) to replace the performance function in order to reduce the computational burden [31]. The response surface is constructed based on a selected set of samples. The obtained closed-form expression of the performance function is then used to calculate the failure probability. The response surface approach provides a fast approximation of the performance function that can be used to identify important combination of variables and discern the nature of the input-output relationships. Often polynomial based response surfaces are used; however, with the increasing number of random variables the number of performance function evaluations greatly increases thus making the approach computationally expensive. In this method we express the limit state function in the space spanned by the input variables, like the following,

$$g(\boldsymbol{\xi}) \approx \hat{g}(\boldsymbol{\xi}) = a_0 + \sum_{i=1}^{N} a_i \xi_i + \sum_{i=1}^{N}\sum_{j=1}^{N} a_{ij}\xi_i\xi_j \tag{2.63}$$

Here, N is the number of input random variables, a_i are the unknown coefficients which can be determined from the least square process of the error given by,

$$\text{error}(\mathbf{a}) = \sum_{k=1}^{NF} (g(\boldsymbol{\xi}^k) - \hat{g}(\boldsymbol{\xi}^k))^2 \tag{2.64}$$

Here k denotes the selected sample points of the input variables. Minimization of the Eq.(2.64) leads to,

$$\hat{g}(\boldsymbol{\xi}^k) = (1, \xi_i^k, \xi_i^k\xi_j^k)^T (a_0, a_i, a_{ij}) = \mathbf{V}^T(\boldsymbol{\xi}^k)\mathbf{a} \tag{2.65}$$

or,

$$\mathbf{a} = (\mathbf{V}^T\mathbf{V})^{-1}\mathbf{V}^T g(\boldsymbol{\xi}^k) \tag{2.66}$$

As sample points 2^N fitting points from all the possible combinations of $(\pm\xi_1, \cdots, \pm\xi_N)$. Here $\xi_i = \mu_i \pm \sigma_i$.

2.3.5. CURTAILED RESPONSE SURFACE METHOD

To reduced the number of performance function evaluations Artificial neural network (ANN) based or Gaussian process regression (GPR) based response surfaces have been proposed and tested [32],[33],[34]. It is necessary to construct the response surface in the neighborhood of the most probable failure region in order to obtain an accurate estimate of reliability, especially for nonlinear, multimodal performance functions [35],[36]. Another way of constructing the response in the neighborhood of the failure regions is the curtailed response surface [37] given by,

$$g(\boldsymbol{\xi}) \approx \hat{g}(\boldsymbol{\xi}) = a_0 + \sum_{i=1}^{N} a_i\xi_i + \sum_{i=1}^{N} a_{ii}\xi_i^2 \tag{2.67}$$

Here Exactly $2N+1$ fitting points are selected as follows,

$$\begin{aligned} \boldsymbol{\xi}^1 &= \mu_{\boldsymbol{\xi}} \\ \boldsymbol{\xi}^{2i} &= \mu_{\boldsymbol{\xi}} - f\sigma_i\mathbf{e}_i \\ \boldsymbol{\xi}^{2i+1} &= \mu_{\boldsymbol{\xi}} + f\sigma_i\mathbf{e}_i \\ \boldsymbol{\xi}_M &= \mu_{\boldsymbol{\xi}} + (\boldsymbol{\xi}^* - \mu_{\boldsymbol{\xi}})\frac{g(\mu_{\boldsymbol{\xi}})}{g(\mu_{\boldsymbol{\xi}}) - g(\boldsymbol{\xi}^*)} \end{aligned} \tag{2.68}$$

Here f is a constant number. The value $f = 3$ is used in this Chapter. $\boldsymbol{\xi}^*$ is the vector of design values obtained by HLRF method. $\nabla_{\mathbf{Y}} g(\mathbf{Y})$ is obtained by chain rule $\nabla_{\mathbf{Y}} g(\mathbf{Y}) = \nabla_{\boldsymbol{\xi}} g(\boldsymbol{\xi})\mathbf{J}_{\boldsymbol{\xi},\mathbf{Y}}$, where, from Eq.(2.67) $\frac{dg(\boldsymbol{\xi})}{d\xi_i} = a_i + 2a_{ii}\xi_i$. This approach requires $4N+3$ evaluations of the limit state functions in total.

2.3.6. RESPONSE SURFACE BY POLYNOMIAL CHAOS EXPANSION

The response surface can be prepared in the space of Hermite polynomial also [38]. The response $\mathbf{U}(\mathbf{x}, \boldsymbol{\xi})$ of a structural system can be represented as a Polynomial Chaos Expansion (PCE) as following,

$$\mathbf{U}(\mathbf{x}, \boldsymbol{\xi}) = \sum_{i=0}^{P-1} \psi_i(\boldsymbol{\xi}) U_i(\mathbf{x}) \tag{2.69}$$

Here P is the number of terms in the expansion, $\psi_i(\boldsymbol{\xi})$ are the Hermite polynomials, $\boldsymbol{\xi}$ is the vector of independent standard normal variables and $U_i(\mathbf{x})$ are the associated coefficients. Hermite polynomials have the property of ortho-normality, so,

$$< \psi_i(\boldsymbol{\xi}) >= 0, \qquad < \psi_i(\boldsymbol{\xi})\psi_j(\boldsymbol{\xi}) >= 0, \qquad i \neq j, \qquad \psi_0(\boldsymbol{\xi}) = 1 \tag{2.70}$$

The ortho-normal property of Hermite polynomials can be exploited in the method of Galerkin's projection [39] where the associated coefficients of each Hermite polynomial in the response surface expansion can be obtained as the following,

$$U_i(\mathbf{x}) = \frac{< \mathbf{U}(\mathbf{x},\boldsymbol{\xi})\psi_i(\boldsymbol{\xi}) >}{< \psi_i(\boldsymbol{\xi})^2 >} \tag{2.71}$$

The idea is to evaluate the response $\mathbf{U}(\mathbf{x},\boldsymbol{\xi})$ at some collocation points (like Gauss-Patterson collocation points) and also find the values of $\psi_i(\boldsymbol{\xi})$ at those particular collocation points. With those values at the disposal the expectation $< \mathbf{U}(\mathbf{x},\boldsymbol{\xi})\psi_i(\boldsymbol{\xi}) >$ can be computed numerically, which leads to the desired coefficient $U_i(\mathbf{x})$ at a location $\mathbf{x}$. Alternatively, instead of Galerkin's projection method, least square method can be employed to obtain the coefficients $U_i(\mathbf{x})$ [40]. This process will follow the very same path as outlined for the quadratic response surface.

2.3.7. IMPORTANCE SAMPLING METHOD

A class of method, called Importance sampling (IS) is developed to improve the efficiency issue of MCS [41]. In IS the generation of samples is controlled by a sampling distribution concentrated in the important (high-probability density) region of the failure domain. This method combines the fast convergence of FORM with the robustness of Monte Carlo simulation. The basic idea is to recast the expression for failure probability P_f in Eq.(2.32) to,

$$P_f = \int_{G(\mathbf{Y})\leq 0} \frac{\varphi_{\mathbf{Y}}(\mathbf{Y})}{\psi_{\mathbf{Y}}(\mathbf{Y})} f_{\mathbf{Y}}(\mathbf{Y})\mathrm{d}\mathbf{Y} \tag{2.72}$$

where $f_{\mathbf{Y}}(\mathbf{Y})$ is the M dimensional sampling distribution. The estimate of P_f given a sample $\mathbf{Y}^k$ drawn from f is therefore given by,

$$P_{f,IS} = \frac{1}{N}\sum_{k=1}^{N} 1_{D_f(\mathbf{Y}^k)} \frac{\varphi_{\mathbf{Y}^k}(\mathbf{Y}^k)}{\psi_{\mathbf{Y}^k}(\mathbf{Y}^k)} \tag{2.73}$$

here $1_{D_f(\mathbf{Y}^k)} = 1$ whenever $G(\mathbf{Y}^k) \leq 0$ and 0 otherwise.

Exact convergence of FORM is not necessary to obtain accurate results, even an approximate sampling distribution can significantly improve the convergence rate compared to standard MC sampling. In this Chapter maximum 1000 samples are for IS. It is reported in literature that for systems with a high number of stochastic input variables, the computational effort needed to construct a suitable sampling distribution in Importance sampling may exceed that of MCS [42],[43],[44],[45].

2.3.8. DIRECTIONAL SIMULATION

A method that treats high dimensional reliability problem efficiently is the Directional Sampling (DS) method. A detailed discussion on this can be found in the work of Grooteman [46] and Waarts [14]. In this method, instead of sampling random points in the entire stochastic domain like in MCS, random directions are generated and the failure probability content is determined for each of these directions. This technique takes advantage of an implicitly available LSF through finite element response to obtain samples

extremely close to the LSF. In DS, for each simulated direction, a line search is performed to locate the intersection point of that direction with the limit state function. At the beginning of the process, the actual stochastic space of the problem is transformed to standard normal space **u**. A direction vector $\boldsymbol{u}_i$ in the **u** space can be written as,

$$\boldsymbol{u}_i = \lambda_i \boldsymbol{\theta}_i \tag{2.74}$$

Here, $\boldsymbol{\theta}_i$ is the unit vector in i^{th} direction. λ_i is the distance to the limit state surface $G = 0$ from the origin, along the i^{th} direction. The Figure 2.1) demonstrates the line search procedure for a particular direction $\boldsymbol{\theta}_i$, in the space where G is a function of the uni-variate parameter λ_i alone. At $\lambda_i = 0$, (denoted by the point 0 in Figure 2.1) the point on the limit state surface (denoted by the point (a)), is obtained by finite element method. Then along $\boldsymbol{\theta}_i$ a starting value for λ_i (point 1) is assumed. Equivalent sample point within the **u** space is found through Eq.(2.74) and the corresponding point, (b), on G is evaluated.

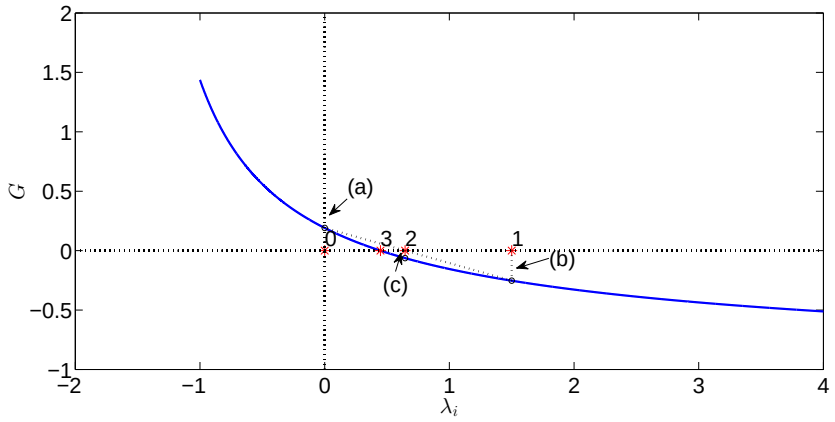

Figure 2.1: Demonstration of the line search for a particular direction $\boldsymbol{\theta}_i$. The limit state function G is plotted as a function of the uni-variate parameter λ_i, along the direction $\boldsymbol{\theta}_i$.

A linear interpolation is done by joining the two points (a) and (b). The intercept of $G = 0$ and this interpolated line is obtained. From this, a new value of λ_i, (point 2), is obtained. This gives a third point (c) on the curve G. Using the three available points, (a), (b) and (c), a quadratic interpolation is done and a new value of λ_i at $G = 0$ is obtained (point 3). This process continues till the intercept point of G and i^{th} direction (final λ_i) is found having a pre-defined limit-state function error tolerance (denoted as tol). Usually this line search takes $3-4$ iterations per direction. The failure probability for N such directions can be estimated as,

$$P_f = \frac{1}{N}\sum_{i=1}^{N} P_{fi} = \frac{1}{N}\sum_{i=1}^{N}(1-\chi_n^2(\lambda_i^2)) \tag{2.75}$$

where n is the number of random variables. $\chi^2_n(\lambda_i^2)$ is the cumulative Chi-square distribution of dimension n. DS can be applied for any irregular limit state surface and operates only on data points obtained directly from FE analysis. The advantage of this method is particularly evident when the number of stochastic input variables is low, but for high stochastic dimension DS can be just as inefficient as MCS.

2.3.9. DIRECTIONAL ADAPTIVE RESPONSE SURFACE

Several authors have used response surfaces in conjunction with directional important sampling methods to improve the efficiency of directional important sampling. Nie *et al.* [47] made an adaptive directional sampling technique which applies a neural network in order to distinguish important regions on the surface of unit hyper sphere. Grooteman [46] developed a response surface based adaptive directional importance sampling where a quadratic response surface is used as the functional type of the response surface to account for the failure probabilities in the unimportant regions of the limit state function. Waarts [14] compared the efficiency of DARS method against various other reliability algorithms for simple finite element based cases. DARS works along the same principle outlined for DS. However, instead of carrying out actual function evaluation based line searches for all directions, DARS distinguishes the important part(s) of the limit state surface with the unimportant part. The actual line searches are reserved for the important part only. This way around increases the efficiency of DS. For the unimportant part of the LSF a fully quadratic response surface of the nature of Eq.(2.76) is used for line search.

$$\hat{G}(\mathbf{u}) = a_0 + \sum_{i=1}^{n} a_i u_i + \sum_{i=1}^{n}\sum_{j=1}^{n} a_{ij} u_i u_j \tag{2.76}$$

This response surface is used instead of the real limit-state function, for the directions pointing towards distant regions of the limit state surface from the origin of $\mathbf{u}$. This method is called the Directional adaptive response surface method (DARS), which is adopted in this thesis. Unlike DS, which uses NLFEA based exact line search for all sampled directions, DARS requires exact line search for only few 'important'directions . The whole procedure completes over several iterations. In each iteration the algorithm tries to find out new important directions from the set of all sampled directions, in addition to the important directions already found from the previous iterations. At the end of each iteration an exact line search is performed for the newly found important directions and the response surface ($\hat{G}$) is updated, based on all the important limit state points. Whether an i^{th} direction is important or not is judged based on the criterion $\lambda_i \leq \lambda_{min} + \lambda_{add}$. The sum $\lambda_{min} + \lambda_{add}$ is the threshold radius enclosing the closest region of the limit state surface from the origin. Here λ_{min} is the current shortest distance from the origin to the exact limit state surface $G = 0$. The term λ_{add} works as an offset which increases the chances of finding an important direction. λ_i is the distance found by inexact line search (based on $\hat{G} = 0$). This iterative process continues over and over again till no new important direction emerges. In the end, all the λ_i (whether found based on G or final $\hat{G}$) are used in Eq.(2.75) to obtain P_f. As such, the λ_is based on final $\hat{G}$ makes only minor contribution to the overall P_f. But the response surface plays a critical role in steering the procedure towards the most important region of the limit state

surface $G = 0$. The fact that $\hat{G}$ is updated in each iteration, makes the process adaptive and despite several iterations, eventually takes less number of NLFE evaluations compared to DS to attain comparable accuracy in P_f. While it is expected that un-important directions would intersect the limit state surface further from the important ones, some rare exceptions do occur. This is because during the iterations, the premature response surface might deem some direction to be important. In later iterations, with an updated response surface, it might turn out that those directions are not close to the important region.

2.3.10. ADAPTIVE KRIGING MONTE CARLO SIMULATION

The adaptive Kriging Monte Carlo simulation (AK-MCS) is a state of the art reliability algorithm which employes Gaussian process regression based meta model to approximate the behavior of the actual limit state function [48], [49]. Experimental design based samples are generated at the beginning and initially the meta model is only accurate close to these points. Then samples are added in a guided way so that the meta model updates in each iteration and the experimental design gradually concentrates in the region close to the limit state surface. Once this meta model finally converges based on a predetermined criterion, it is used as a surrogate function in a Monte Carlo simulation to determine the failure probability.

The details of Gaussian process regression method or Kriging is discussed in Chapter 5. The rest of the algorithm is described here. The AK-MCS algorithm is described here following the algorithm outlined by Schöbi *et al.* [49]. An initial experimental design χ is generated by a Latin Hypercube sampling and corresponding exact response Υ is computed. A Kriging meta model is constructed based on $[\chi, \Upsilon]$. A large set of candidate samples are generated and the corresponding limit state function values are predicted by the meta model. These candidate samples are then ranked according to an enrichment criterion. A selection step determines the sample(s) χ^* to be added to the experimental design of the meta model and their corresponding exact limit state function values Υ^* are evaluated. The meta model is then updated based on these enriched set of experimental design. This process continues till the iterations are terminated through a convergence measure (stopping criterion) with respect to the statistics of interest in order to stop the design enrichment algorithm reliably.

The ranking of the candidate samples are done by learning functions. A learning function estimates the expected value of information gained with respect to the statistics of interest when a sample $\mathbf{x}$ is added to the experimental design of the meta model. There are various learning function proposed in the literature, one among them, the U function [48] is used in this work. The U-function is based on the concept of miss-classification and it is intrinsic to the nature of Gaussian process meta model. For each sample $\mathbf{x}$ there is a nonzero probability that the prediction mean $\mu_{\hat{G}}(\mathbf{x}) > a$ (safe domain), in reality $S(\mathbf{x}) \leq a$ (failure domain, where $S(\mathbf{x})$ is the mechanical response of the structure). This event is termed as miss-classification. Prediction by Gaussian process regression for a given sample is a Gaussian random variable described by the first two moments $\mu_{\hat{G}}(\mathbf{x}), \sigma_{\hat{G}}(\mathbf{x})$. The probability of miss-classification is then,

$$
\begin{aligned}
P_m &= \min\Big\{\Phi\Big[\frac{\mu_{\hat{G}}(\mathbf{x})-a}{\sigma_{\hat{G}}(\mathbf{x})}\Big], \Phi\Big[\frac{a-\mu_{\hat{G}}(\mathbf{x})}{\sigma_{\hat{G}}(\mathbf{x})}\Big]\Big\} \\
&= \Phi\Big[-\frac{|\mu_{\hat{G}}(\mathbf{x})-a|}{\sigma_{\hat{G}}(\mathbf{x})}\Big]
\end{aligned} \tag{2.77}
$$

This function $U(\mathbf{x}) = -\frac{|\mu_{\hat{G}}(\mathbf{x})-a|}{\sigma_{\hat{G}}(\mathbf{x})}$ is called the U-function. The probability of miss-classification is maximum when $|\mu_{\hat{G}}(\mathbf{x})-a|$ is close to zero, or in other works, the sample $\mathbf{x}$ is extremely close to the limit state surface. When the sample is far from the limit state surface, the probability of miss-classification is low. For each candidate sample its associated probability of miss-classification is evaluated based on Eq.2.77. The sample with maximum P_m is added to the existing set of experimental design for enrichment of the experimental design. The convergence measure (or stopping criterion) is based on the accuracy of the meta model around the limit state surface rather than on the estimation of the statistics of interest. The learning function U is seen to give more weight to the points in the close neighborhood of the predicted limit state rather than further ones with high Kriging variance. This learning function is therefore faster in converging towards an accurate probability of failure at the stopping condition. The choice of this learning function U is rather natural, because it is easy to understand that the U value is directly linked to the Kriging variance and prediction. Echard *et al.* [48] used the stopping criterion

$$
\min[U(\mathbf{x})] \geq 2 \tag{2.78}
$$

which indicates that the probability of miss-classification must be smaller than $\Phi(-2)$ for all candidate samples in order to stop the iteration. Schöbi *et al.* [49] used a different strategy for convergence criterion. They defined a lower and upper boundary of the limit state function with,

$$
\mu_{\hat{G}}(\mathbf{x}) \pm k\sigma_{\hat{G}}(\mathbf{x}) = a \tag{2.79}
$$

where k typically has the value 1.96. Based on these limit state boundary a convergence criterion is set as,

$$
\frac{\hat{P}_f^+ - \hat{P}_f^-}{\hat{P}_f^0} \leq \varepsilon_{\hat{P}_f} \tag{2.80}
$$

here $\hat{P}_f^{\pm} = P[\mu_{\hat{G}}(\mathbf{X}) \pm k\sigma_{\hat{G}}(\mathbf{X}) \leq a]$ are the upper and lower bound failure probabilities and $\hat{P}_f^0 = P[\mu_{\hat{G}}(\mathbf{X}) \leq a]$. $\mathbf{X}$ is the set of all the samples. When the lower and upper limit state boundaries are close to each other (i.e., a small limit state margin), then the estimate of the statistics are of interest (such as failure probability) is accurate.

As the meta model Schöbi *et al.* used the polynomial chaos Kriging model, which has a set of orthogonal basis functions, instead of simple Kriging used by Echard *et al.* The authors called the resulting method PC Kriging (or PC-AK-MCS) The authors also exploited high performance computing architecture by selecting multiple candidate samples at a time (and evaluating their exact response parallelly) instead of single candidate sample for enrichment. In this work however, multiple candidate selection is not used.

2.4. RANDOM VARIABLE METHOD VERSES RANDOM FIELD MODEL

The issue of how the randomness in the material properties can be modeled, requires due consideration. One simple approach is to model the randomness as random variable. However, this implies homogenization of material property in the spatial extent of the structure, which in turn, introduces additional epistemic uncertainties into the model. To make matter worse this variation does not confine itself in spatial extant of the structural component, but also varies from sample to sample. For some cases ignoring this spatial inhomogeneity while modeling material randomness could significantly undermine the accuracy of the reliability analysis. A more accurate representation of the uncertainties within the spatial extent of the structural component would be to adopt random field models. Random field models are more robust and can model the spatial fluctuations in the properties, as well as the ensemble variations. On the other hand modeling the uncertainty as a random field demands sophisticated means of analysis. Two among the random field modeling approaches found in the literature are discussed briefly in the sequel.

2.4.1. OPTIMAL LINEAR EXPANSION

The Optimal linear expansion (OLE) method is termed as a point discretization method. In this method a spatial discretization of the system geometry (the mesh) is utilized for the approximation of the mechanical response of the structure [50]. An input random field can be expressed by OLE as the following,

$$\mathbf{E}(\mathbf{x},\boldsymbol{\xi}) \approx \hat{\mathbf{E}}(\mathbf{x},\boldsymbol{\xi}) = \mathbf{E}_0 + \sum_{i=1}^{N} \varphi_i(\mathbf{x})\boldsymbol{\xi}_i \tag{2.81}$$

The shape functions $\varphi_i(\mathbf{x})$ at every point $\mathbf{x}$ are determined by minimizing the variance of the error given by $\text{var}[\mathbf{E}(\mathbf{x},\boldsymbol{\xi}) - \hat{\mathbf{E}}(\mathbf{x},\boldsymbol{\xi})]$ subject to the condition that $\hat{\mathbf{E}}(\mathbf{x},\boldsymbol{\xi})$ has the same mean as $\mathbf{E}(\mathbf{x},\boldsymbol{\xi})$ (or $\text{expectation}[\mathbf{E}(\mathbf{x},\boldsymbol{\xi}) - \hat{\mathbf{E}}(\mathbf{x},\boldsymbol{\xi})]$).

OLE is particularly attractive when Finite Element method is used to assess the propagation of the uncertainty of the input to the response of the structural system, because OLE allows the use of different set of discretization than FE discretization for the same problem.

2.4.2. KARHUNEN-LOEVE EXPANSION METHOD

The Karhunen-Loeve expansion method or K-L expansion method is a series expansion method, where the random field is exactly represented as a series involving random variables and deterministic spatial functions. The approximation is then obtained as a truncation of the series. In this method a random field $\mathbf{E}(\mathbf{x},\boldsymbol{\theta})$ is described in the space of standard normal variables θ like the following,

$$\mathbf{E}(\mathbf{x},\boldsymbol{\theta}) = \sum_{i=0}^{N} \theta_i E_i(\mathbf{x}) \tag{2.82}$$

where,

$$< \theta_i >= 0, \qquad < \theta_i \theta_j >= 0, \qquad i \neq j, \theta_0 = 1 \tag{2.83}$$

The coefficients $E_i(\mathbf{x})$ are obtained by using the covariance matrix R_{EE} of random field $\mathbf{E}(\mathbf{x},\boldsymbol{\theta})$,

$$\int R_{EE}(\mathbf{x},m)\Phi_i(m)\mathrm{d}m = \lambda_i\Phi_i(\mathbf{x}) \tag{2.84}$$

$$E_i(\mathbf{x}) = \sqrt{\lambda_i}\Phi_i(\mathbf{x}) \tag{2.85}$$

One issue with K-L expansion is that bases of this expansion are the standard normal variables. So, it is best used to expand a Normally distributed random field. A log-Normal random field with K-L expansion can be obtained by the following,

$$f(\mathbf{x},\boldsymbol{\theta}) = \exp(\mathbf{E}(\mathbf{x},\boldsymbol{\theta})) = \exp\Big(\sum_{i=1}^{N}\theta_i E_i(\mathbf{x})\Big) \tag{2.86}$$

In order to maintain the correlation structure of the input random field through this process of nonlinear transformation it is necessary to simulate an intermediate covariance matrix R'_{EE}. There is an exception in the case of transformation between normal and log-normal spaces however. There exists an exact relationship between correlation coefficients in normal and log-normal spaces.

2.4.3. RELEVANCE OF RANDOM FIELD FOR RC STRUCTURES

Some comments are in order regarding the applicability of random field discretization for RC structures. The consideration of spatial inhomogeneity while modeling material randomness makes the reliability estimates more realistic. On the other hand, random field discretization introduces additional random variables. The number of additional random variables due to random field discretization depends on the correlation length of a random field in the spatial extent. Correlation length is a measure of inhomogeneity of a material property. For small correlation length, the homogenization effect, discussed in material science, takes over. Effective properties are average ones over a critical window width. Smaller correlation length leads to finer random field discretization, resulting in more number of input random variables. Increase in random variables puts additional computational burden and complexity on the reliability calculation. So unless there is a significant improvement in the accuracy of the reliability estimate, the additional computational burden can be a wasteful endeavor. According to the JCSS Probabilistic Model Code the default correlation length for concrete compressive strength is 5 m [51]. The correlation length of 5 m means that only for structures in excess of $15-20$ meters the random field approach is going to be effective. For structures of smaller dimensions there will be little variation in the material property for concrete in the spatial domain. It is expected that a random variable model will be sufficiently accurate in such cases.

One concern could be that how to quantify modeling uncertainty for a FE model when random field is considered, because when random field modeling is considered, it is necessary to use the same spatial distribution of material property as used in the experiment. Random field for a material property is obtained by testing the material properties in from several different locations of the structure. In the NLFEA model those

same measured values needs to be considered in those exact same locations. This is how the modeling uncertainty for the random field can be quantified.

2.5. NUMERICAL EXAMPLES

The reliability methods discussed in this chapter are demonstrated with two numerical examples in this section. These two example serves as a demonstrative examples to compare the performance of various different structural reliability algorithms discussed in this chapter.

2.5.1. FIRST EXAMPLE

For the first example a point mass hanging from the ceiling by wire is considered (Figure 2.2). The weight is $S = 100\,\text{kN}$, the diameter and the tensile strength of the wire are denoted by d and f. The limit state function for this problem is given by,

$$g = \frac{\pi d^2 f}{4} - S \tag{2.87}$$

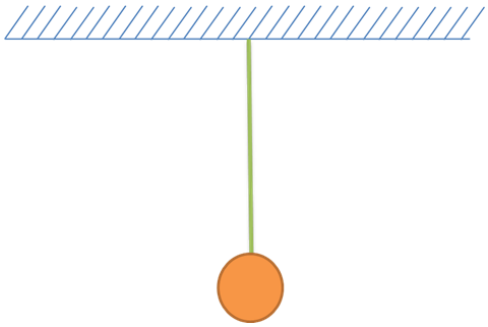

Figure 2.2: Ball hanging from ceiling

The mean and standard deviation of f are $290\,\text{N/mm}^2$ and $25\,\text{N/mm}^2$. The mean and standard deviation of d are 30 mm and 3 mm. In this problem f and d are distributed Log-Normally. The reliability of this problem is attempted with various methods discussed in this chapter. The number of limit state function evaluations (LSFE) and the corresponding β are summarized in the Table 2.2.

Table 2.2: The comparison of reliability results for the first example

	MCS	FORM	SORM	IS	DARS	PC-AKMCS
β	3.25	3.24	3.24	3.25	3.26	3.30
LSFE	10^5	20	32	1020	63	13

2.5.2. SECOND EXAMPLE

For the second example a slender beam is considered for which the Young's modulus E is modeled as a log-normal random field (Figure 2.3). The length, depth and width of the beam are 10 m, 0.16 m and 0.5 m respectively. The beam has a uniformly distributed load of 1000 N/m. 10 finite element discretization have been taken (11 nodes with 2 degrees of freedom per node).

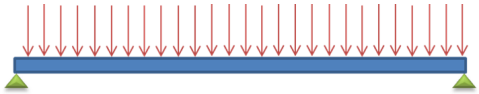

Figure 2.3: Beam with random Modulus of elasticity

The mean value of Young's modulus E is taken to be 2×10^{11} N/m^2 with 20% coefficient of variation. The correlation structure of the random field is represented with Eq.(2.19). This random field has been discretized using an Optimal linear expansion scheme described earlier in this Chapter. Along the length of the beam, four OLE discretization has been considered, which gives 5 OLE nodes and as many correlated random variables (in the original Log-normal space) and OLE shape functions. The log-normal random field is described in the space of log-normal random variables ξ_i. Here,

$$\xi_i = \exp(\mu_{ln} + \sigma_{ln} R'_{ij} Z_j) \tag{2.88}$$

Where, Z_i are Gaussian random variables. The quantities μ_{ln} and σ_{ln} are Log-normal mean and standard deviation corresponding to Gaussian mean and variance μ_n and σ_n. These quantities are related according to the following relations,

$$\mu_{ln} = \ln\left(\frac{\mu_n^2}{\sqrt{\mu_n^2 + \sigma_n^2}}\right) \tag{2.89}$$

$$\sigma_{ln} = \sqrt{\left(\ln\left(\frac{\mu_n^2 + \sigma_n^2}{\mu_n^2}\right)\right)} \tag{2.90}$$

R'_{ij} in the equation signifies the transformed correlation coefficient between ξ_i and ξ_j obtained through Nataf's transformation.

As a limit state function the following has been used,

$$g(\mathbf{U}(\boldsymbol{\xi})) = g(\mathbf{U}(\boldsymbol{\xi}((Y)))) = G(\mathbf{Y}) = 1 - \frac{U_{midpoint}}{0.0006} \tag{2.91}$$

where $U_{midpoint}$ is the deflection at the midpoint of the beam.

Various reliability methods like FORM, SORM, DS, PCE (Galerkin), IS, DARS and PC-AKMCS are used to obtain the reliability, and these results are compared with the Monte Carlo method. The number of finite element analysis (FEA) and the corresponding β are given in the Table 2.3. For MCS, DS and DARS a coefficient of variation of failure probability of 0.1 is used as termination criterion for sampling. The PDF of the deflection at the midpoint by Response surface is plotted and compared to Monte Carlo simulation

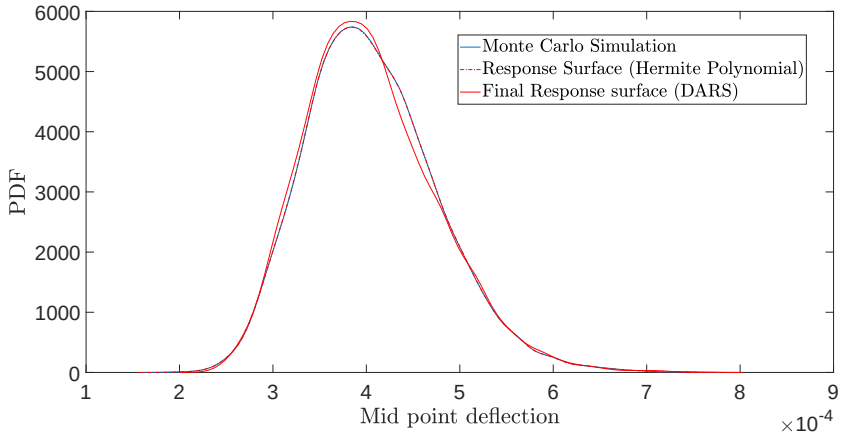

Figure 2.4: Comparison of probability density functions of the mid point deflection

Table 2.3: The comparison of reliability results for the second example

	MCS	FORM	SORM	DS	PCE	IS	DARS	AK-MCS
β	2.37	2.37	2.37	2.37	2.34	2.37	2.38	2.35
FEAs	10^5	35	92	1197	243	1035	84	41

in Figure 2.4. The PDF by the final response surface obtained from DARS is also provided in the same figure.

2.5.3. DISCUSSION ON THE EXAMPLES

Perturbation method has not been considered for the numerical examples. Because for a finite element problem implementation of this method is relatively difficult as it requires extensive intrusive manipulations of the stiffness matrix. The result obtained by this method is reported to be less accurate since the reliability index is evaluated at the mean value but not at the design point [52]. The manipulations and implementation effort required by Perturbation method for nonlinear problems are even more involved while they still suffer from the same shortcomings. Curtailed response surface method also has been ignored in the examples. Because The lack of cross terms in curtailed response surface means that only $4N+3$ function evaluations may not be sufficient to get an accurate result. FORM gives quite accurate result with least number of function evaluations for both the examples, but it requires the gradient of the limit state function. Also design point is obtained by an iterative optimization scheme where convergence can be an involved issue for large number of random variables. SORM is even better in terms of result for the second example, while it requires some additional computational effort in comparison to FORM, but calculation of the hessian of the limit state function is most definitely not a viable option for non-linear problems. Some methods which do

not require hessian can remedy this situation [30]. IS, DARS, PC-AKMCS all these methods produced highly accurate results for the example. DS however took substantially larger number of function evaluations compared to DARS. Implementation of Galerkin's projection method can be problematic for large number of input random variables, as with increase in input random variables result in exponential increase in the number of collocation points and as a result the number of finite element analysis.

2.6. CONCLUDING REMARKS FOR THE SECOND CHAPTER

Several finite element based reliability methods have been reported in this Chapter and they are demonstrated through some numerical examples. Based on the results of these examples we can speculate about their suitability for the reliability of RC structure problems. First order reliability method (FORM) and Second order reliability method (SORM) are among the earliest reliability algorithms. FORM and SORM approximate the limit state function at the design point with a first order and incomplete second order function respectively. They employ constrained optimization methods to determine the design point and its distance from the origin in the standard normal space. The FORM and SORM algorithms are known to have difficulty converging to a correct failure probability when the structure in question has multiple failure modes (system effect). The resulting failure probability can be incorrect if all the failure modes are described using a single limit state function. FORM can be applied in cases with system effect when different parts of the limit state function, corresponding to each failure mode, can be expressed as distinct functions. But for the cases where the limit state function is described using finite element analysis, expressing each part of the limit state function as distinct functions is too difficult. This is especially unlikely in nonlinear finite element analysis of reinforced concrete structures that are based on (2D or 3D) continua formulations and that simulate the failure process, as is applied in the thesis. A modified FORM (and SORM) algorithm has been described by Der Kiureghian and Dakessian [53] which can detect multiple design points, when the failure modes are described by a single limit state function. FORM and SORM's inaccuracy in case of highly non-linear limit state function has been attested by several authors [46]. Highly nonlinear limit state function is also quite likely for a NLFEA based limit state function of a RC structure. Monte Carlo simulation (MCS) is the simplest method for calculating response variability. But even though convergence and accuracy is guaranteed in MCS, the randomness of the sampling points demands large number of samples, especially for estimation of small failure probability with low variance. Run time of each NLFEA computationally a RC structure prohibits the use of large number of simulations. Higher stochastic dimensions also rule out methods like the non-intrusive Galerkin's projection method [19]. Directional sampling (DS) offers improved performance over crude MCS, it samples directions in the standard normal space. The probability content for each direction is evaluated by an one-dimensional integral which has a closed-form solution in the standard normal space. This method has poor efficiency for high number of random variables.

The Directional adaptive response surface method (DARS) is known to be efficient as well as accurate and robust from the literature. It overcomes practical obstacles associated with many other structural reliability algorithms concerning efficiency, robustness and accuracy. Based on several different kinds of limit state function Waarts [14] demon-

strated that the number of exact limit state function evaluations for DARS is not significantly influenced by the number of input random variables. The author stated that for high dimensional problems only few directions are likely to have influence. DARS will perform significantly better than DS in terms of efficiency for these problems. Waarts also concluded that FORM and DARS are equivalent in terms of efficiency on component level. Grooteman [46] compared the efficiency of DARS and FORM for a linear limit state function (a linear-hyper plane limit state surface), for different numbers of input random variables. He showed that with the increase of the input random variables, DARS becomes more efficient compared to FORM as long as linear or incomplete quadratic response surfaces are used for DARS. It must be pointed out though that these conclusions are based on few selected cases, and they may not hold generally.

The effectiveness of DARS and AK-MCS have been demonstrated mainly for simple algebraic limit state functions or at best, simple finite element based limit state functions in the literature [46],[14],[54], [49]. For most practical structures (or systems), the structural responses have to be calculated by a numerical procedure such as finite element analysis, because the limit state function is not available as an explicit, closed-form function of the input variables. In many applications the limit state function described by finite element is smooth and poses little difficulty for the reliability algorithm. But in some applications, like reinforced concrete (RC) structures, the nonlinear finite element analysis (NLFEA) failure simulations can be a source of irregularity, leading to a noisy limit state function. Computational noise occurs in all nonlinear FE problems, where a tolerance criterion determines the convergence of the iterative solution. Noisy limit state functions or performance functions are not exclusive to the failure analysis of RC structures only but often encountered in computational fluid dynamics based optimization problems [55],[56],[57]. Directional integration along each direction is performed by finding the distance of the limit state surface $G(\mathbf{X}) = 0$ along that direction from the origin. This is done by an iterative process called line search. Even though small noise in finding the distance to the limit state surface is immaterial in calculating the probability, a highly noisy limit state function can pose major difficulties for the uni variate root finding and the overall efficiency might decrease. The practical issues concerning the reliability analysis for cases of limit state functions under numerical noise have gained little attention in literature. The performance of adaptive directional importance sampling algorithms or adaptive Kriging algorithms for such cases has not been reported. In the subsequent chapters RC structural examples will be introduced which will help to test the performances of DARS and AK-MCS for limit state functions under numerical noise.

3

NLFEA MODELING IN STRUCTURAL RELIABILITY

3.1. INTRODUCTION

THE NLFEA solution strategy is an essential element of reliability analysis of RC structures. It was mentioned in the Chapter 1 that in the process of abstraction from the structure to the mechanical model, and then the abstraction from the mechanical model to the finite element model, NLFEA introduces a potential for significant uncertainties and scatter in the result in all steps from idealization of the physical problem, discretization into finite elements, numerical material modeling and selection of solution procedures. Guidelines are often used to streamline the choices made in tailoring the solution strategy. The Dutch Guideline is used in this thesis for formulating such solution strategy. The formulation is done after extensive review of the solution strategies found in the RC literature. This solution strategy will serve as the foundation for the NLFEA based reliability analysis in the forthcoming chapters.

3.2. NLFEA SOLUTION STRATEGY FOR RC BEAM

In the context of NLFEA, solution strategy means choices made regarding kinematic relationship, constitutive modeling, equilibrium, material modeling, boundary conditions etc [17]. The modeling choices and parameters influence the predicted structural response significantly. If the choices are not calibrated properly the scatter in results will be big, with some results being unrealistic. NLFEA guidelines for RC structures have been prescribed in order to minimize the error associated with human judgment. The framework issued by Dutch Ministry of Infrastructure and the Environment or Dutch Guideline (DG) [18, 58] in short, lays a framework for devising such a solution strategy. For the solution strategy in this thesis several options have been experimented with, remaining within the framework of the Dutch Guideline. In this work the adopted solution strategy draws its inspiration from other Dutch Guideline based solution strategies in literature, like [59] (DG based) and [60]. However, the major influence has been the solu-

tion strategy developed by Evangeliou [15]. Each major aspects of the solution strategies, like constitutive modeling, kinematic compatibility, loading and boundary conditions are discussed separately. The similar strategies found in literature are also discussed in parallel.

3.2.1. CONSTITUTIVE MODELING

CONCRETE

- For concrete, a total strain based rotating crack or fixed crack model was recommended in [18] as constitutive model. Compared to the fixed model, the rotating model usually results in a lower limit failure load because it does not suffer as much from spurious stress locking. In this thesis the smeared cracking approach is used with a fixed total strain crack model.

- When using a fixed crack model, it is necessary to assign a shear retention factor (SRF). The SRF reflects the relative amount of shear stiffness that should be retained at an integration point after cracking, and should be assigned a sufficiently high value to avoid numerical instabilities due to ill-conditioning of the material stiffness matrix and a sufficiently low value to reduce the transfer of shear stresses across cracks due to rotation of the stress field after cracking.

- A constant SRF of 0.1 was used in [59] (DG based) and [60]. An isotropic linear-elastic material model based Young's modulus and Poisson ratio has been prescribed in [18]. Regarding shear behavior, for fixed crack models a variable shear retention model was strongly recommended in [18]. The aggregate interlock effect is modeled with a damage based variable SRF in this thesis. This implies that the secant shear stiffness degrades at the same rate as the secant tensile stiffness does due to cracking.

- An exponential softening diagram was recommended in [18] for tensile behavior of concrete. In the absence of exponential softening a multi-linear approximation of the exponential uni-axial stress-strain diagram can be used. The exponential softening model in tension is chosen in this thesis.

- The apparent Poisson ratio should be reduced after crack initiation. Poisson's ratio was kept constant at the value of 0.15 until initiation of cracking in [59] (DG based) and [60]. The reduction of the Poisson's effect upon cracking is accounted with a damage based concept [61] in this thesis. The effect of confinement, although of limited importance for a 2D model, is modeled as suggested by Selby and Vecchio [62].

- The compressive behavior should be modeled such that the maximum compressive stress is limited. Parabolic stress strain diagram with softening branch was suggested in [18], which is adopted in the chosen solution strategy. The softening branch should be based on the compressive fracture energy value in order to reduce mesh size sensitivity during compressive strain localization. The lateral effect of cracking on the compressive strength is modeled with the model suggested by Collins and Vecchio [63].

- As per the recommendation in [18], tension-compression interaction needs to be addressed and taken into account in the modeling of concrete structures subjected to multi-axial stress state, where as compression-compression interaction could be ignored as per the strategies.

- Existing cracks in the structure should be taken into account when ever detailed information about location and crack widths is available, because existing cracks basically reduce the stiffness in a local region of the structure. This can be modeled using a reduced tensile strength, reduced Young's modulus and reduced fracture energy [18]. Since the amount of reduction is difficult to assess, the existing crack pattern should be recreated using multiple load cases that lead to the observed pattern. Alternatively the cause of existing cracks is modeled explicitly.

- An automatic procedure for determining the crack band width is recommended [18]. The preferred method is a method based on the initial direction of the crack and the element dimensions. Alternatively, a method based on the area or volume of the finite element can be used. In this thesis an automatic procedure, available in DIANA, to determine crack band width has been chosen based on area of element.

REINFORCEMENT

- As model for reinforcement, an elasto-plastic material model with hardening was recommended for both steel bar and pre-stressing steel by the authors in [18]. The stress-strain behavior of the reinforcement bars is modeled as elastic-perfectly plastic in this thesis.

3.2.2. KINEMATIC COMPATIBILITY

- Regarding finite element discretization, elements with quadratic interpolation of the displacement field was recommended by the authors in [18]. Preferably a quadrilateral shape or a hexahedral shape in 2D and 3D, respectively.

- Quadrilateral eight node iso-parametric plane stress elements and twenty node iso-parametric solid brick elements were used in the 2D and 3D based model respectively in [60]. A rectangular mesh of aspect ratio 1 is applied in this thesis. 2D plane stress quadrilateral elements of length 25 mm are chosen with quadratic interpolation and 3×3 Gauss integration. The steel plates are modeled with the same quadrilateral elements.

- As for numerical integration, full integration was recommended in [18], because reduced order integration for quadratic elements can lead to spurious modes when the stiffness of the element becomes small due to extensive cracking. The solution strategy in [59] used 20 node solid elements and three-node truss elements for concrete and reinforcement respectively. This gives rise to the danger of under integration, which is circumvented by selecting reduced integration.

- For reinforcement, the same order of interpolation as the concrete elements should be used [18].

- It was suggested in [18] that the finite element mesh has to be generated using an algorithm that produces regular meshes with less than 5% of distorted elements.
- While there is no restriction regarding minimum element size, the maximum element size is limited to ensure that the constitutive model does not exhibit a snap-back in the stress-strain relationship.
- Concrete-reinforcement interaction is the main mechanism for stress redistribution after cracking in concrete structures with bonded reinforcement. Effects like tension stiffening is governed by the number of cracks that are present after a stabilized crack patterns has developed.
- A conservative assumption is to ignore the tension-stiffening component and only account for the energy dissipated in the cracks that develop during the loading process. If the element size is smaller than the estimated average crack spacing, the tension-softening model can be used. Otherwise, the amount of energy that can be dissipated within a finite element should be related to the average crack spacing and the size of the element.
- Slip between reinforcement and concrete and dowel action of reinforcement should also be accounted for with appropriate model. Embedded reinforcement elements with no slip were used in [18], [58] and [60]. The reinforcement is modeled as embedded in this thesis, i.e. perfect bond is assumed between the reinforcement bars and the surrounding concrete surface.
- Bond slip and tension softening are recommended to be used in [59] for medium scale analysis, i.e. when the element size is in the order of the reinforcing bar diameter, and perfect bond and tension stiffening should be used for large-scale analysis.

3.2.3. LOADING AND BOUNDARY CONDITIONS

- It was recommended in [18] that unless the objective of the analysis is to study the detailed behavior of the loading and support points, the support and loading plates should be modeled such that local stress concentrations are reduced.
- It was suggested in [18] that interface elements having no-tension behavior should be inserted between the loading plate and concrete in order to properly reproduce the actual load transfer mechanism. Linear interface elements are applied between the concrete beam surface and the steel plates used for loading and support.
- For 2D model a fully reinforced and cantilevered upper beam, with linear elastic concrete was used in order to avoid damage of the upper beam due to the concentrated load in [60].
- During analysis dead weight, permanent loads, and, if appropriate, pre-stressing should be applied first to the structure, the variable loads are increased until a clear failure mode is present or if a significant load reduction has been achieved [18].

3.2.4. EQUILIBRIUM

- Equilibrium between internal and external forces should be achieved iteratively using a Newton-Raphson method with an arc-length procedure [18]. A standard Newton-Raphson solution procedure with line searches was used in all the analysis, for a stable and robust solution procedure [58], [60]. For the equilibrium iterations in this thesis, a Quasi-Newton method based on a secant stiffness is selected. A line-search technique is adopted to boost the convergence rate. The maximum number of iterations for each load step is set at 100, in order to relieve convergence requirements for few possible spurious load steps where the amount of crack opening rate is high.

- Energy-norm together with a force-norm should be used as convergence criterion to determine equilibrium [18], which is adopted in this thesis. A norm based on displacements only should be avoided. 10^{-2} tolerance for force norm and 10^{-4} tolerance for energy norm were suggested in [58]. Convergence criteria on both force-norm and energy-norm with tolerances of respectively 10^{-2} and 10^{-3} was used, in [58], [59](DG based) and [60], though allowing the analysis to proceed beyond non-converged load steps as non-convergence does not necessarily imply failure. A tight tolerance of 10^{-3} is selected in order to avoid load path sensitivity.

- In [60] The load steps were explicitly defined with initial steps about a third of the displacement value that initiated flexural cracking. The loading sequence comprised five initial load steps of 0.1 mm, with following step sizes of 0.5 mm until failure. In this thesis a displacement control based loading is selected. The displacement corresponding to the loading capacity of the beam has been determined for the mean values of the material properties. 1.25% of this displacement is selected as the incremental load step size.

3.3. PERFORMANCE OF THE NLFEA SOLUTION STRATEGY FOR RC BEAM

The comparative performance of this solution strategy, for the mean material properties, can be seen in Figure 3.1. The results are based on beam A75A2, selected from the experiments of Yang *et al.* [64]. R_{NLFEA} and R_{EXP} are the predicted and experimentally obtained response respectively.

In Figure 3.1 the predicted load displacement curve is observed to have a steep gradient initially. Later the two load displacement curves become almost parallel. The steep inclination is absent in the experimental result because a used beam, with cracks, is used in the experiment. For the NLFEA a loading-unloading-loading cycle can be used. However, we are following here the basic assumption that was made in the test setup. The test procedure assumes that when the supporting condition does not change, and there is no clear flexural shear crack, the crack pattern of the previous loading-unloading does not affect the shear capacity of the loading that follows [64]. This assumption implies that an initial difference in stiffness will have a minor influence on the obtained failure load. The figure shows that the predicted capacity is indeed reasonably close to the experimental one.

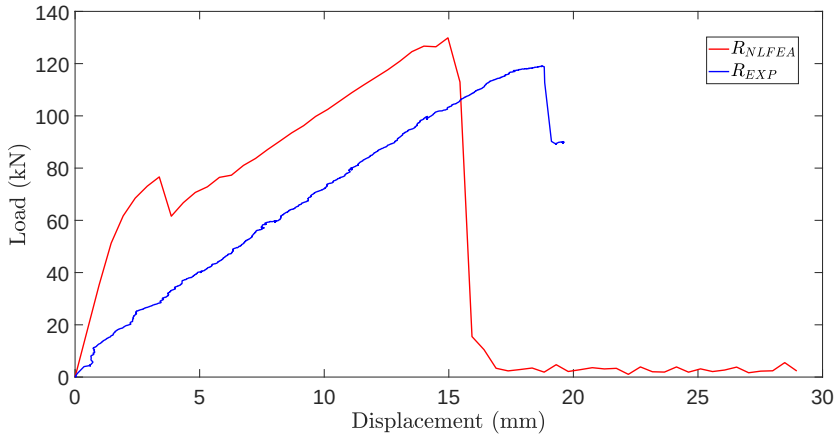

Figure 3.1: Comparison of load vs displacement curve

3.3.1. DEMONSTRATIVE TEST CASES: THREE RC BEAMS

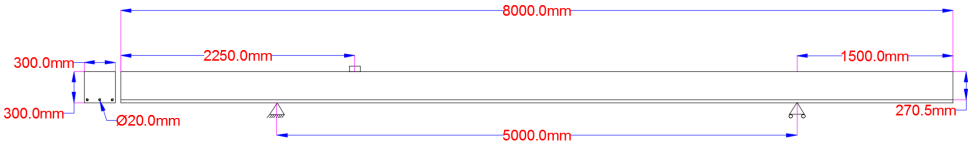

Figure 3.2: Schematics of the reinforced concrete shear beam and the point of loading

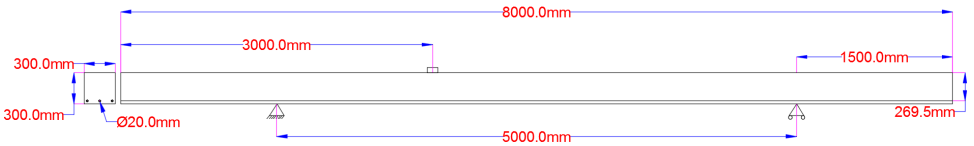

Figure 3.3: Schematics of the reinforced concrete mixed beam and the point of loading

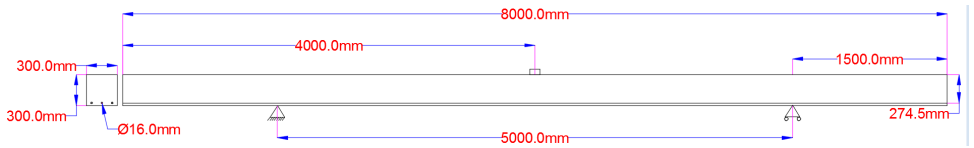

Figure 3.4: Schematics of the reinforced concrete bending beam and the point of loading

Three RC beams are selected in this thesis as demonstrative examples. These beams are largely inspired by RC beams experimentally studied by Yang *et al.* [64]. The first beam fails in shear (Figure 3.2), the second one fails in mixed mode (Figure 3.3) and the third one fails in bending (Figure 3.4). These beams will be referred to as shear beam, mixed beam and bending beam respectively in this work. The concrete compressive strength (f_c), tensile strength (f_t), tensile fracture energy (G_F), compressive fracture energy (G_c), Young's modulus (E_c) and reinforcement yield strength (f_y) represent all the possible random variables considered for these three beams. The stochastic properties for the random variables are obtained from Yang *et al.* and Wiśniewski *et al.* [65] (summarized in Table 3.1). All the stochastic variables for this beam are properties which cannot have negative values. Therefore, they are assumed to follow log-normal distribution. For concrete, the compressive fracture energy G_c has been obtained by the relation $G_c = 250G_F$, provided by Nakamura *et al.* [66], where the mean value of G_F is used.

Table 3.1: The mean properties for the three RC beams

Cases	f_c [MPa]	f_t [MPa]	G_F [N/mm]	E_c [MPa]	f_y [MPa]	G_c [N/mm]
Shear	78.2	5.13280	0.1266	42675	550	31.64
Mixed	77.5	5.09860	0.1258	42547	550	31.45
Bending	78.5	5.14739	0.1269	42729	550	31.73

The bending beam represents the more general structural reliability problem of RC structures where a ductile failure mode is expected. Typically, these include all structures where the primary flexural reinforcement start to yield and finally rupture and the moment of failure. On the contrary the shear beam represents the RC structures where the concrete properties are dominant. Typically, this category includes various examples of RC beams and slabs with expected shear and punching failures. The mixed beam represents practical RC structures in which the failure mode is unknown on beforehand. A typical example is a multi-girder bridge structure in which the individual girders are expected to have limited shear capacity and in which the joints between the girders are supposed to provide sufficient load redistribution via the other girders.

3.3.2. NUMERICAL NOISE ASSOCIATED TO THE NLFEA PREDICTION

The NLFEA solution strategy can numerically introduce pronounced noise in the capacity prediction for RC structures. This noise will result into a noisy limit state function, which may entail performance and efficiency related issue for the reliability analysis. To demonstrate this noise three stochastic cases are conceived based on the three RC beams. For these three cases the concrete tensile strength f_t, tensile fracture energy G_F and reinforcement yield strength f_y are considered random. The mean values for these parameters are already given in Table 3.1, the standard deviations are summarized in Table 3.2. The variables f_t and G_F are considered to be perfectly correlated, so that $f_t$and G_F can be described by just one random variable, u_{f_t}, in the standard normal space. The random variable f_y is considered to be independent with the other two variables. All three random variables are considered to be log-normally distributed. The limit state

function G is given by Eq.(3.1),

$$G = \frac{R_{NLFEA}}{F} - 1 \tag{3.1}$$

Table 3.2: Standard deviations of stochastic properties for the three beams considered

Case	f_t [MPa]	G_F [N/mm]	f_y [MPa]
Shear	0.8503	0.0309	30
Mixed	0.8503	0.0309	55
Bending	0.8503	0.0309	65

where R is the load capacity of the beam and F is the applied load on the beam whose value is 80 kN. The calculations are done in the standard normal space, so the variables f_t, G_F and f_y are transformed to their corresponding standard normal variables u_{f_t}, u_{G_F} and u_{f_y}. Several equally spaced points along the negative u_{f_t} axis are created for the shear and mixed beams. Along this specific direction only the concrete tensile strength f_t (along with fracture energy G_F) decreases, both of which have major influence on shear resistance. For the bending beam, the same exercise is done along the negative u_{f_y}, since reinforcement yield strength primarily governs bending failure. From Figures 3.5 and 3.6 it follows that NLFEA predictions are noisy for shear dominant (where concrete governs the failure) cases. A Gaussian process regression (GPR) is performed on the data. The noise variance of the noisy data is calculated as the mean square error, where the mean value of G at some particular value of u_{f_t} (or u_{f_y} for the bending beam) is obtained by GPR. For bending dominated cases (where reinforcement govern the failure) the NLFEA predictions fall in a relatively smooth pattern (Figure 3.7).

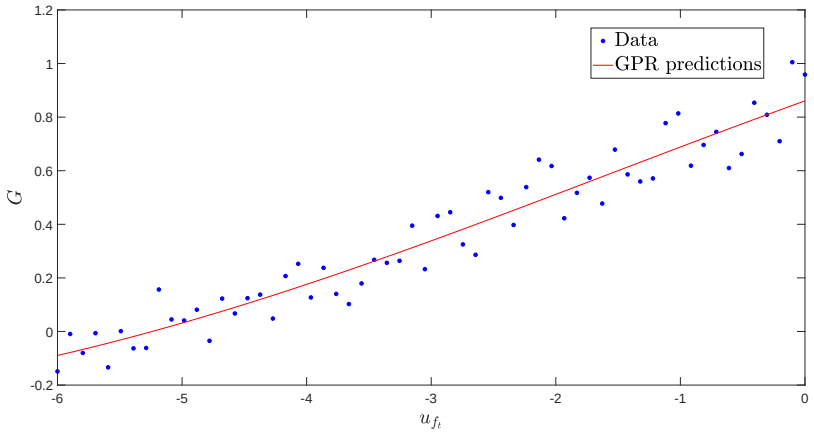

Figure 3.5: Shear beam. Noise variance is 0.0043

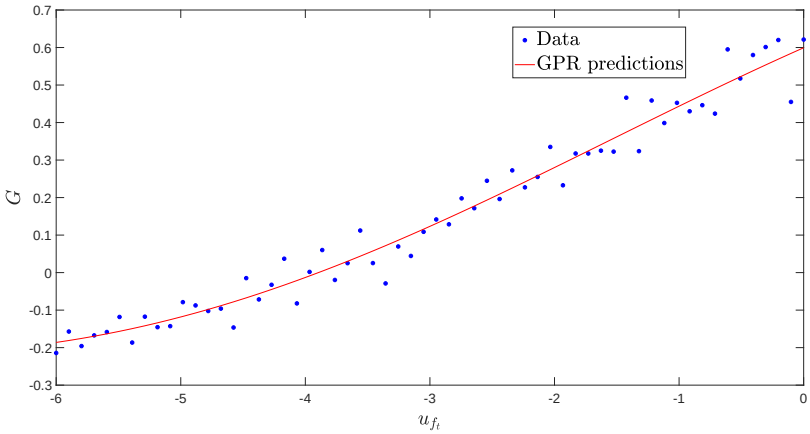

Figure 3.6: Mixed beam. Noise variance is 0.0019

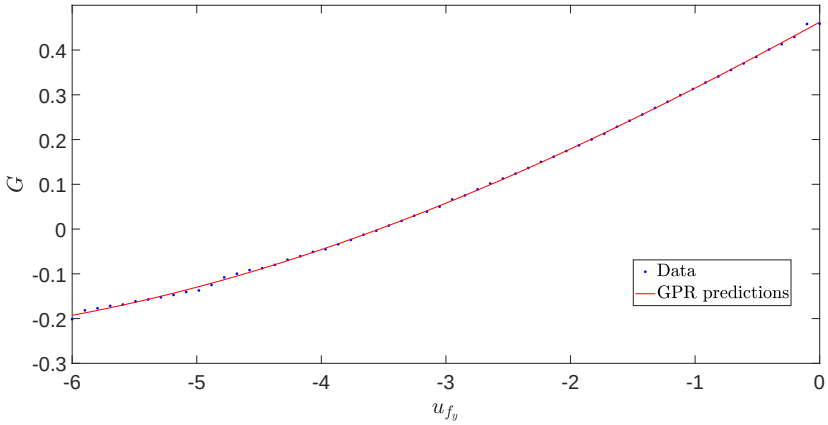

Figure 3.7: Bending beam. Noise variance is 9.66×10^{-6}

To gain further insight into the reason behind this noise in G for the shear dominated beams, several equally spaced points along the negative u_{f_t} axis are created for the shear beam and the NLFEA predicted capacities are plotted. In Figure 3.8 the capacity of the beam doesn't always decrease with decrease in f_t. The third point from the right side suddenly shows more capacity than the adjacent second point, which had lower concrete tensile strength. The displacement versus capacity comparison for these three points (in Figure 3.9) shows that the three load paths are almost coincident for the large part. This is expected, as the difference of f_t values are little for these three points. None of the three curves suddenly stop during ascendency due to non convergence. All

three of them fail in shear. The reason to why the curve with $f_t = 2.62$ would show more capacity than that of $f_t = 2.64$, lies with the plot of relative energy variation corresponding to the NLFEA iterations (Figure 3.10), for the 3^{rd} point.

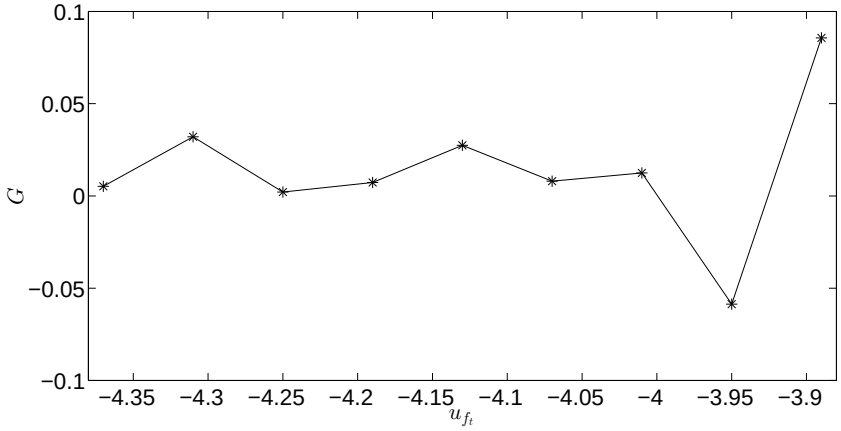

Figure 3.8: f_t vs G, along the negative u_{f_t} axis. The line search tolerance used is 0.01

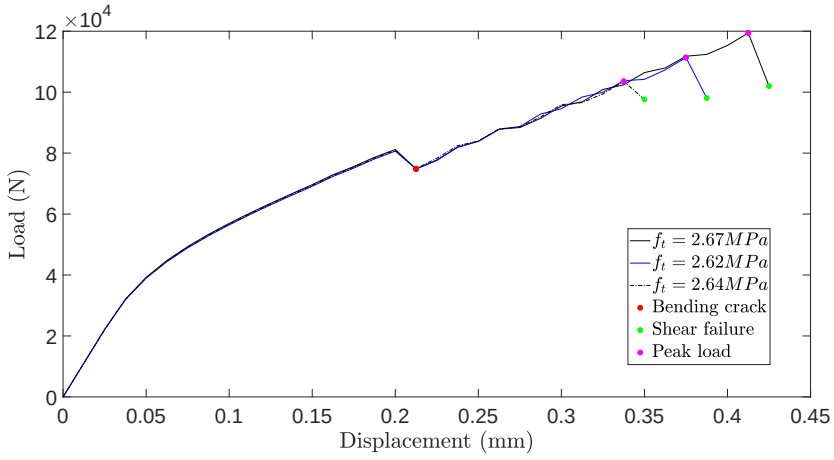

Figure 3.9: Displacement versus capacity curve for the first three consecutive points on the negative u_{f_t} axis.

A convergence criterion in a NLFEA can be a source of noise in the predicted capacity. There are several occasions in Figure 3.10 when an iteration, for a load step, almost converged. Even though small load steps are chosen, load path sensitivity cannot completely be ruled out.

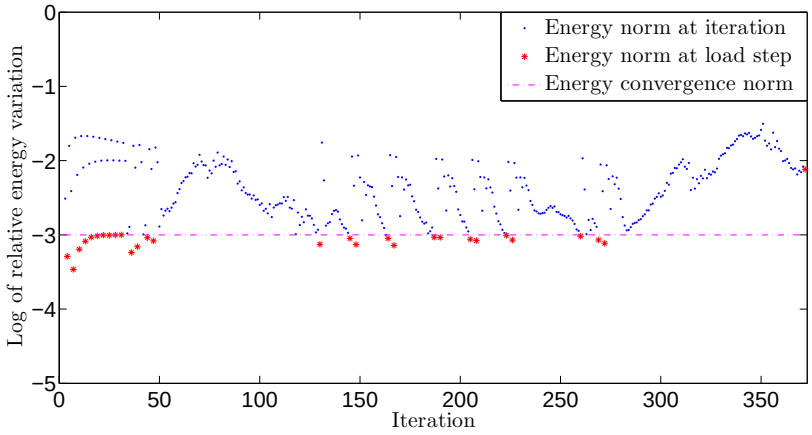

Figure 3.10: The relative energy variation with each load step during a deterministic NLFEA iterations. For this deterministic NLFEA the value $f_t = 2.62\,\text{MPa}$ is used.

3.3.3. PREDICTION OF FAILURE MODE

The failure mode predicted by NLFEA for RC structures during a reliability analysis is an object of interest in the reliability literature. The possibility that the failure mode can change between mean and design parameters, during a reliability analysis, was voiced by Schlune *et al.* [67]. It is for this reason the failure mode of the three stochastic cases at their respective design points are looked into with interest. From Figures 3.11 and 3.12 it follows that the shear beam and the bending beam fails in shear and bending respectively, as indicated by the maximum principle strain contour plots. The Mixed beam however has two design points. At the design point on the failure boundary where reinforcement yield strength f_y remains constant, the mixed beam fails in shear (Figure 3.13). The other design point, on the failure boundary where concrete tensile strength f_t remains constant, the mixed beam fails in bending (Figure 3.14). The locations of the design points in the standard Normal space for all the different failure modes are summarized in the Table 3.3.

Table 3.3: Design points for the three beams. The design point is specified both in the 2-D standard Normal space and the original Log normal space.

Beam type, failure mode	u_{f_t} [-]	u_{f_y} [-]	f_t [MPa]	G_F [N/mm]	f_y [MPa]
Shear beam, shear failure	−5.43	0	2.07	0.03	549.18
Bending beam, bending failure	0	−3.53	5.08	0.12	360.41
Mixed beam, shear failure	−3.60	0	2.77	0.05	547.27
Mixed beam, bending failure	0	−4.13	5.03	0.12	362.48

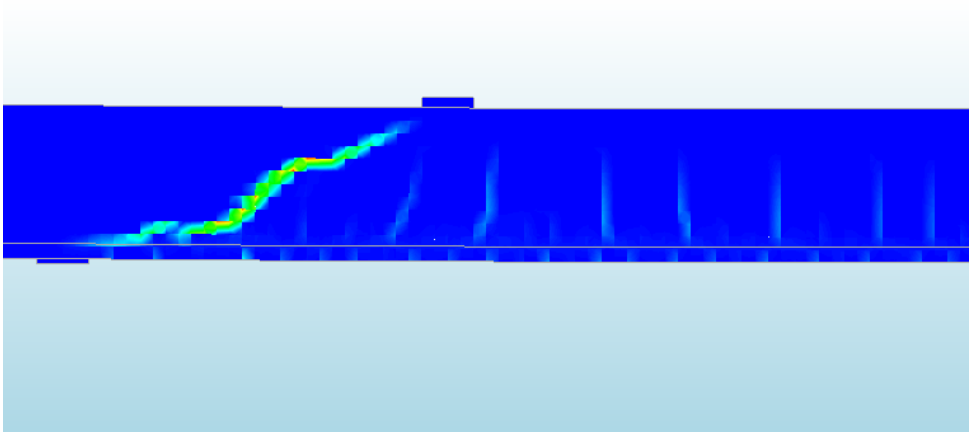

Figure 3.11: Maximum strain contour at the design point for the shear beam. The contour plot indicates shear failure.

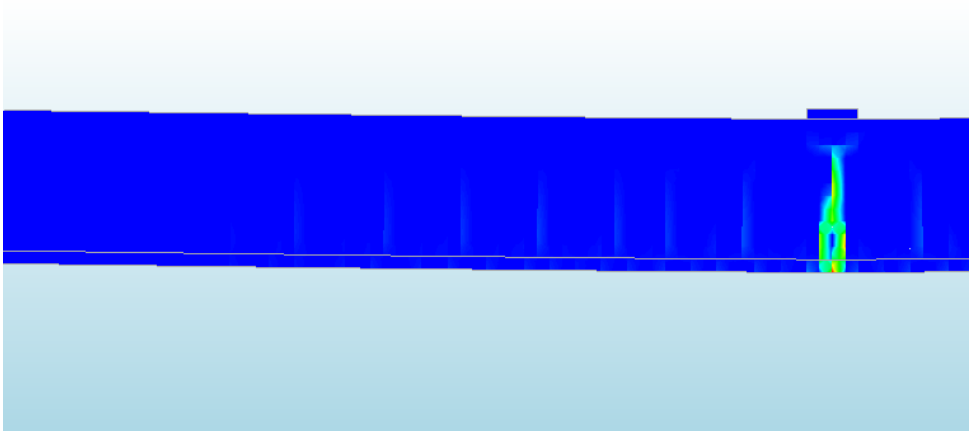

Figure 3.12: Maximum strain contour at the design point for the bending beam. The contour plot indicates bending failure.

3.4. MODELING UNCERTAINTY FOR NLFEA SOLUTION STRATEGY

The assessment of reliability of RC structures needs to incorporate the uncertainty that arises from the numerical scheme used for the analysis. If the reliability calculation of a RC structure does not account for this additional scope of uncertainty, then the estimated reliability will be incorrect.

Modeling uncertainty is a measure of discrepancy between experimentally obtained peak load and predicted peak load by FE, when the same material properties are used

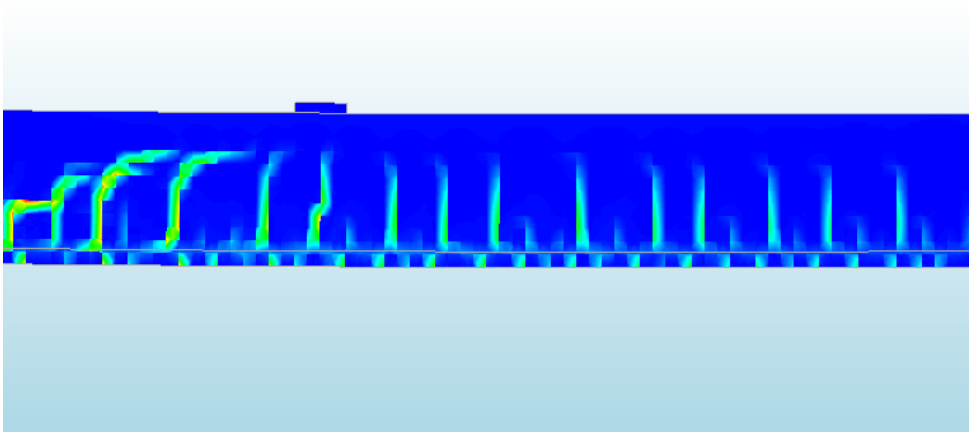

Figure 3.13: Maximum strain contour at one of the two design points for the mixed beam. This design point is on the failure boundary for which f_y remains constant. The contour plot indicates shear failure.

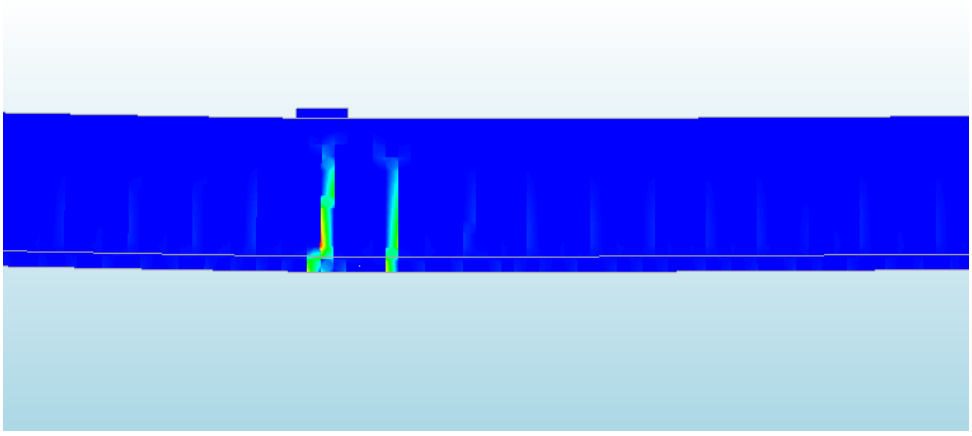

Figure 3.14: Maximum strain contour at one of the two design points for the mixed beam. This design point is on the failure boundary for which f_t remains constant. The contour plot indicates bending failure.

in both experiments and FE model. The actual load bearing capacity (experimentally obtained) R_{Exp} of a structure can be related to the predicted load bearing capacity of the structure R_{FEM} by the following relations,

$$R_{Exp} = \vartheta R_{FEM} \tag{3.2}$$

$$R_{Exp} = \vartheta + R_{FEM} \tag{3.3}$$

Among these two relations, the one given by Eq.(3.2) has been adopted in the present

report as it has been used in the reliability context by Eurocodes. Following that, the modeling uncertainty ϑ can be expressed as,

$$\vartheta = \frac{R_{Exp}}{R_{FEM}} \tag{3.4}$$

The philosophy behind multiplying ϑ with R_{FEM} follows straight from the definition of ϑ in Eq.(3.4). The idea is that each realization of the material parameters would produce a capacity prediction R_{FEM} by NLFEA, which will then be multiplied with the corresponding realization of ϑ.

The literature in the context of modeling uncertainty can be divided in two approaches [68]. In the first approach the modeling uncertainty is determined based on blind prediction contests. Several participants come with their own solution strategies and model an RC structure, whose experimental results are withheld from the participants. The ratios ϑ are calculated by each contestant based on their own respective solution strategies. From the population of different values of ϑ, the mean μ_ϑ and coefficient of variation cov_ϑ are determined. In the second approach one particular solution strategy is applied to several different RC structures of a particular type. From the population of predicted peak loads for each of these structures μ_ϑ and cov_ϑ are obtained. These two approaches are discussed in the sequel.

3.4.1. QUANTIFICATION BASED ON CONTEST

The first approach was taken by Schlune *et al.* [67]. The authors collected the results from the modeling completions for various RC structure types, grouped them according to the failure modes and computed the modeling uncertainty specific to each failure mode. Modeling uncertainty for bending failure was computed based on the round robin test of over-reinforced beams under 4-point bending [69]. Four beam types were tested, three times each. One small beam with normal strength concrete, one large beam with normal strength concrete, one beam made of high strength concrete and one beam of fiber reinforced high strength concrete. For shear type failures, the modeling uncertainty is quantified based on a competition on four different types of shear panels [70]. For shear and bending failures in slabs Jaeger *et al.* were referred [71, 72]. In these papers, the slabs without shear reinforcement failed in shear, the rest failed in bending. The beams failing in shear were not part of the investigation by Schlune *et al.* A TNO report [73] can be referred for this part, where three different types were tested for shear failure. The summary of modeling uncertainties corresponding to different failure modes are presented in Table 3.4.

One interesting observation can be made from Table 3.4. The shear failure mode consistently produces a higher coefficient of variation compared to bending. Two reasons can be identified behind this. One reason is that the shear failure is dominated by the concrete tensile strength. Whereas bending failure is often due to reinforcement yielding, so the failure is dominated by the reinforcement yield strength. The variability associated with concrete properties is higher compared to steel properties. As a result, failure modes dominated by concrete show a higher variability. Another reason is the numerical noise associated with the NLFEA prediction of shear failure.

Table 3.4: ϑ based on round robin contest

Failure mode	μ_ϑ	cov_ϑ (%)
Bending in RC beams	0.93 – 1.02	10 – 26
Bending in RC slabs	0.89 – 1.12	3 – 11
Shear in RC beams	0.77 – 1.02	21 – 42
Shear in RC panels	0.73 – 1.05	11 – 39
Shear in RC slabs	0.72 – 1.00	24 – 34

3.4.2. QUANTIFICATION BASED ON UNIFORM SOLUTION STRATEGY

The second approach of calculating the modeling uncertainty is relatively more frequent in literature. In a validation study of guidelines issued by the Dutch Ministry of Infrastructure and the Environment (also called *Dutch Guidelines*), Hendriks *et al.* [18] applied the guidelines based solution strategy to thirteen different RC structures, mostly consisting of beams and some slabs. Nygaard [60] formulated a solution strategy for RC walls based on the *Dutch Guidelines* and applied it on six different RC walls. Engen *et al.* [17] used thirty eight benchmark cases, consisting of short and slender walls, beams, deep beam and frames, to quantify the modeling uncertainty. The summary of the results is given in Table 3.5.

Table 3.5: ϑ based on single solution strategy

Contribution	μ_ϑ	cov_ϑ (%)
Hendriks *et al.*[18]	1.11	23
Nygaard [60]	1.21	6.6
Engen *et al.*[17]	1.10	10.9

The values μ_ϑ and cov_ϑ can be used directly as modeling uncertainty mean and coefficient of variation if the number of samples is high. Because high number of samples diminishes the statistical uncertainty associated with these parameters. In the case of small number of sample cases Bayesian inference has to be used in order to account for the uncertainty in the modeling uncertainty mean and coefficient of variation.

3.4.3. DISCUSSION ON THE HIGH SPREAD OF RESULTS IN SOME OCCASIONS

One interesting phenomena is the fact that some authors find large cov_ϑ for their solution strategies. Before we try to explain why that might be, it is useful to note that there is apparently no correlation between the complexity of the analytical model and the accuracy of the resulting prediction. Simple models can produce predictions that are just as good or just as bad as those arrived at by use of complex models [70]. The many diverse analytical methods available are quite sensitive to the material properties and adopted modeling techniques. While most of these methods can be vigorously defended on a theoretical basis, they do not always represent actual concrete response.
At the very outset it can be remarked that it is expected that the uncertainties of the structural response depend on whether the failure mode is governed by the concrete or the

reinforcement, and expected to be particularly high if the failure mode is governed by the tensile strength of the concrete. In fact from the work in [74] it can be concluded that resistance of reinforced concrete beams failing in bending is found to have a lower co-efficient of variation than beams failing in shear, something we observe in the results in Table 3.4 as well. But it would be interesting to know the reason for this. It is seen that if all the redistribution, i.e. the plastic dissipation, is assigned to the concrete, the structure is likely to fail in a brittle manner due to the low redistribution capacity of the concrete. The brittle failure modes governed by the concrete have a higher inherent physical uncertainty and are often more difficult to predict with a high accuracy compared to the ductile counterpart of failure modes governed by the reinforcement, which results into higher variance of reaction force for this failure mode. The modeling uncertainty of the ductile failure modes, on the other hand, have a lower contribution from physical uncertainties due to the lower physical uncertainties inherent to the reinforcement steel.

The sources for the high inherent uncertainty of the brittle failure modes are the spatial variability and the mean and standard deviation of the material properties within the concrete batch, and the correlation between the cylinder strength and other parameters of the concrete [17]. The brittle failure can be represented by a series system failure, where the minimum value (or the weakest) value of the material property governs the failure. Ductile failure on the other hand can be represented by parallel system, where the failure happens at the aggregate value of the material property. Aggregate value of a material property is less prone to statistical uncertainty compared to the minimum value. Even though these variations are not controlled in the underlying experiments, and are usually not considered explicitly in the NLFEA, they are implicitly included in the modeling uncertainty.

However, this only partly explains why shear failure modes have higher co-efficient of variation compared to the bending ones. Another possible reason is the numerical noise associated with the NLFEA prediction for shear failure, as demonstrated earlier in this chapter. Shear failure has been observed to be quite sensitive to the arbitrary choices made in the solution strategy. For example, it was seen in the Figure 3.10 that shear failure cases could be highly load path sensitive. Slight variation in the convergence criterion might produce significantly different outcome of capacity prediction. This irregular behavior of NLFEA prediction for shear failure cases can be a potential source of high co-efficient of variation.

3.4.4. CRITIC OF DIFFERENT APPROACHES TO FIND MODELING UNCERTAINTY

The accuracy of the mechanical models depends on the approximations in the numerical solution procedure and the mathematical idealization of the problem, and as such, nobody expects that the solution strategies adopted in engineering analysis will be spot on. The blind round robin prediction contests are a way to select an optimal solution strategy, where different authors came with their own solution strategies, based on their own assumptions for constitutive relations, element discretization etc. to find out which solution strategy results into the closest prediction.

It is a fact that different sets of solution strategy can result into a wide variety of predicted response, like it is seen from the prediction contests. But, then, it is also a reasonable expectation that the average of these predictions (for a specific case) might even out the

deviations and produce a response which is closer to the actual response. For example like in [70] it was observed that the average of the predicted response was within 15% of the actual response.

The concept of modeling uncertainty is associated with a model (or solution strategy). A change of solution strategy is expected to result in different parameters for the modeling uncertainty that need to be quantified. Individual modeling uncertainties can have biases, but if we take inspiration from the above discussion and obtain cumulative modeling uncertainty based on several solution strategies, then the resulting modeling uncertainty might be an even better one. In this approach, the modeling uncertainty is obtained by taking an arithmetic mean of all the $\frac{R_{Exp}}{R_{FEM}}$ ratios from different authors. It is the same as saying that all the solution strategies used are assigned equal probability, and the mean modeling uncertainty is obtained as the weighted sum (where associated probability works as weight) of all the individual means from each authors.

This is how Schlune *et al.* [75] obtained the modeling uncertainty mean and cov_ϑ, for different kind of structures. However, the weakness in Schlune's approach was that he used one type of structure, he used only one contribution from each authors to calculate the mean and cov_ϑ of the modeling uncertainty, specific to that type of structure. Even though the mean can be calculated this way, determining the standard deviation this way is perhaps not mathematically meaningful. Because this standard deviation will not represent the variability of any particular solution strategy.

Of the two approaches to modeling uncertainty described in this section, the second approach has better justification in favor of it. Because a modeling uncertainty characterizes the bias and variability of a specific solution strategy. The first approach is based on the philosophy that a cumulative modeling uncertainty based on several different solution strategies mitigates the biases of individual solution strategies. In doing so, the resulting modeling uncertainty does not represent any specific solution strategy. However, in a reliability analysis, only one particular solution strategy is used. The modeling uncertainty by the first approach may not reflect the true variability and bias associated with the solution strategy used for the reliability analysis.

3.4.5. STATISTICAL INFERENCE OF MODELING UNCERTAINTY FROM LIMITED DATA

In assessing a model, or in using a model for prediction purposes, one has to deal with two broad types of uncertainties, aleatory uncertainties also known as inherent variability or randomness and epistemic uncertainties. The former are those that are inherent in nature; they cannot be influenced by the observer or the manner of the observation. The epistemic uncertainties are those that arise from our lack of knowledge, our deliberate choice to simplify matters, from errors in measuring observations, and from the finite size of observation samples [76]. It is important to account for these uncertainties in the model prediction, particularly when the sample size is relatively small. The Bayesian updating framework is ideally suited for this purpose. In the Bayesian approach to statistics, anything unknown (like the truth of hypotheses or the values of parameters) is treated as random, and as such, is described by a probability distribution. A typical Bayesian analysis can be outlined in the following steps [77, 78]. The data is assumed to be outcomes of a random variable. First we need to formulate a probability model

for the data, i.e. the type of distribution the random variable follows. Then decide on a prior distribution, which quantifies the uncertainty in the values of the unknown model parameters (such as mean and variance) before the data are observed. Based on the data and the probability model formulated, the likelihood function is constructed. The likelihood is then combined with the prior distribution to determine the posterior distribution, which quantifies the uncertainty in the values of the unknown model parameters after the data are observed. Based on the posterior distribution, most likely value of the parameters can be estimated and predictive distribution of the random quantity can constructed. For example, let's say there are observations $x_1, x_2, \cdots, x_n$ of a random variable X. All these observations are independent of each other. Let's assume that X has a probability density function $f_X(x|\theta)$ conditioned on the unknown parameter θ. The individual observations of X can be described by independent random variables $X_1, X_2, \cdots, X_n$ all of which can be assumed to have same marginal PDFs, conditioned on θ. As all these random variables are independent, according to the multiplication theorem for independent events, the conditional density can be obtained as,

$$f_{X_1,X_2,\cdots,X_n}(x_1, x_2, \cdots, x_n|\theta) = \prod_i^n f_X(x_i|\theta) \tag{3.5}$$

The above equation can be written as,

$$L(\theta|\hat{x}) = \prod_i^n f_X(x_i|\theta) \tag{3.6}$$

where the left hand side of equation 3.6 denotes likelihood function. $\theta|\hat{x}$ signifies that $\hat{x}$ is fixed as data and it is the parameter θ which varies. Parameter values where the likelihood is high are those that have a high probability of producing the observed data. The prior distribution of the unknown parameter θ is assumed to be $f_\theta(\theta)$. Combining the likelihood with the prior density, by means of Bayes' theorem, we obtain the posterior distribution of θ conditioned on the observed data $\hat{x}$ as,

$$f_\theta(\theta|\hat{x}) = \frac{L(\theta|\hat{x}) f_\theta(\theta)}{f_X(\hat{x})} \tag{3.7}$$

The term $f_X(\hat{x}) = \int_{-\infty}^{\infty} L(\theta|\hat{x}) f_\theta(\theta) \mathrm{d}\theta$ is a constant at the time when the data is observed, so we can say that the posterior density is proportional to the product of the likelihood and the prior density,

$$f_\theta(\theta|\hat{x}) \propto L(\theta|\hat{x}) f_\theta(\theta) \tag{3.8}$$

where $f_X(\hat{x})$ is merely the required constant to normalize the product of the likelihood and prior density. It is necessary to find this constant though, because this constant makes the right hand side of Eq.(3.8) a proper PDF (which integrates to one).
We can combine the posterior density of the parameter θ and the probabilistic model for the random variable X (i.e. $f_X(x|\theta)$) to obtain the predictive distribution of X conditioned on the observed data set $\hat{x}$.

$$f_X(x|\hat{x}) = \int_{-\infty}^{\infty} f_X(x|\theta) f_\theta(\theta|\hat{x}) \mathrm{d}\theta \tag{3.9}$$

In the event of multiple models (denoted by M_k with associated parameter set θ_k), the predictive density of a random quantity X can be written as [78],

$$f_X(x) = \sum_k^m P(M_k) \int_{-\infty}^{\infty} f_X(x|\theta_k, M_k) f_{\theta_k}(\theta_k|M_k) \mathrm{d}\theta_k \tag{3.10}$$

Upon an observation x of the random quantity X, the posterior probability can be updated as,

$$P(M_k|x) = \frac{P(M_k) \int_{-\infty}^{\infty} f_X(x|\theta_k, M_k) f_{\theta_k}(\theta_k|M_k) \mathrm{d}\theta_k}{\sum_k^m P_k(M_k) \int_{-\infty}^{\infty} f_X(x|\theta_k, M_k) f_{\theta_k}(\theta_k|M_k) \mathrm{d}\theta_k} \tag{3.11}$$

and the posterior density of the parameters θ_k can be updated as,

$$f_{\theta_k}(\theta_k|M_k, x) = \frac{f_X(x|\theta_k, M_k) f_{\theta_k}(\theta_k|M_k) \mathrm{d}\theta_k}{\int_{-\infty}^{\infty} f_X(x|\theta_k, M_k) f_{\theta_k}(\theta_k|M_k) \mathrm{d}\theta_k} \tag{3.12}$$

The choice for likelihood and prior density varies from case to case. In the absence of any knowledge of the parameters, defuse priors are assumed. One such choice of defuse prior can be 1, which is also improper prior since this does not result in 1, when integrated from negative to positive infinity. The parameter X , in our case is modeling uncertainty ϑ. In the context of structural reliability, the limit state function can be expressed as,

$$G = \frac{\vartheta R_{FEM}}{F} - 1 \tag{3.13}$$

Where F is the action effect. Once we have the posterior distribution $f_\vartheta(\vartheta|\hat{\vartheta})$ we can generate samples for ϑ along with other input stochastic quantities. This posterior distribution $f_\vartheta(\vartheta|\hat{\vartheta})$ accounts for the uncertainty in the mean and standard deviation of ϑ. These samples will be useful in quantifying the reliability based on some structural reliability algorithm. Reliability analysis in this approach will account for the epistemic uncertainty associated with the mean and standard deviation of ϑ in the failure probability outcome. It can be assumed that ϑ is independent (hence un-correlated) to other input stochastic parameters (like material properties).

3.4.6. PROBABILISTIC MODELING OF MODELING UNCERTAINTY

The probability density function of modeling uncertainty ϑ, has two parameters, mean (μ) and standard deviation (σ). In the Bayesian analysis frame work, these two parameters need to be estimated, contingent on the observations. Several probabilistic models can be chosen to model the modeling uncertainty distribution, and the prior probability density of the parameters. Here we are going to discuss a few of them.

The Gaussian or normal distribution is one of the most widely used in statistics. Estimating its parameters using Bayesian inference and conjugate priors is also widely used. Conjugate prior is the one where prior and post prior distribution belongs to the same distribution family. If we assume that the standard deviation σ is known a priory, then it is only the mean that needs to be estimated based on our data set. Let's assume that the modeling uncertainty is normally distributed, $f_\vartheta(\vartheta) \propto N(\vartheta|\mu, \sigma^2)$ where σ is known.

Let's assume a conjugate prior $f_\mu(\mu) \propto N(\mu|\mu_0,\sigma_0^2)$ for the unknown μ. Here μ_0 and σ_0 are mean and standard deviation of μ. Based on Eq.(3.12) the posterior density of μ can be obtained as, $f_\mu(\mu|\hat{\vartheta},\sigma^2) \propto N(\mu|\mu_n,\sigma_n^2)$, where,

$$\sigma_n^2 = \frac{\sigma^2\sigma_0^2}{n\sigma_0^2+\sigma^2} \tag{3.14}$$

$$\mu_n^2 = \sigma_n^2\left(\frac{\mu_0}{\sigma_0^2}+\frac{n\bar{\vartheta}}{\sigma^2}\right) \tag{3.15}$$

Here $\bar{\vartheta}$ is the population (data) mean and n is the size of the data. The posterior predictive density of ϑ can be given by, $f_\vartheta(\vartheta|\hat{\vartheta}) = N(\vartheta|\mu_n,\sigma_n^2+\sigma^2)$.
If we chose to believe that both μ and σ are unknown, then we need an estimate of both these parameters based on our observations. Like before we assume that $f_\vartheta(\vartheta) \propto N(\vartheta|\mu,\sigma^2)$ but for the parameters, we assume a prior density as Normal-Inverse-Chi Squared distribution, i.e. joint density function, $f_{\mu,\sigma}(\mu,\sigma) \propto NI\chi^2(\mu_0,\kappa_0,\nu_0,\sigma_0^2)$. Here μ_0 and σ_0 are prior estimates of mean and standard deviation of ϑ, where as κ_0 and ν_0 are the measures of how strong our believe is in prior mean and standard deviation respectively. The post prior density of the parameters is estimated as, $f_{\mu,\sigma}(\mu,\sigma|\hat{\vartheta}) \propto NI\chi^2(\mu_n,\kappa_n,\nu_n,\sigma_n^2)$.
where,

$$\nu_n = \nu_0 + n$$

$$\kappa_n = \kappa_0 + n$$

$$\mu_n = \frac{\kappa_0\mu_0 + n\bar{\vartheta}}{\kappa_n}$$

$$\sigma_n^2 = \frac{1}{\nu_n}\left(\nu_0\sigma_0^2 + \sum_i(\vartheta_i-\bar{\vartheta})^2 + \frac{n\kappa_0}{\kappa_n}(\mu_0-\bar{\vartheta})^2\right) \tag{3.16}$$

The posterior mean is μ_n and the posterior variance is $\frac{\nu_n}{\nu_n-1}\sigma_n^2$. The predictive posterior distribution can be given as, $f_\vartheta(\vartheta|\hat{\vartheta}) = t_{\nu_n}(\mu_n, \frac{1+\kappa_n}{\kappa_n}\sigma_n^2)$, a non-central t distribution.

If the mean value μ is assumed to be known, then standard deviation σ needs to be estimated from the data. Like before we assume $f_\vartheta(\vartheta) \propto N(\vartheta|\mu,\sigma^2)$. For the parameter σ we can assume an inverse chi-squared prior distribution inverse $\chi^2(\nu',s')$ with prior parameters ν' and s'. Then the posterior distribution would be inverse $\chi^2(\nu",s")$ with posterior parameters $\nu"$ and $s"$ which are given by,

$$\nu" = \nu' + n$$

$$s"^2 = \frac{\nu' s'^2 + ns^2}{\nu' + n}$$

here n is the sample size and s is the sample standard deviation. With no prior knowledge, the posterior distribution will have the parameters $\nu" = n$ and $s" = s$. The predictive probability density of the modeling uncertainty is given by,

$$f_{\vartheta}(\vartheta|\hat{\vartheta}) = \frac{1}{s"\sqrt{\nu"}B(\frac{1}{2},\frac{\nu"}{2})}\left(1+\frac{(\vartheta+\mu)^2}{s"^2\nu"}\right)^{-\frac{\nu"+1}{2}} \tag{3.17}$$

While it is convenient to assume Normal distribution for the Likelihood of ϑ, literature strongly suggests use of Log-Normal distribution. The predictive density, mean and variance obtained for ϑ with normal assumption for the Likelihood, can be easily adjusted for Log normal assumption of the Likelihood. If it is indeed assumed that ϑ is Log normally distributed, then for the ease of operation ϑ is first converted into Normal distribution. The corresponding values of mean λ and and standard deviation ς in the normal space can be adjusted by the following equations,

$$\lambda = \ln(\mu) - 0.5\ln\left(1+\frac{\sigma^2}{\mu^2}\right) \tag{3.18}$$

$$\varsigma^2 = \ln\left(1+\frac{\sigma^2}{\mu^2}\right) \tag{3.19}$$

3.5. QUANTIFICATION OF MODELING UNCERTAINTY

The solution strategy tailored by Evangeliou [15] has been discussed in Section 3.3. The modeling uncertainty for this solution strategy is determined on the basis of beams tested in labs by Yang [64].

3.5.1. DESCRIPTION OF THE EXPERIMENTS

Yang *et al.* carried out a large test series in order to determine the minimum average shear stress that can cause shear failure of a specimen with different depth and concrete strength. The experiments were conducted by varying the reinforcement ratio and loading conditions. In the report, the Eurocode [79] provisions on v_{min} were discussed and compared with the test results.

The Eurocode v_{min} expression defines the shear capacity of reinforced concrete members without shear reinforcement and with relatively lower longitudinal reinforcements. This concept has been widely applied in the evaluation of the concrete slabs in buildings or bridges. It is believed that many of the bridges designed according to the old design code could not fulfill the requirements of the Eurocode, and preliminary analysis on the concrete slab bridges, according to the Dutch ministry of Infrastructure and the Environment, showed that a large amount of the slab bridges in the Dutch highway system do not have sufficient shear capacity as per the requirement outlined by Eurocode. The authors attempted to determine the actual v_{min} through experiments.

Yang *et al.* used in total 107 reinforced concrete beam specimens without shear reinforcement. All the specimens are 5000 mm long prismatic beams. The depth of the beams varied between 300 mm, 500 mm and 800 mm. Most of the specimens have the same longitudinal reinforcement in both tensile and compressive zone. The concrete cover was 25 mm. A limited number of stirrups were placed in the center and the ends

of the specimens to guarantee the anchorage and support the reinforcement cage. No shear reinforcement was present in the tested span. Five test series were planned in the research program. Within each test series, several specimens with different reinforcement configurations were casted. Of the five test series used in the experiments, the series A, B and C are of interest for this work. The differences between them are listed in Table 3.6

Table 3.6: The details of the experimental RC beams of Yang *et al.* [64]

Specimen	h mm	d mm	Concrete	Rebar mm	ρ_l
$A12$	300	265	HC	3Φ20	1.16%
$A90$	300	265	HC	1Φ12 + 2Φ20	0.90%
$A75$	300	267	HC	3Φ16	0.74%
$A60$	300	267	HC	1Φ10 + 2Φ16	0.58%
$B70$	500	465	HC	3Φ20	0.67%
$B50$	500	465	HC	1Φ16 + 2Φ20	0.58%
$C90$	300	265	LC	1Φ12 + 2Φ20	0.90%
$C75$	300	267	LC	3Φ16	0.74%
$C60$	300	269	LC	3Φ12	0.42%

Where h is height, d is the depth of the reinforcement from the top and ρ_l is the reinforcement ratio, i.e. the ratio of the area of cross section of the reinforcement and the area of cross section of the concrete beam cover. Within each test series, the reinforcement ratio of the specimens varies. For each reinforcement ratio, several tests with different shear slenderness ratio were executed. The names of the tests were defined to indicate the basic variables of the tests.

The effect of concrete strength to the shear capacity is limited. To investigate the influence of the concrete strength, a large difference of concrete strength was applied between test series A, B and C. Compressive tests and splitting tensile tests were carried out on 150 mm cubes. A summary of the concrete strengths of both mixtures is given in Table 3.7.

Table 3.7: The summary of the input parameters used in the experiments by Yang *et al.* [64]

Concrete type	High strength (HC)		Low strength (LC)	
	Strength MPa	cov	Strength MPa	cov
Compressive strength	76.67	4.34%	27.2	3.49%
Tensile strength	5.9	16.87%	2.9	4.19%

The normal ribbed bar with characteristic yield strength 500 MPa was employed in the tests, while the mean yield strength was about 550 MPa.

The target of the experimental research was to search the boundary shear stress under which the flexural shear failure occurs on the specimen while the strain of the longitudinal reinforcement approaches or reaches the yielding strain in the steel bars. Within

the test program, all the specimens were loaded by three point bending. The test series started from placing the point load at a location relatively further away from the support so that flexural failure was obtained, which is defined by the yielding of the longitudinal reinforcement. The specimen was unloaded afterward, and the point load was moved to a loading position closer to the support. The same loading procedure was repeated until flexural shear failure was obtained. The distance between two loading points was usually constant. After the shear failure was reached, the integrity of the shear span of the specimen was affected. Additional tests have to be carried out on specimens with different supporting conditions. The additional tests were executed with the point load located between the last flexural failure and the first shear failure, so that a refined critical position is obtained. The test procedure assumes that when the supporting condition does not change, and there is no clear flexural shear crack, the crack pattern of the previous test does not affect the shear capacity of the next test. Nevertheless, an additional test with the same boundary conditions were carried out, whenever possible, on un-cracked span, so that the effect of the existing cracks can be evaluated. The testing procedure was designed to ensure that as much information could be obtained from every beam. The basic assumption is that an observed onset of bending failure will not affect the results of the shear capacity once the load has been subsequently moved in the direction of the support. The other end of the beam is tested subsequently to verify this assumption by immediately applying the load at the critical loading position.

The so called flexural failure was defined by the yielding of the longitudinal reinforcement in this test program. By shear failure the authors referred to the flexural shear failure. In such failure mode, the specimen loses its capacity at the moment when unstable secondary cracks develop along the tensile reinforcement and the compressive zone. When such failure occurs, no additional test was carried out in the same span. The mixed mode is, on the other hand a failure mode between flexural failure and shear failure. With this failure mode, the yielding of the tensile reinforcement usually occurred first, meanwhile, the secondary cracks initiated at the tips of one of the flexural cracks further away from the loading point. Such failure mode typically occurs when the position of the point load is between that of a flexural failure test and a shear failure test.

3.5.2. EVALUATION OF MODELING UNCERTAINTY

The ratio $\frac{R_{Exp}}{R_{FEM}}$ has been calculated for 53 of the beam cases of Yang. The results are tabulated in the Table A.1. In that Table the specifications of each beam, such as the distance a of the loading point from the left support, depth d of the reinforcement bars from the top fiber, concrete compressive strength f_c, the diameter of the reinforcement bar, is registered. Along with these specifications the experimental capacity of the beams R_{Exp}, NLFEA predicted capacity R_{FEM} and the ratio $\vartheta = \frac{R_{Exp}}{R_{FEM}}$ are tabulated. The repeated experiments are grouped together. Modeling uncertainty is in fact itself influenced by the random material parameters. This is why it is useful to have repeated experiments, in order to uncouple the modeling uncertainty from the material uncertainty.

Due to the sufficiently large number of data Bayesian inference is not used for determining the statistical properties of ϑ from the data. The mean (0.971) and standard deviation (0.1327) for ϑ are directly found from the data set Since the ratios $\frac{R_{Exp}}{R_{NLFEA}}$ are posi-

tive quantities, it is hypothesized that ϑ for the adopted NLFEA solution strategy is Log-normally distributed. The Lilliefors test is performed to test whether the null hypothesis

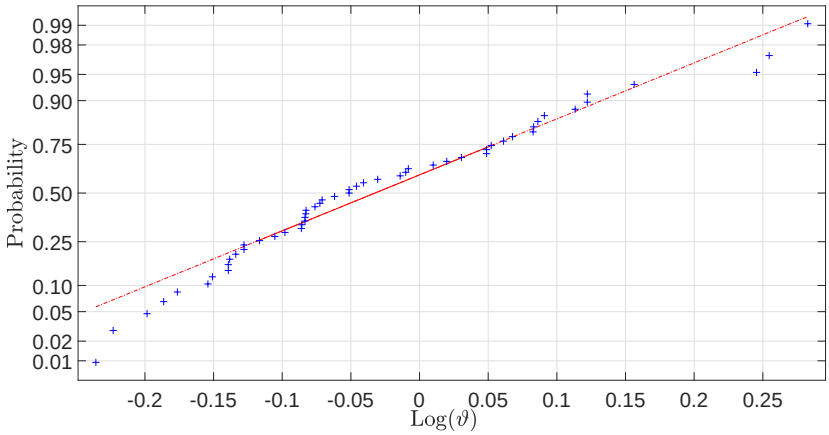

Figure 3.15: Probability plot of the logarithm of the data. The figure shows that the logarithm of the data follows Normal distribution.

that the data (for ϑ) follows Log-normal distribution is true or not. The Lilliefors test is a two-sided goodness-of-fit test suitable when the parameters of the null distribution are unknown and must be estimated. From the test the null hypothesis is confirmed with 1% confidence level. The probability plot of the logarithm of the data from Figure 3.15 also shows that the logarithm of the data follows Normal distribution. This corroborates with the Lilliefors test result.

3.6. SEMI-PROBABILISTIC VERIFICATION FROM LITERATURE

Semi-probabilistic reliability methods are often used in RC literature [80] to avoid using a large number of NLFEA. In such a semi-probabilistic reliability method it is assumed that the probability distribution of resistance is already known. In semi-probabilistic reliability method it is assumed that the probability distribution of resistance is already known. Based on this assumption it is checked whether the safety criterion, $R_d \geq F_d$ is met or not. R_d is the design resistance and F_d is the design action effect. The design resistance could be obtained by the partial safety factor method, where the representative values of the parameters (either mean or characteristic) are divided by respective safety factors (calculated based on the parameters' distribution type and coefficient of variation) to obtain the design values of those parameters. If it is assumed that the stochastic parameters are log normally distributed, then according to Eurocode 1990 [79], the design value f_{id} for the parameter f_i can be found as,

$$f_{id} = \frac{\mu_i \exp(-\alpha_i \beta_n \sigma_i - 0.5\sigma_i^2)}{\gamma_{Rd}} \tag{3.20}$$

Here α_i is the sensitivity factor of the parameter f_i, μ_i is the mean, β_n is the target reliability index and $\sigma_i = \ln(1 + cov_i^2)$ can be found from the updated coefficient of variation cov_i. γ_{Rd} is the parameter quantifying the uncertainty associated with the NLFEA model. In the partial safety factor method it is assumed that the NLFEA with design parameters as input leads to the design resistance R_d.

Another approach to find R_d is the global resistance safety factor where,

$$R_d = \frac{R_m}{\gamma_R \gamma_{Rd}} \tag{3.21}$$

here, R_m is the mean value of the resistance, which is obtained by NLFEA at the mean parameter values. γ_R is the global resistance safety factor. This expression has been prescribed by *fib* Model Code 2010 [80]. A slightly different expressions for R_d, based on mean material resistances, is given by Allaix *et al.* [81]. If the structural resistance is assumed to follow a lognormal distribution, then following Cervenka [82], we have the expression,

$$\gamma_R = \exp(-\alpha_R \beta_n cov_R) \tag{3.22}$$

where, α_R is the sensitivity factor of resistance, β_n is target reliability and cov_R is the coefficient of variation of resistance, which depends on the coefficient of variations of material, model and geometrical uncertainties. cov_R can be determined with any of the methods by Cervenka [83], Schlune *et al.* [67] or Roseblueth [84]. The use of the partial safety factor approach is better suited for member level safety evaluation. Global resistance safety factor approach on the other hand is applicable to the safety evaluation at the system level, which automatically takes into account the interactions of different parts of the whole structural system [2].

The semi-probabilistic reliability methods require only few NLFEA. Their efficiency makes them attractive methods. However, the underlying assumptions which go into these approaches are might produce conservative estimates of the reliability. For example, the values of influence coefficients (α_i) in partial safety factor approach, are assumed to be 0.8 for dominating and 0.32 for non-dominating parameters [85].These values are prescribed based on calibration. Moreover, semi-probabilistic methods disregard correlations between the input random variables, which may have significant influence on the outcome. In order to confirm whether semi-probabilistic methods produce conservative estimates of safety, it is necessary that the performance of semi-probabilistic safety formats are compared with a NLFEA based full probabilistic reliability method at member level.

3.7. CONCLUDING REMARKS FOR THE THIRD CHAPTER

The NLFEA solution strategies for the RC structures are reviewed in this Chapter. A solution strategy is adopted based on the review. The test cases, three RC beams, one failing in shear one in bending and one in mixed mode, are selected in this Chapter. These beams will serve as the subject of demonstration in the coming Chapters. The numerical challenges associated with NLFEA solution strategies are demonstrated in this Chapter. It is seen, that the shear beam has a pronounced noisy limit state function, where as the bending beam has a relatively smooth limit state function. It is also seen that the mixed

beam has two design points, one leading to a bending failure another leading to a shear failure.

The modeling uncertainty pertaining to the adopted solution strategy is determined based on experimental results. Two approaches to finding modeling uncertainty are reviewed. The approach where the modeling uncertainty for an NLFEA solution strategy is determined based on the results for several RC structures, is adopted in this thesis. Due to the relatively large number of data set Bayesian updating method is not used, because with large number of data the statistical uncertainty for the stochastic parameters, mean and standard deviation, diminishes significantly. Instead the mean and standard deviation for ϑ are calculated directly, while assuming that ϑ follows a Log-normal distribution.

It can be questioned whether the choice of combining the data for all failure modes to calculate the modeling uncertainty is justified or not. Because the standard deviation of ϑ would be much larger for shear failure than for flexural failure. A different modeling uncertainty parameter ϑ for each failure mode would have been more reasonable. However, the data for all failure modes were combined (to obtain a single ϑ) from the sake of simplifying the reliability analysis. Because if different modeling uncertainty parameters were used for different failure modes, then all those different modeling uncertainty parameters have to be used as separate random variables. During the reliability analysis, for a particular realization, whenever the structure fails in some failure mode, only the corresponding modeling uncertainty realization would be used to produce the value of the limit state function. This approach has the practical difficulty that during a reliability analysis failure mode needs to identified quantitatively for each of the NLFEA, from one realization to another. One possibility is to measure the Ductility index, introduced by Engen *et al.* [17], for each NLFEA of RC structure. The Ductility index quantitatively determines whether the failure is brittle or ductile in nature. Such approach is not considered in this thesis however.

4

RELIABILITY ANALYSIS OF A RC BEAM FAILING IN SHEAR BY A DARS METHOD, ACCOUNTING FOR MODELING UNCERTAINTY

4.1. INTRODUCTION

THE limited examples of available literature on NLFEA based full probabilistic reliability study of RC structure is lacking in one major aspect. In none of these works the modeling uncertainty associated with a NLFE model has been accounted for. A finite element model of a structure is an abstraction of the physical structure with a number of assumptions, generalizations, and idealizations. In NLFEA the process of abstraction from the structure to the mechanical model, and then the abstraction from the mechanical model to the finite element model, introduces a potential for significant uncertainties. The assessment of reliability of RC structures needs to incorporate the uncertainty that arises from the numerical scheme used for the analysis. This uncertainty, termed as modeling uncertainty in literature, was quantified in the previous chapter based on experimental results of 53 benchmark cases [64].

In this chapter the reliability of RC beams has been investigated with one of the important sampling methods, called directional adaptive response surface (DARS) method. The specific implementation of DARS with commercial FE package DIANA [61] has been validated with a couple of simple test problems. The test problems were chosen such that they had reference reliability results with Monte Carlo analysis. Then a case study, a RC beam failing in shear, is chosen. The NLFE solution strategy for RC beams have been formulated following the guidelines issued by Dutch Ministry of Infrastructure and the Environment [18]. Along with material parameters, the modeling uncertainty associated with the solution strategy is used as an additional random variable in this work. The

spatial variability of the random variables is ignored in this work, i.e., only the random variable method is used. Sensitivity analysis with FORM on the final response surface obtained from DARS, is performed to obtain the sensitivity factors α_i for each random variables. These factors give a quantitative measure of the relative importance of the random variables.

4.2. VALIDATION OF THE SPECIFIC IMPLEMENTATION OF DARS

The algorithm of DARS has been discussed in the Chapter 2. The specific implementation of DARS in the commercial FE package DIANA has been validated based on three test cases. For these simple test cases the limit state functions are available in analytical form. This makes reliability analysis by means of Monte Carlo simulation possible, which is used as benchmark for comparison. The relative simplicity of the test cases also allow the opportunity to study the effects of three parameters used in DARS and critically asses their appropriate values. Two of the parameters, λ_{add} and tol, have been introduced in subsection 2.3.8. The third parameter is the threshold coefficient of variation of the failure probability estimator P_f (from Eq.(2.75)), cov_{P_f}.

4.2.1. THE TEST PROBLEMS

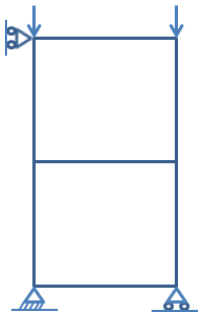

Figure 4.1: Two concrete element under compression

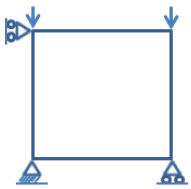

Figure 4.2: A single concrete element under compression

As test cases, a two element model (one concrete element on top of the other, Figure 4.1) and a single element model (Figure 4.2) have been chosen. The dimension of each element is $100 \times 100 \times 300\,\text{mm}^3$ where 300 denotes the thickness of the plane stress

element. The compressive strengths of the two elements in Figure 4.1, f_{c1} for the top element and f_{c2} for the bottom element are the two stochastic quantities. The single element (Figure 4.2) has a compressive strength f_{c2}. The modeling uncertainty ϑ is also an input stochastic variable for some cases. In total three cases are considered. Table 4.1 lists the random variables for each case. The schematizations should be conceived as academic test cases in which we can also study the numerical process. It is not the intention that these should represent detailed analyses of compressive tests, which would require more thought on the boundary conditions and the required FEM discretization.

Table 4.1: Input random variables

Cases	f_{c1}	f_{c2}	ϑ	Structure
First	random	random	-	Figure 4.1
Second	-	random	random	Figure 4.2
Third	random	random	random	Figure 4.1

The modeling uncertainty ϑ is included just for the sake of demonstration. The summary of all the input random variables for these three cases is given in Table 4.2. All the random variables are considered to be independent.

Table 4.2: Input random variables

Stochast.	Distribution	Mean	Std.
ϑ	Normal	1	0.1
f_{c1}	Normal	60 MPa	9 MPa
f_{c2}	Normal	30 MPa	4 MPa

The NLFEA solution strategy, common for all three test cases, is different compared to the one that is specific to RC beams. The solution strategy chosen for the test cases is specific for compressive loading. A parabolic stress strain behavior has been chosen for concrete in compression. A deterministic value of compressive fracture energy of $G_c = 11.037\,\text{N/mm}$ is selected. A displacement controlled compressive load has been applied in 170 load steps. The load increment in each step is 0.004 mm. The regular Newton Raphson method is used for solving the system of nonlinear equations. A force convergence norm is used as a convergence criterion for the equilibrium iterations, as force equilibrium is better satisfied with a force norm.

The total load bearing capacity in analytical form for the first and third case is $A_c \min(f_{c1}, f_{c2})$ and for the second case it is $A_c f_{c2}$. $A_c = 100 \times 300\,\text{mm}^2$ is the cross section area. The limit state function has been defined based on the total support reaction force R. As force on the structure $F = 200000\,\text{N}$ is considered for all three cases. So, for the first case the analytical limit state function G_A is,

$$G_A(f_{c1}, f_{c2}) = \frac{A_c \min(f_{c1}, f_{c2})}{F} - 1 \tag{4.1}$$

and the corresponding FE based limit state function G is denoted as,

$$G(f_{c1}, f_{c2}) = \frac{R(f_{c1}, f_{c2})}{F} - 1 \tag{4.2}$$

Similarly, for the second case,

$$G_A(f_{c2}, \vartheta) = \frac{\vartheta A_c f_{c2}}{F} - 1 \tag{4.3}$$

$$G(f_{c2}, \vartheta) = \frac{\vartheta R(f_{c2})}{F} - 1 \tag{4.4}$$

and for the third case,

$$G_A(f_{c1}, f_{c2}, \vartheta) = \frac{\vartheta A_c \min(f_{c1}, f_{c2})}{F} - 1 \tag{4.5}$$

$$G(f_{c1}, f_{c2}, \vartheta) = \frac{\vartheta R(f_{c1}, f_{c2})}{F} - 1 \tag{4.6}$$

Note that for the second and third case that, even though G is function of all three random variables, the modeling uncertainty ϑ does not enter the nonlinear finite element analysis to calculate R. However, ϑ is used as a base variable to construct the response surface to approximate G. Also note that, the reliability calculations are not done in the space of original random variables. The random variables are transformed into independent standard normal variables, with 0 mean and standard deviation 1. The variables f_{c1}, f_{c2} and ϑ are transformed into $u_{f_{c1}}$, $u_{f_{c2}}$ and u_ϑ respectively in the standard normal space. The response surface is then fitted in the space of standard normal variables.

4.2.2. STUDY OF THE PARAMETERS cov_{P_f}, λ_{add}, tol

The accuracy of the result of DARS is directly influenced by the number of sampled directions and line search convergence criterion tol. The line search convergence criterion has been defined as $\left|\vartheta\frac{R}{F} - 1\right| \leq tol$ (ϑ to be ignored when it is not an input random variable). The parameter λ_{add} also has an influence on the outcome. While it is intuitively understood that a larger number of sampled directions would increase the accuracy of the reliability analysis, the price paid in terms of computational cost puts a prohibitive limit on sampling large number of directions. A compromise, balancing in terms of acceptable accuracy and viable amount of computation, has to be reached. The acceptable degree of accuracy is a more involved question however. In most cases it is unlikely that the limit state function would be available in analytical form. So, it would be impossible to know the actual reliability with Monte Carlo simulation, which could have served as a reference. There needs to be some indirect measure of accuracy, which can be used as a criterion to stop sampling directions, as soon as that criterion is met. cov_{P_f} is used as such criterion for DARS. From Eq.(2.75) it is seen that failure probability P_{fi} for i^{th} sampled direction is dependent on λ_i. For large numbers of sampled directions, the important directions will band together around the nearest region of the limit state surface from the origin, resulting in relatively low variability among the corresponding distances λ_i to the origin. Consequently, the corresponding failure probabilities, P_{fi},

will also have less variability. This is the rational behind choosing the coefficient of variation of P_f, cov_{P_f} as a stopping criterion for sampling directions. In each iteration of DARS directions are sampled until the value of cov_{P_f} becomes less than or equal to a user prescribed threshold value. By the end of the last iteration many of the sampled directions, which started out unimportant in the first iteration, will turn out to be important, yielding a substantial value of associated P_{fi}. As a result the final variability of P_f will be lower compared to the first iteration.

As a measure of confidence on the procedure, a confidence interval has been constructed based on the variability of P_f. If P_f from Eq.(2.75) is the estimator of failure probability with standard deviation σ_{P_f}, then for a given confidence level of γ the confidence interval would be,

$$P_f - Z_\gamma \frac{\sigma_{P_f}}{\sqrt{N}} \leq P_f \leq P_f + Z_\gamma \frac{\sigma_{P_f}}{\sqrt{N}} \tag{4.7}$$

where,

$$Z_\gamma = \Phi^{-1}\left(\frac{\gamma+1}{2}\right) \tag{4.8}$$

Φ is the CDF of the Normal distribution. This interval is the range in which the failure probability is expected to belong. γ is the probability that DARS would be able to produce a failure probability within this bound. When no reference result for $P_f$is available, the length of confidence interval gives an extra measure of how trustworthy the estimate of P_f is. To study the performance of cov_{P_f} as a threshold criterion of sampling, P_f has been plotted against varying cov_{P_f}, along with confidence interval and number of required NLFEA, for all the three test cases in Figures 4.3, 4.4 and 4.5. A confidence level of 95% (or $\gamma = 0.95$) is used. The reference P_f by Monte Carlo simulation have been indicated with horizontal dashed lines. $\lambda_{add} = 1$ and $tol = 0.01$ have been assumed for this study.

Some discussions are in order regarding the appropriate choice of cov_{P_f}. The Eurocode [79] recommends a $\beta = 3.8$ for a 50 years reference period for the ultimate limit state of ordinary structures. Based on this recommendation Waarts [14] worked out that a convergence criterion of $cov_{P_f} = 0.57$ would be sufficient to ensure with 95% confidence that the error in β is within acceptable limit of 8% error in the estimation of β. This was shown in [14] to lead to enough accuracy for practical structural engineer problems in relation to safety classes defined in [79].

For the first and second case, cov_{P_f} has been varied from 0.2 to 0.45 in steps of 0.05. For the third problem however, the range of cov_{P_f} considered was $0.3 - 0.55$, as DARS failed to achieve a cov_{P_f} lower than 0.25 with in 300 sampled directions.

From Figures 4.3, 4.4 and 4.5 it follows that for all three cases, the difference of P_f by DARS with the reference value (by MCS) increases as cov_{P_f} increases. In these figures the mean value(s) of the P_f, corresponding to each cov_{P_f} are marked with a star $(*)$, which appears exactly at the midpoint of each of these confidence interval lines (vertical blue lines). The corresponding number of NLFEAs are also indicated along side the confidence intervals. One thing to notice in these examples is that there is significant bias in the estimate of mean failure probability P_f, compared to the reference value (obtained with MCS), when the target cov_{P_f} is relatively higher. For example, $cov_{P_f} = 0.45$ produced the highest bias in the estimate of P_f in all the three examples, and at $cov_{P_f} = 0.2$

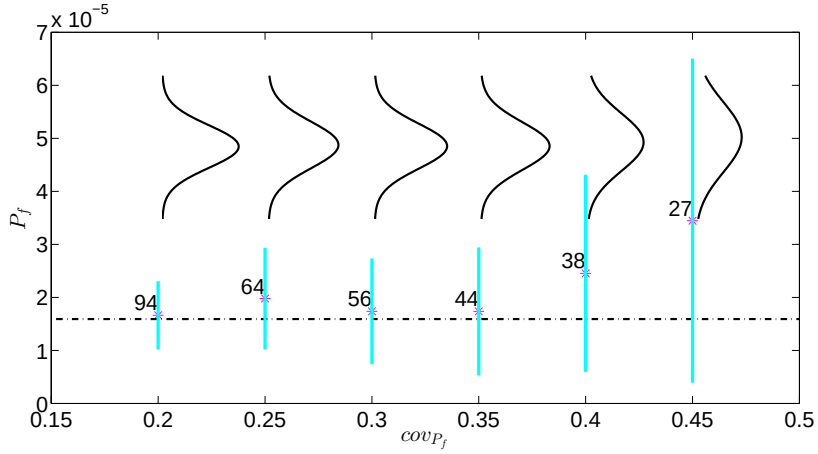

Figure 4.3: First case: Random f_{c1},f_{c2}. cov_{P_f} vs P_f: $\lambda_{add} = 1$ and $tol = 0.01$

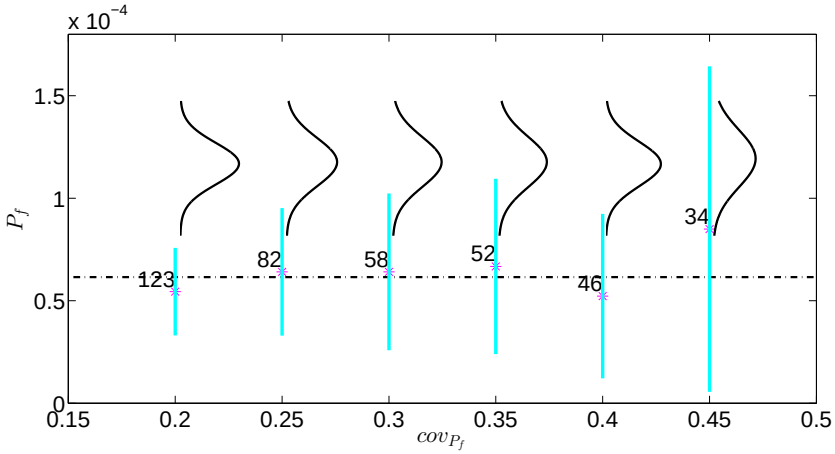

Figure 4.4: Second case: Random f_{c2}, θ. cov_{P_f} vs P_f: $\lambda_{add} = 1$ and $tol = 0.01$

the estimated P_f almost matched the reference value by MCS. The explanation is that the total number of randomly sampled directions decreases with the increase in cov_{P_f}. This can make the failure probability estimator, P_f, biased for larger value of cov_{P_f}. Low sampling density also increases the standard deviation σ_{P_f}. This fact is attested by the distributions of P_f (which is Normally distributed), given against cov_{P_f} for all three problems as inset. Consequently, according to the expression of Eq.(4.7), the confidence interval (for a confidence level $\gamma = 0.95$) increases with increasing cov_{P_f}.

One interesting observation from the Figures 4.3, 4.4 and 4.5 is that the confidence interval shrinks much more rapidly when the value of cov_{P_f} is higher. But as the value

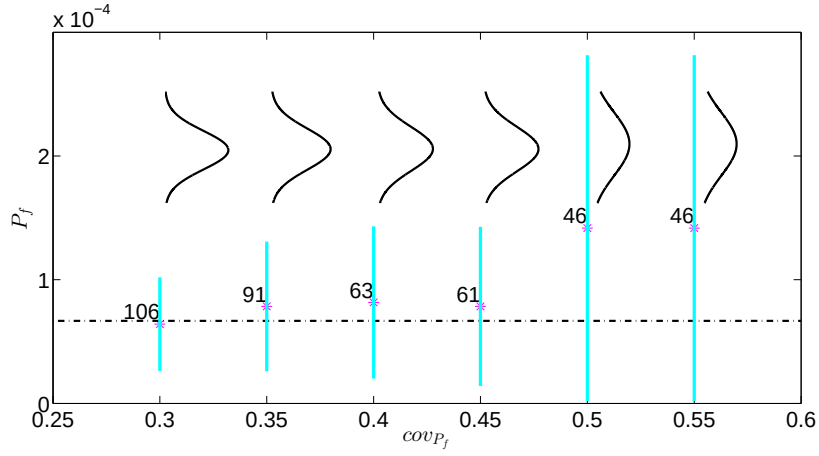

Figure 4.5: Third case: Random f_{c1}, f_{c2}, ϑ. cov_{P_f} vs P_f: $\lambda_{add} = 1$ and $tol = 0.01$

of cov_{P_f} reduces, the width of the confidence interval does not decrease as drastically (for example, at $cov_{P_f} = 0.25$ and $cov_{P_f} = 0.2$). It suggests that lowering the cov_{P_f}, and thereby increasing the sampling density beyond a certain level, the obtained information about the failure probability through directional simulation does not differ significantly. It can be argued that too small cov_{P_f} unnecessarily increases the number of (exact) simulated directions around the important region of the limit state surface, without adding any additional information.

To study the influence of λ_{add} and tol on the reliability analysis, $cov_{P_f} = 0.4$ for the first case and $cov_{P_f} = 0.45$ for the second and third problem have been selected.

The entity $\beta = \Phi^{-1}(P_f)$, the number of NLFEA and the number of sampled directions are plotted against λ_{add} and tol for all three problems, to see what influence these two parameters have on the reliability analysis. From Figures 4.6, 4.7 and 4.8 it follows that the test cases the β doesn't depend on λ_{add}, as for a given value of tol β doesn't change along the λ_{add} axis. Also, beyond $tol = 0.1$ for first problem (Figure 4.6) and $tol = 0.01$ for second and third problem (Figure 4.7 and Figure 4.8), β remains constant along the tol axis. The number of NLFEA however, as can be seen from Figures 4.9, 4.10 and 4.11, depends on λ_{add} and tol. So for these test cases the λ_{add} doesn't influence the accuracy of the reliability analysis, but it certainly influences the computational effort, for the simple cases considered in this section.

In light of the discussion of the DARS procedure in Section 2.3.8, it can be said that a large λ_{add} improves the possibility of finding an important direction, by relaxing the criterion of deciding whether a direction is important or not. This is particularly useful when the limit state surface has uneven fluctuations. But a too large λ_{add} would mean that a larger number of directions would be deemed as important, thereby increasing the total number of NLFEA. But many of these directions will actually be further from the important region and contribute insignificantly to the P_f (or to $\beta = \Phi^{-1}(P_f)$). This

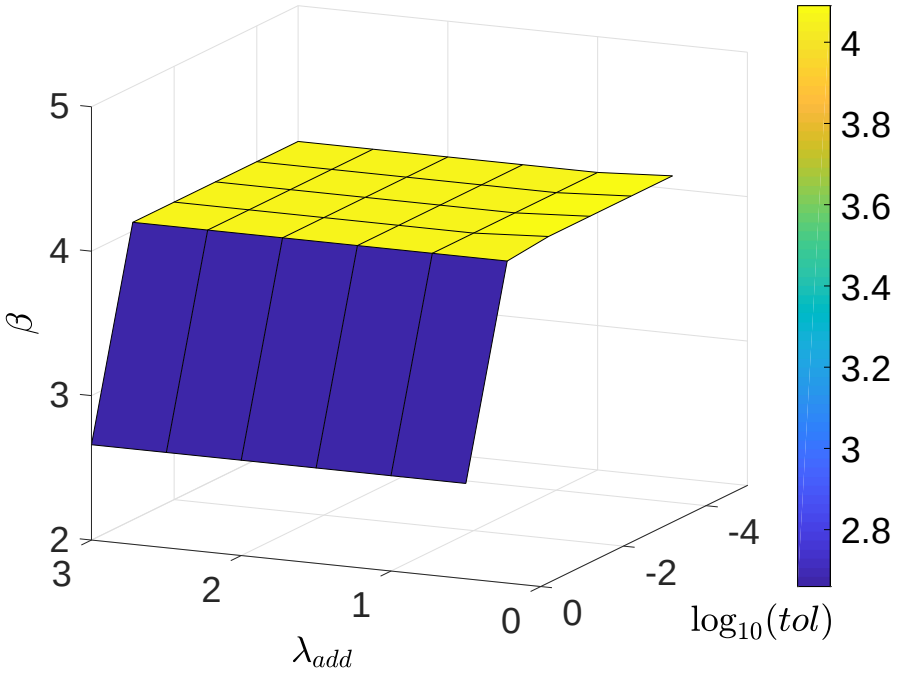

Figure 4.6: First case: Random f_{c1},f_{c2}. λ_{add} and $\log_{10} tol$ vs $\beta = \Phi^{-1}(P_f)$: $cov_{P_f} = 0.4$

Table 4.3: Reliability results of the test problems with DARS

Case	cov_{P_f}	λ_{add}	tol	Directions	G^*_{NLFEA}	NLFEA	λ_{min}	β	β_{Ref}
First	0.4	2	0.01	33	10	30	4.17	4.06	4.16
Second	0.45	1	0.01	24	7	34	3.88	3.76	3.84
Third	0.45	1	0.01	80	13	61	3.88	3.78	3.82

notion is supported by Figures 4.12, 4.13 and 4.14 where it can be seen that the number of sampled directions does not increase with increasing λ_{add}. A too small λ_{add} however might discard nearly all directions as un-important, resulting in a slow update of the response surface, requiring a lot of iterations and hence, increasing the number of NLFEA. Depending on the nature of of the limit state surface, there can be an optimum λ_{add}, as is the case in Figure 4.9, where the number of NLFEA is lowest at $\lambda_{add} = 2$ for a tol less than 0.1. tol acts as a termination criterion of line search. While it is desired to get as close as possible to the limit state surface, a too tight tol will not contribute significantly to the accuracy of the analysis beyond a certain value, except increasing the computational cost. Also, the limit state surface, which is defined based on capacity estimates by

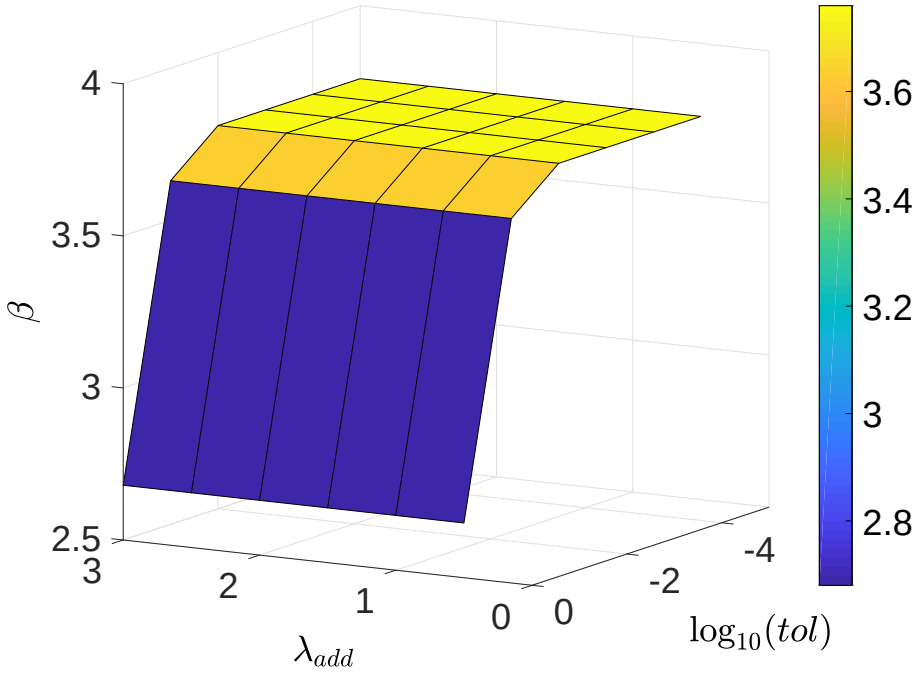

Figure 4.7: Second case: Random f_{c2}, ϑ. λ_{add} and $\log_{10} tol$ vs $\beta = \Phi^{-1}(P_f)$: $cov_{P_f} = 0.4$

NLFEA, is itself not exact. Because NLFEA uses a convergence criterion of its own. So, it will not be meaningful to try to satisfy the limit state equation exactly.

4.2.3. COMPARISON AGAINST REFERENCE RESULTS

With appropriate choices of cov_{P_f}, λ_{add} and tol in due consideration of accuracy and computational effort, the reliability results for the three problems are summarized in Table 4.3. The β is defined as $\beta = \Phi^{-1}(P_f)$, where P_f is the failure probability from Eq.(2.75). β_{ref} denotes the reference value found by Monte Carlo, by $\beta = \Phi^{-1}(P_{ref})$. P_{ref} is the failure probability by Monte Carlo. The reference results have been generated by Monte Carlo simulation on the analytical limit state functions. The number of samples for the Monte Carlo is selected based on the criterion, $N \geq \frac{1}{cov^2_{P_f}}(\frac{1}{P_f} - 1)$. A target $cov_{P_f} = 0.1$ and an expected P_f in the order of 10^{-5} is used in this criterion to determine the minimum number of required Monte Carlo samples (10^7) for all three cases. It should be mentioned that based on this target $cov_{P_f} = 0.1$ the required number of samples in MCS can be determined dynamically during the MCS. However, the purpose of this exercise here is not to compare the efficiency of DARS against MCS, but rather obtaining a reference value in order to verify the accuracy of DARS results. That's why 10^7 samples are

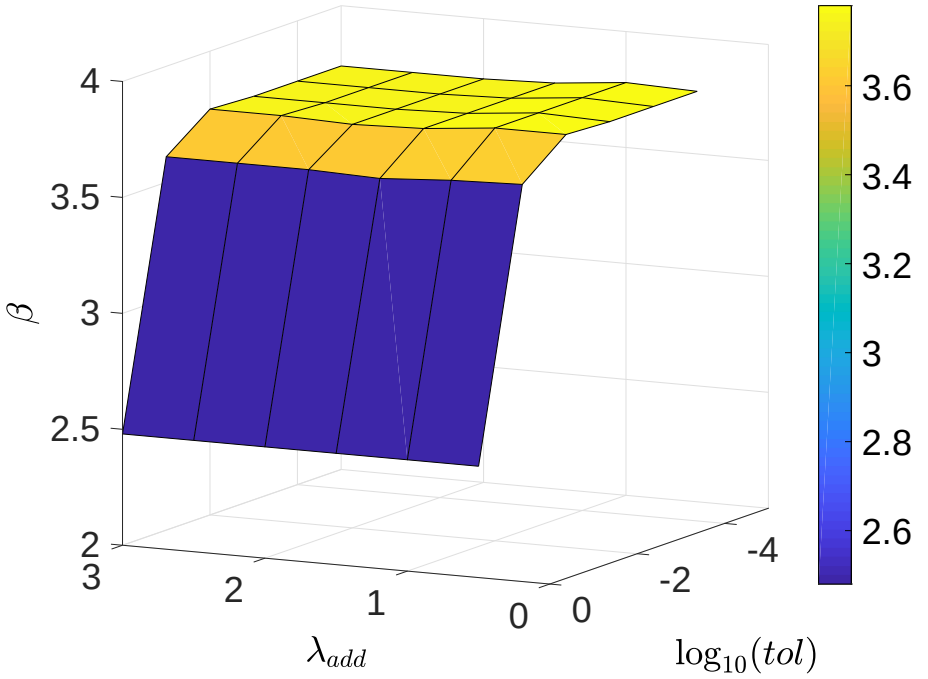

Figure 4.8: Third case: Random f_{c1}, f_{c2}, ϑ. λ_{add} and $\log_{10} tol$ vs $\beta = \Phi^{-1}(P_f)$: $cov_{P_f} = 0.4$

used. The λ_{min} denotes the minimum distance, obtained by DARS, from the origin to the limit state surface. DARS manages to produce β values which are reasonably close to the reference results for all the cases. The $G = 0$ and the final $\hat{G} = 0$ are plotted along with directions (important or otherwise) in Figures 4.15 and 4.16 for first and second case respectively. For the third case, only the $\hat{G} = 0$ is plotted to increase the visibility (Figure 4.17).

The intersection points of the $G = 0$ hyperplane with the important directions and $\hat{G} = 0$ with un-important directions have been denoted with G^*_{NLFEA} and G^*_{RS} respectively throughout this thesis. Along the important directions, the line search interim points are denoted by G_{NLFEA}. The G^*_{NLFEA} point with minimum distance λ_{min} from the origin to $G = 0$, is considered to be the design point obtained by DARS.

From Figures 5.1 and 5.2 it can be seen that the final $\hat{G} = 0$ coincides with $G = 0$ in the most important region (in the vicinity of the design point) of $G = 0$. For the first problem the analytical limit state surface consists of two half lines in the space of the standard Normal space as,

$$\begin{aligned} u_{f_{c1}} &\geq -5.22 \\ u_{f_{c2}} &\geq -4.25 \end{aligned} \tag{4.9}$$

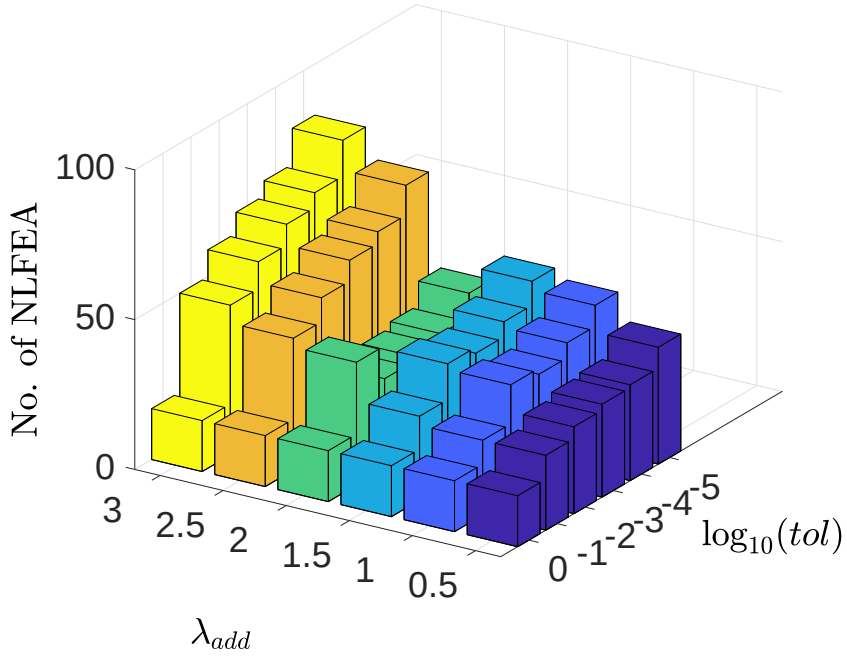

Figure 4.9: First case: Random f_{c1},f_{c2}. λ_{add} and $\log_{10} tol$ vs No. of NLFEA: $cov_{P_f} = 0.45$

Table 4.4: The design point and λ_{min} for the first and second case

Method	First case			Second case		
	$u_{f_{c1}}$	$u_{f_{c2}}$	λ_{min}	$u_{f_{c2}}$	u_ϑ	λ_{min}
FORM	0	−4.25	4.25	−3.49	−1.68	3.88
DARS	0	−4.17	4.17	−3.53	−1.61	3.88

For the second problem, the analytical limit state surface in the standard normal space is,

$$15000(0.1u_\vartheta + 1)(4u_{f_{c1}} + 30) - 200000 = 0 \tag{4.10}$$

the design point for the first and second problems can be obtained by FORM analysis on Eq.(4.9) and Eq.(4.10). The result compares reasonably well with the design point and λ_{min} obtained by DARS (Table 4.4).

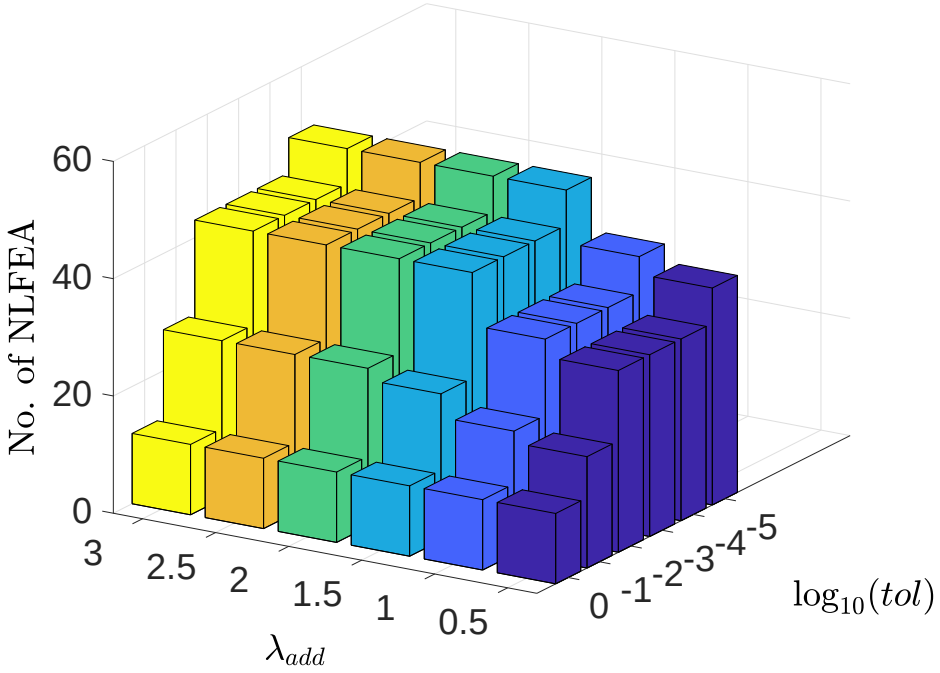

Figure 4.10: Second case: Random f_{c2}, ϑ. λ_{add} and $\log_{10} tol$ vs No. of NLFEA: $cov_{P_f} = 0.45$

4.3. CASE STUDY: BEAM FAILING IN SHEAR

In the previous section the simple test cases had relatively smooth limit state surfaces. The shape of the limit state functions of actual structures may be more complicated and irregular compared to those simple problems. Waarts [14] applied DARS on a number of structures, which are typical of civil engineering practice. He compared those results with other methods for accuracy and efficiency. But even those structures were so chosen such that the finite element part was relatively simple and the limit state functions were relatively well behaving. When it comes to DARS reliability analysis of RC structure, there is a paucity of demonstrative examples in literature. NLFEA based reliability analysis of RC structures with DARS has several critical elements of its own, which will be studied in detail in Section 4.3.1. Among the several RC beams experimentally studied by Yang *et al.* [64], a beam A122A1 (Figure 3.2) which failed in shear in the experiment, has been selected for a case study. In the experiments stirrups were also part of the beam configuration, which is not used in this work. The stochastic properties are obtained from Yang *et al.* and Wiśniewski *et al.* [65] (summarized in Table 4.5). The model uncertainty ϑ has been quantified from the 53 experimental beams considered by Yang *et al.* Given the large number (53) of benchmark cases, Bayesian inference is not used. All the stochastic variables for this beam, including ϑ, are properties which cannot have

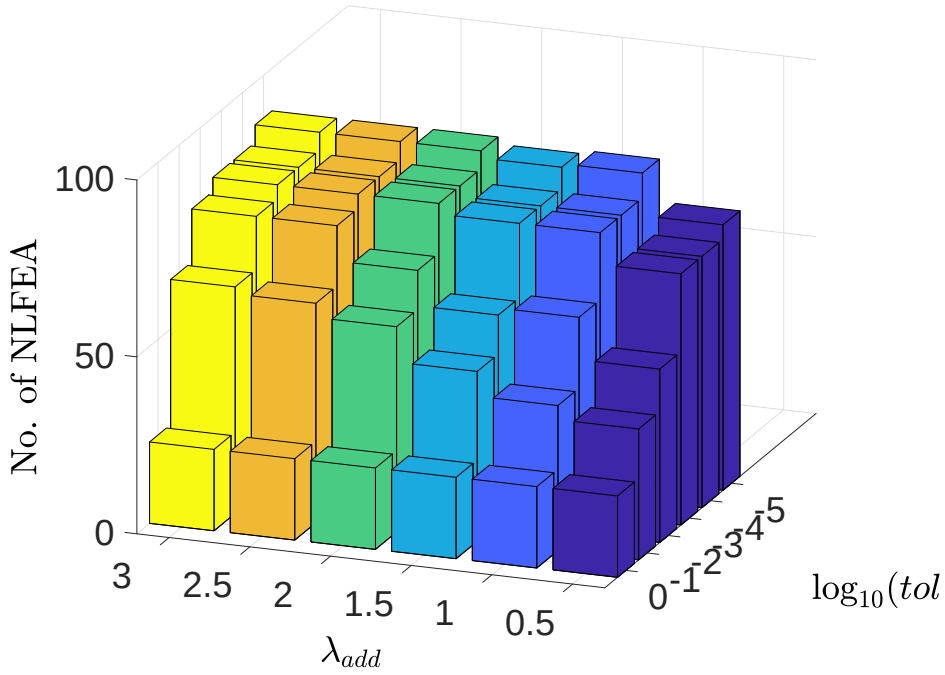

Figure 4.11: Third case: Random f_{c1}, f_{c2}, ϑ. λ_{add} and $\log_{10} tol$ vs No. of NLFEA: $cov_{P_f} = 0.45$

negative values. Therefore, they are assumed to follow Log-normal distribution.

Table 4.5: Stochastic properties for the beam in shear

Properties	f_c [MPa]	f_t [MPa]	G_F [N/mm]	E_c [MPa]	f_y [MPa]	ϑ [-]
Mean	78.2	5.13280	0.1266	42675	550	0.971
Std.	9.645	0.8503	0.0309	3198.4	30	0.1327

To gain a deeper insight into the reliability analysis of the RC beam, in total seven cases have been considered. The cases are summarized in Tables 4.6.

The NLFEA solution strategy is a key element of any RC reliability analysis, which has been discussed already in 3. In this Section the line search phenomena in DARS for the RC beam case is expounded first. The modeling uncertainty (ϑ) is not yet considered for that case. Later in this Section four cases with Modeling uncertainty are considered and their results are discussed.

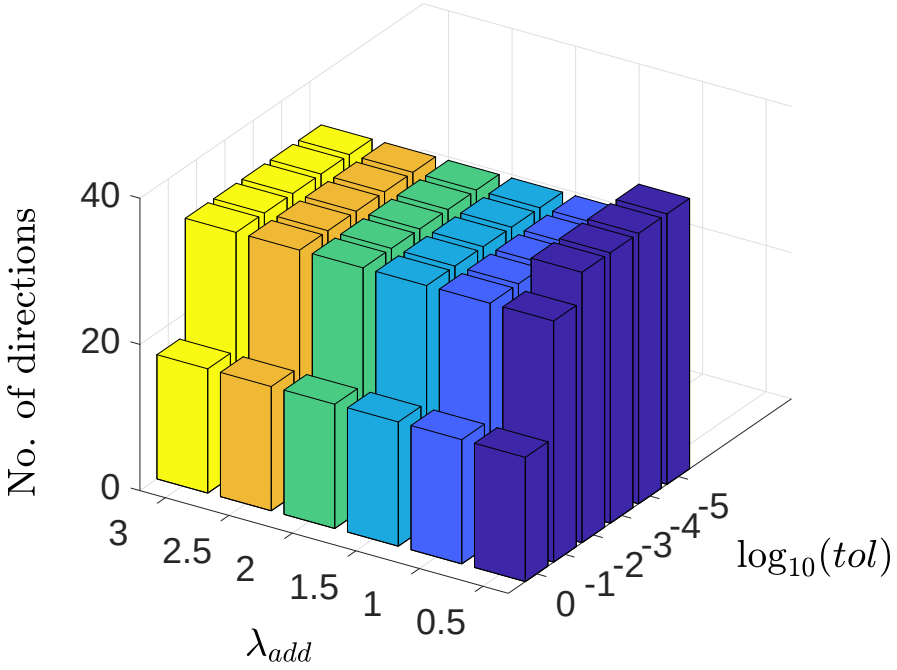

Figure 4.12: First case: Random f_{c1},f_{c2}. λ_{add} and $\log_{10} tol$ vs No. of Sampled Directions: $cov_{P_f} = 0.45$

Table 4.6: Summary of all the beam cases

Case	f_c [MPa]	f_t [MPa]	G_F [N/mm]	E_c [MPa]	f_y [MPa]	ϑ [-]	tol
$1^{st}(a)$	-	✓	✓	-	✓	-	0.01
$1^{st}(b)$	-	✓	✓	-	✓	-	0.1
2^{nd}	-	✓	✓	-	-	✓	0.1
3^{rd}	-	✓	✓	-	✓	✓	0.1
$4^{th}(a)$	✓	✓	✓	✓	✓	-	0.1
$4^{th}(b)$	✓	✓	✓	✓	✓	✓	0.1
5^{th}	✓	✓	✓	✓	✓	✓	0.1

* For the cases $1^{st}(a)$ to $4^{th}(b)$ f_t and G_F are considered to be perfectly correlated, rest are mutually independent. For the 5^{th} case the concrete correlation matrix given by Zimmermann *et al.* [86] is used.

4.3.1. DEMONSTRATION OF LINE SEARCH FOR RC SHEAR BEAM

The key philosophy behind DARS is that instead of simulating large numbers of samples, as typically done in Monte Carlo simulation, only the samples in the most important

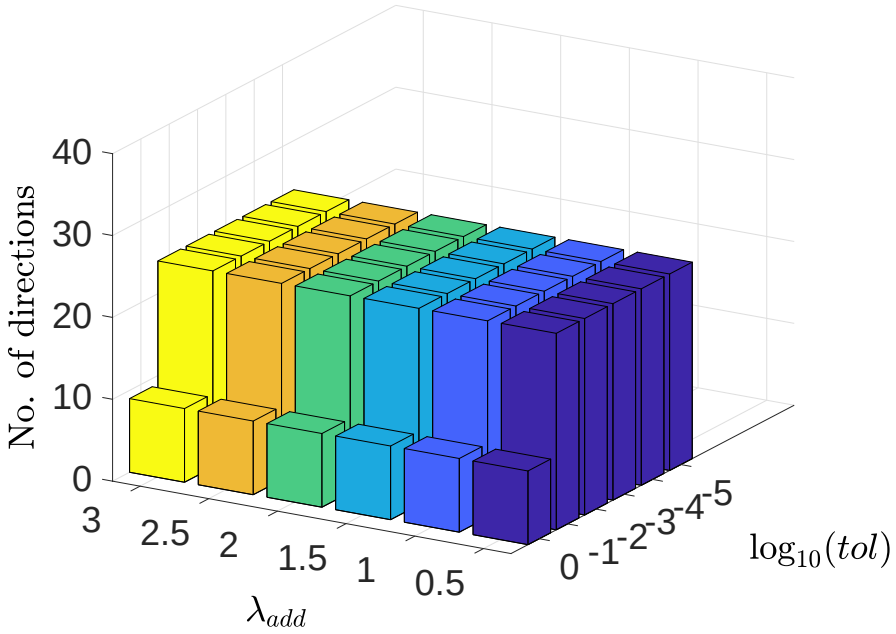

Figure 4.13: Second case: Random f_{c2}, ϑ. λ_{add} and $\log_{10} tol$ vs No. of Sampled Directions: $cov_{P_f} = 0.45$

region of the limit state surface are considered. Such samples are found by a line search along the important directions. The line search procedure has been described in section 2.3.8. The algorithm for the line search works in such a way that after each iteration a new point in the search direction is found, which is then used to improve the polynomial describing the G function. For a smooth and well behaving G function this takes about $3-4$ iterations to locate the important sample near/on the limit state surface $G = 0$.

Table 4.7: Comparison of DARS results for two different values of tol

Case	tol	Directions	G^*_{NLFEA}	NLFEA	λ_{min}	β	β_{FORM}
$1^{st}(a)$	0.01	44	7	63	5.51	5.53	5.51
$1^{st}(b)$	0.1	24	5	17	5.70	5.63	5.35

The G function along a search direction for RC structures however, is rarely smooth. The 1^{st} cases ((a) and (b), Table 4.7), where only the concrete shear strength (f_t), fracture energy (G_F) and reinforcement yield strength (f_y) are random, are selected in this subsection to expound the irregularity that can occur during a line search. The choice of the random variables is inspired by the fact that shear failure is governed by concrete tensile

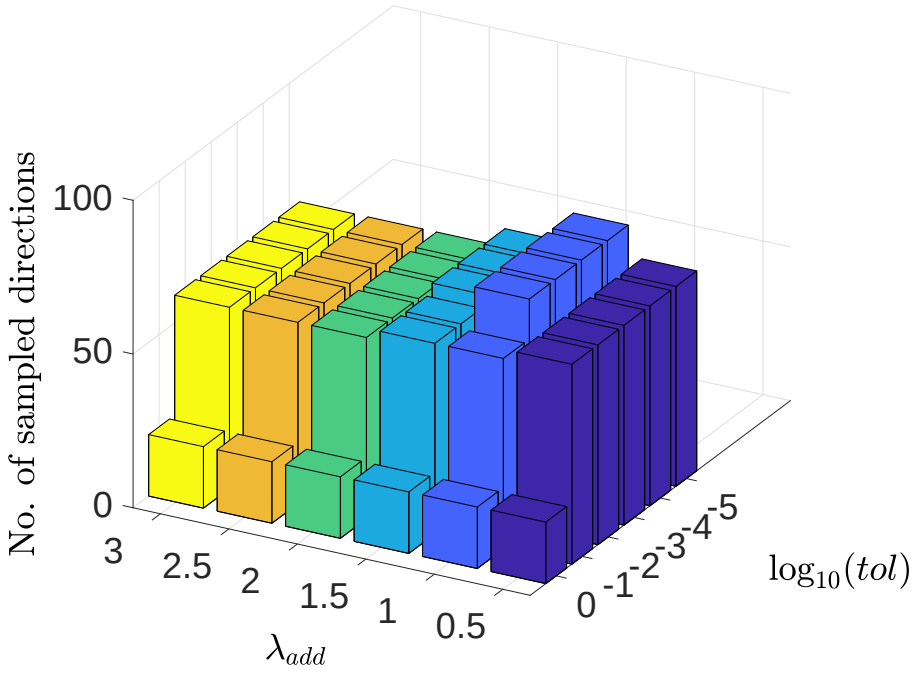

Figure 4.14: Third case: Random f_{c1}, f_{c2}, ϑ. λ_{add} and $\log_{10} tol$ vs No. of Sampled Directions: $cov_{P_f} = 0.45$

properties. A model uncertainty (ϑ) is not taken into account for this case because the exclusion of ϑ make the results more visually explicit. f_t and G_F are considered to be fully correlated. f_y is independent of the other two random variables. This choice of correlations means that the standard normal space would be described by only two random variables, u_{f_t} and u_{f_y}. The limit state function, G, in this case is given by,

$$G = \frac{R_{FEM}}{F} - 1 \tag{4.11}$$

where R is the reaction capacity and F is the applied load on the beam.
In section 4.2.2 the influence of the target cov_{P_f} was studied, based on simple test problems. In that same section it was discussed that a $cov_{P_f} = 0.57$ results in $\leq 8\%$ error in β. While this is a relatively large error, based on the accuracy demanded by Eurocode [79] for engineering practices, this relaxation of error in β is allowed. This consideration is entirely from the perspective of feasibility. In theory, keeping a tight cov_{P_f} as convergence criterion for sampling would result in more accurate result.
However, an unnecessarily too tight cov_{P_f} certainly means larger number of sampled directions and hence NLFEA. Considering how taxing each NLFEA is for RC structures, the number of sampled directions should be kept at bare minimum. So $cov_{P_f} = 0.57$ is used as termination criterion for sampling in rest of this work.

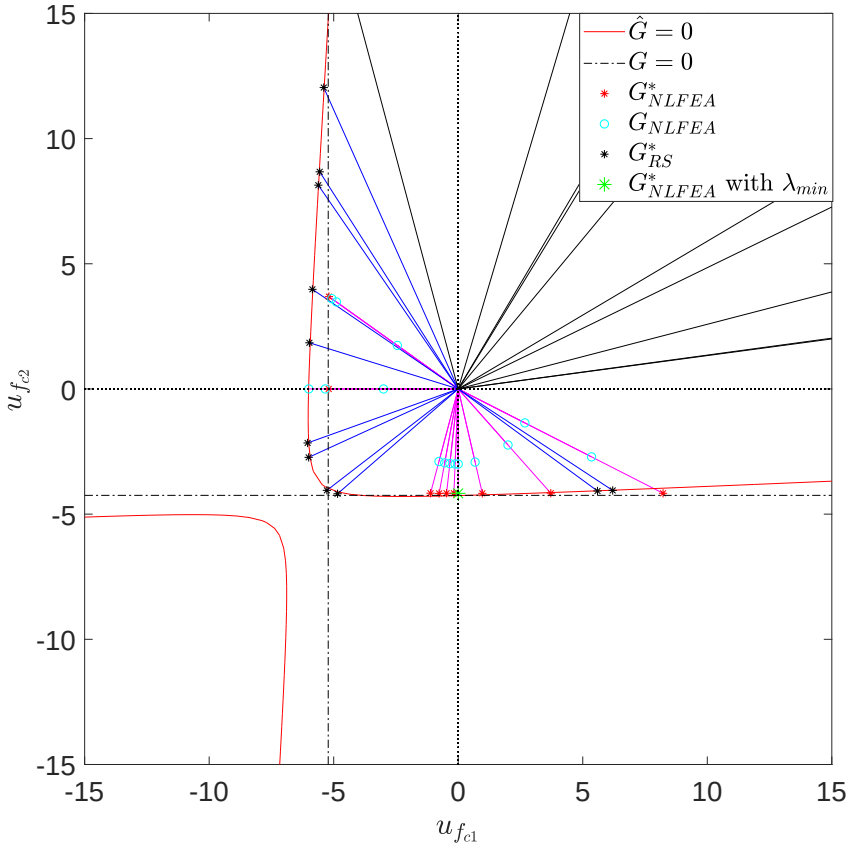

Figure 4.15: $G = 0$, final $\hat{G} = 0$ for the first case

In order to explore the line search phenomena more closely, the two separate cases, $1^{st}(a)$ with line search tolerance $tol = 0.01$ (Figure 4.18) and $1^{st}(b)$ with $tol = 0.1$ (Figure 4.19) are considered. The important samples G^*_{NLFEA}, unimportant samples G^*_{RS} and the final response surface $\hat{G} = 0$ are described in the standard normal space for an applied load of 80 kN. The comparison of the DARS analysis for these two cases is given in Table 4.7. The symbols β and λ_{min} are used in the same sense as before in previous section. β_{FORM} in the Table is the reliability index found based on the FORM analysis on the final response surface $\hat{G} = 0$.

The final response surface $\hat{G} = 0$ in Figure 4.18 is parallel to the u_{f_y} axis. The $\hat{G} = 0$ surface in Figures 4.19 and 4.18 look similar, except that in Figure 4.19 it has a slight negative slope. Since the chosen beam fails in shear, the reinforcement yield strength f_y has almost no influence in the failure of the beam. So the failure surface $\hat{G} = 0$ curve

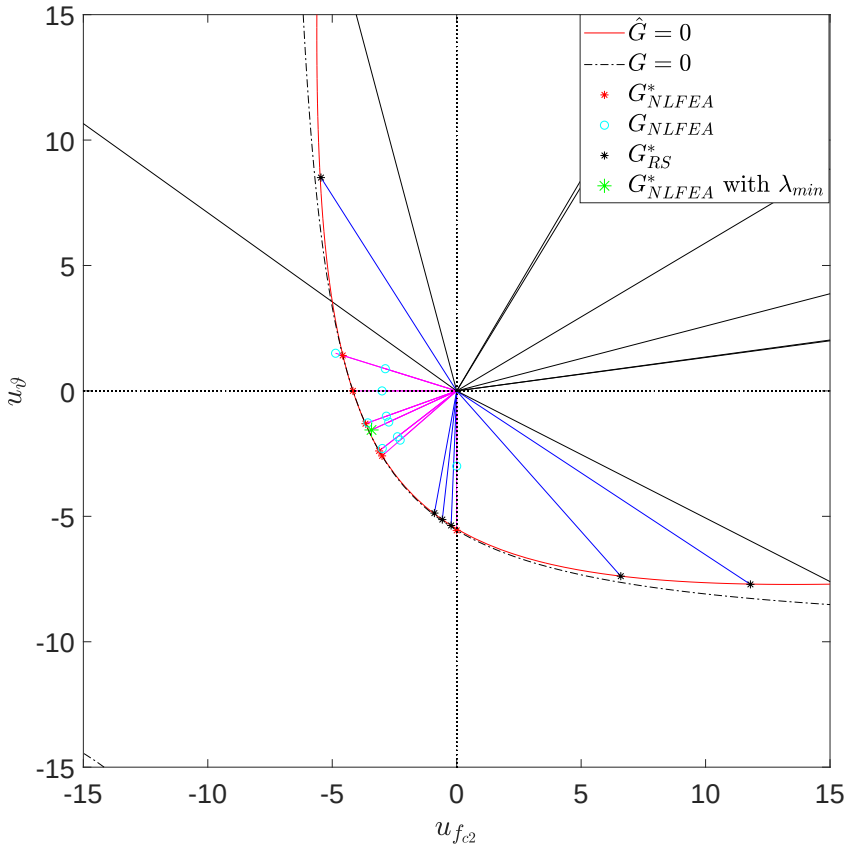

Figure 4.16: $G = 0$, final $\hat{G} = 0$ for the second case

parallel to the u_{f_y} axis for this problem is expected.

The final β value for these two cases are not significantly different. With the less demanding $tol = 0.1$ for case $1^{st}(b)$ the obtained G^*_{NLFEA} points are not as closely located to the $G = 0$, defined by Eq.4.11, compared to $1^{st}(a)$. It is tempting to deduce that $tol = 0.01$ leads to more accurate estimate of reliability. However, close inspection of the line search would reveal that there is more nuance to it than what is apparent. The direction leading to the G^*_{NLFEA} for one specific direction in Figure 4.18 took 10 iterations along that direction (marked in the figure). The plot of the residual G values against the corresponding λ for this direction (Figure 4.20) shows pronounced irregularities. The same direction took only 3 iterations in Figure 4.19 to reach the G^*_{NLFEA}. Also, there are directions in Figure 4.18 which even after 10 iterations could not produce a G^*_{NLFEA} point.

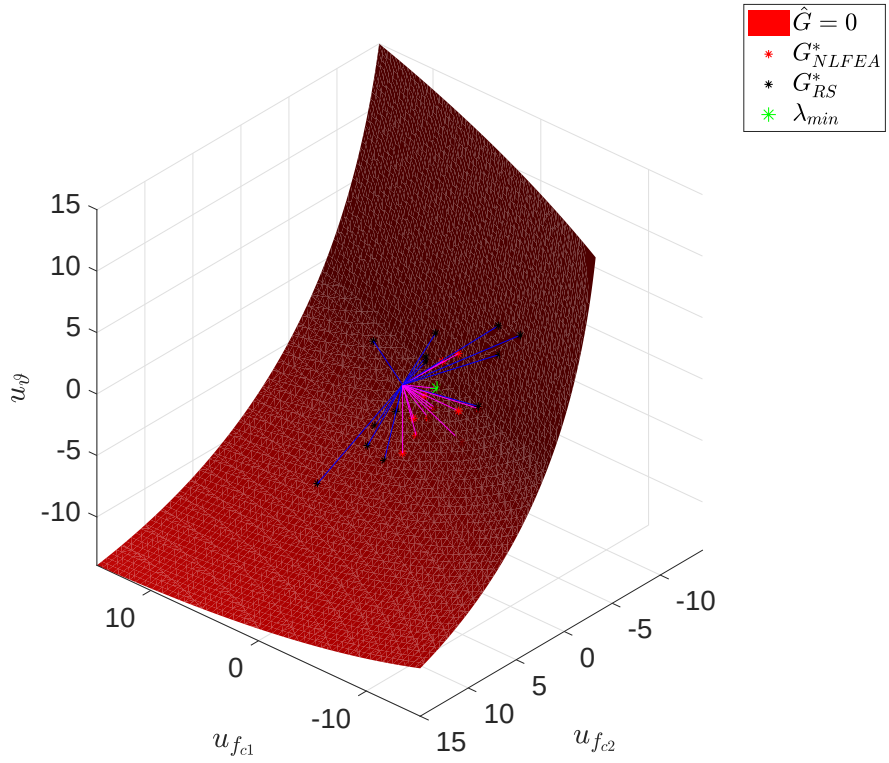

Figure 4.17: $G = 0$, final $\hat{G} = 0$ for the third case

This means, it is entirely possible that during a line search the capacity prediction by NLFEA itself is noisy. In such circumstance, the line search, even after consuming a large number of NLFEA, would lead to an erroneous G^*_{NLFEA}. Keeping a demanding tol, where the NLFEA convergence criterion leads to inaccurate estimates of capacity, will not lead to a realistic reliability estimate.

There is another source of justification for using a relaxed tol. As illustrated in subsection 2.3.8, during a line search the G^*_{NLFEA} point is sought by progressively improving the polynomial describing G function, with each newly available point on the search direction. The hope is that this procedure would guide the line search to locate the G^*_{NLFEA} point. But in presence of irregularities, it might be unrealistic to expect that the polynomial is consistently indicating any trend. In the end, the discovery of a G^*_{NLFEA} point might just be a lucky shot. Spending too many expensive NLFEA in that case would be

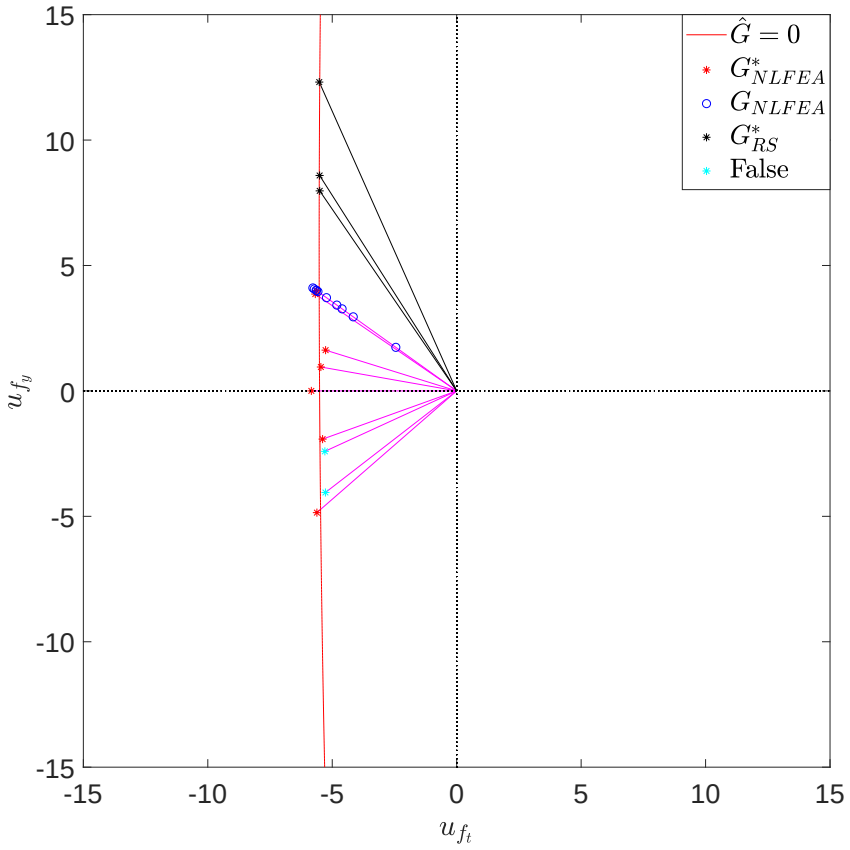

Figure 4.18: The shear beam $1^{st}(a)$ case with f_t, G_F and f_y random. $\lambda_{add} = 3$, $tol = 0.01$ and $cov_{P_f} = 0.57$

wasteful. The total number of NLFEA required for $tol = 0.01$ is 63, where as it took only 17 for $tol = 0.1$ (Table 4.7).

The comparison of the total number of NLFEA is given in Figure 4.21, for varying λ_{add} and tol. The choices for λ_{add} are inspired by Waarts [14] in all cases. From the Figure 4.21 it seems that irrespective of λ_{add}, the relaxed $tol = 0.1$ takes less number of NLFEA. For higher value of $\lambda_{add} = 3.0$, the number of NLFEA increases drastically with $tol = 0.01$. This observation, that smaller a λ_{add} results into more efficiency, is in agreement with the conclusion drawn by Waarts [14]. However, based on a large number of different kind of test examples Waarts concluded that a low value of λ_{add} might compromise the accuracy of the analysis. Keeping the accuracy of result in mind, $\lambda_{add} = 3.0$ value has been used in rest of this chapter.

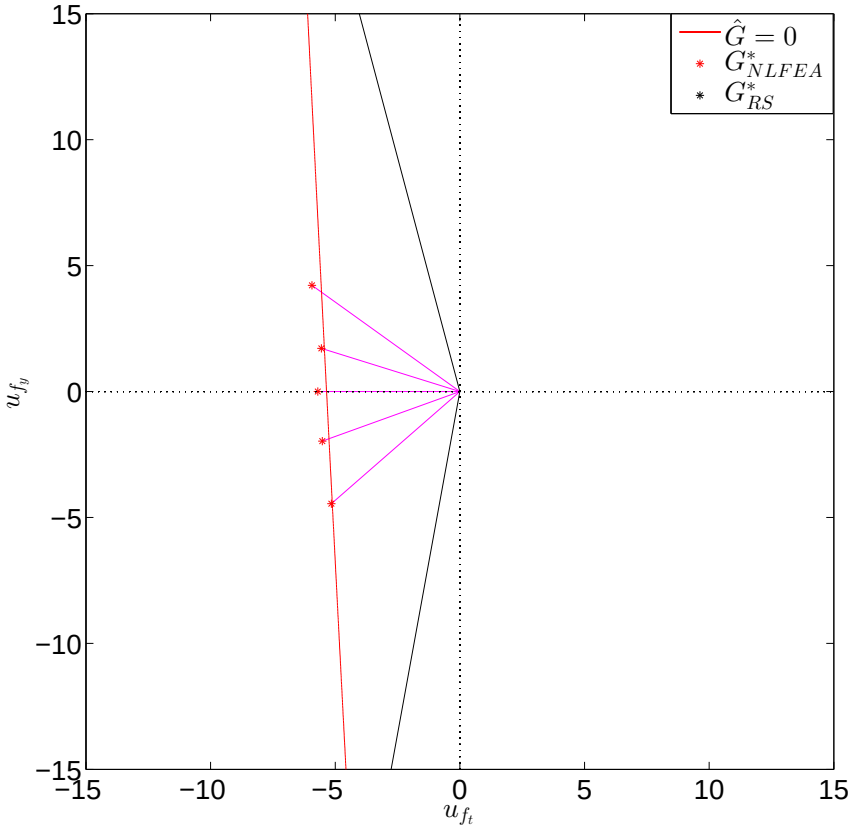

Figure 4.19: The shear beam $1^{st}(b)$ case with f_t, G_F and f_y random. $\lambda_{add}=3$, $tol=0.1$ and $cov_{P_f}=0.57$

4.3.2. RELIABILITY ESTIMATION OF RC BEAM, CONSIDERING ϑ

The assumptions, generalizations and idealizations involved in a NLFEA solution strategy give rise to a source of uncertainty, in addition to the random physical properties.

If the reliability calculation of a RC structure does not account for this additional scope of uncertainty, then the estimated reliability will not be the true reflection of reality. ϑ in a full probabilistic frame work is used by recasting the limit state function given in Eq.(4.11),

$$G=\frac{\vartheta R_{FEM}}{F}-1 \tag{4.12}$$

The philosophy behind multiplying ϑ with R_{FEM} follows straight from the definition of ϑ in Eq.(3.4). The idea is that each realization of the material parameters would

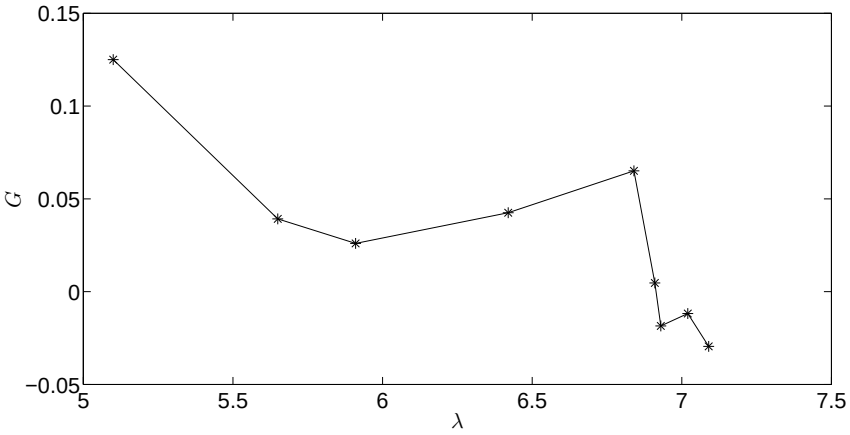

Figure 4.20: λ vs Residual G values for the shear beam $1^{st}(a)$ case.

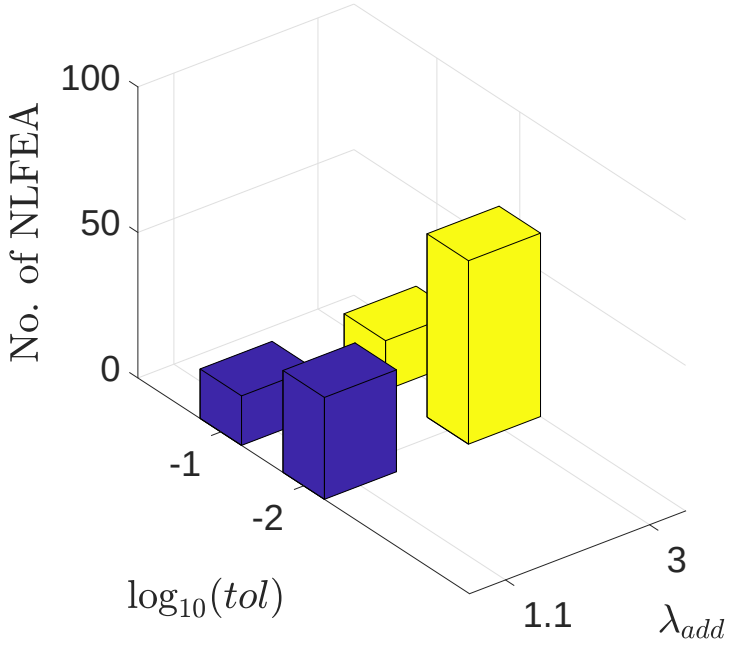

Figure 4.21: λ_{add} and $\log_{10}(tol)$ vs No. of NLFEA for the shear beam. $cov_{P_f} = 0.57$

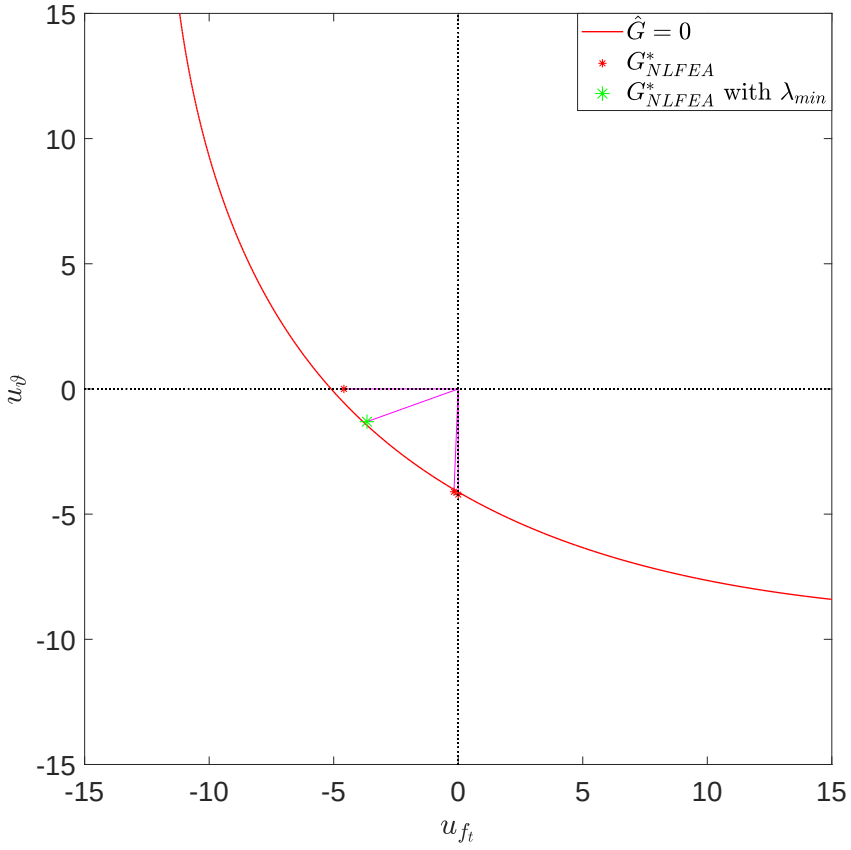

Figure 4.22: The shear beam 2^{nd} case with f_t, G_F and ϑ random. $\lambda_{add} = 3$, $tol = 0.1$ and $cov_{P_f} = 0.57$

produce a capacity prediction R_{FEM} by NLFEA, which will then be multiplied with the corresponding realization of ϑ. One of the opportunities of a full probabilistic reliability analysis with NLFEA is that it allows detail assessment of the effects of the input random variables. Four different cases, described as 2^{nd}, 3^{rd}, $4^{th}(b)$ and 5^{th} in the Table 4.8, are considered in this work. The applied load of $F = 80$kN is considered for all the cases. For concrete, the compressive fracture energy G_c quantity has been assumed to be deterministic in all cases. Its value has been obtained by the relation given in Model code 2010 [87], $G_c = 250G_F$, where the mean value of G_F is used.

The choice for $cov_{P_f} = 0.57$ has been explained earlier in this section. $\lambda_{add} = 3$, which has been used in the previous subsection, is used here as well. Because in the case of noisy limit state functions, a larger $\lambda_{add} = 3$ increases the chances of finding the important directions.

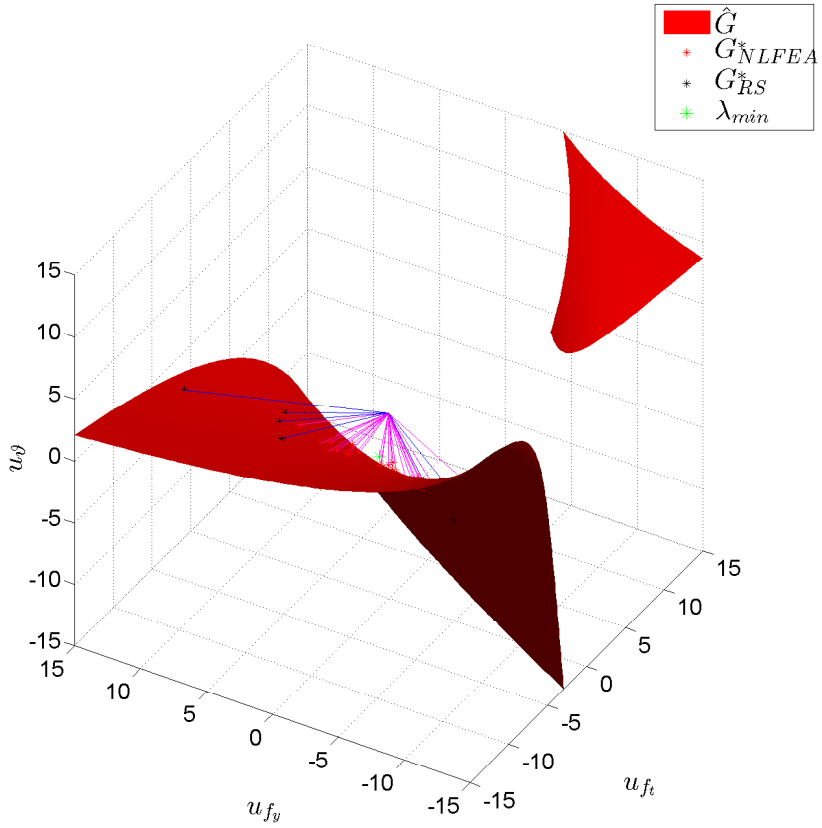

Figure 4.23: The shear beam 3^{rd} case with f_t, G_F, f_y and ϑ random. $\lambda_{add} = 3$, $tol = 0.1$ and $cov_{P_f} = 0.57$

Table 4.8: Summary of DARS results for all four RC shear beam cases considering ϑ

cases	Directions	G^*_{NLFEA}	NLFEA	λ_{min}	β	β_{FORM}
2^{nd} case	13	4	21	3.00	3.72	3.45
3^{rd} case	23	12	30	3.00	3.55	3.18
$4^{th}(b)$ case	31	20	65	3.93	3.16	2.94
5^{th} case	56	33	100	3.86	3.06	3.28

A tighter tol should lead to a more accurate reliability estimate. However, the irregularity of the capacity estimates during a line search cannot be guaranteed against. As discussed

in the previous subsection, a strong scatter of capacity predictions during a line search would render the line search strategy ineffective. So, to avoid this situation the value of $tol = 0.1$ is persisted with.

It is usual practice in semi-probabilistic methods to disregard the correlations between the random variables. For cases 2^{nd} to $4^{th}(b)$ the input random variables are considered uncorrelated, except f_t and G_F which are perfectly correlated. The correlations between the random variables can have substantial effect on the outcome of reliability analysis. In the 5^{th} case the input random variables have a specified correlation matrix. The correlation between all the concrete properties is relatively scarce in literature. The correlation between the compressive strength and other properties of concrete is studied by Rashid *et al.* [88], where a large volume of experimental data was collected from existing literature and analyzed the correlation between various concrete properties. The correlations were determined only for the concrete compressive strength with other properties. In the 5^{th} case the results given in the study by Zimmermann *et al.* [86] is used. The correlation matrix of the concrete properties is given in Table 4.9. In the Table 4.9 there are some negative correlation coefficients. This is however unlikely to happen. There are inadequate references in literature for the correlation of ϑ with other input material parameters. Engen *et al.* [17] found, for a given set of experimental beams, that the correlation coefficient between f_c and ϑ is only 0.013. The model uncertainty ϑ and the reinforcement yield strength f_y are assumed to be independent with respect to all other stochastic parameters for all the cases.

Table 4.9: Correlation of concrete properties

	f_c	G_F	E_c	f_t
f_c	1	−0.25	0.4	−0.11
G_F		1	0.04	0.79
E_c			1	0.00
f_t				1

The important samples G^*_{NLFEA}, unimportant samples G^*_{RS} and the final response surface $\hat{G} = 0$ for the 2^{nd} and 3^{rd} cases are plotted in Figures 4.22 and 4.23 respectively. The important samples, the final response surface etc. are difficult to visualize in higher-dimensional space of the $4^{th}(b)$ and 5^{th} cases. The summary of the reliability results is given in Table 4.8. The comparison of β, β_{FORM}, the total number of sampled directions (along with important directions) and total number of NLFEA calls are shown in the Figures 4.24, 4.25 and 4.26. The total number of directions required to satisfy the sampling criterion $cov_{P_f} \leq 0.57$ depends on the geometry of the LSF. It is observed in Figure 4.25 that for the chosen RC beam model the increase in stochastic dimension consistently increases the required number of sampled directions (along with important directions) to satisfy the sampling criterion. Consequently the total number of NLFEA also increases consistently (Figure 4.26). The total number of NLFEA however does not depend on the number of important directions alone. As seen in the $1^{st}(a)$ case, some directions may take much more NLFEA to meet the convergence criterion than others. So it is possible that even with less number of important directions the number of NLFEA could be

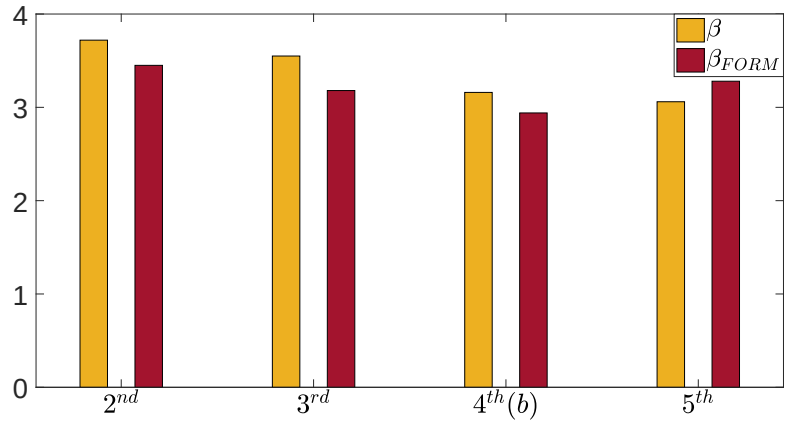

Figure 4.24: Comparison of β and β_{FORM} for the shear beam cases.

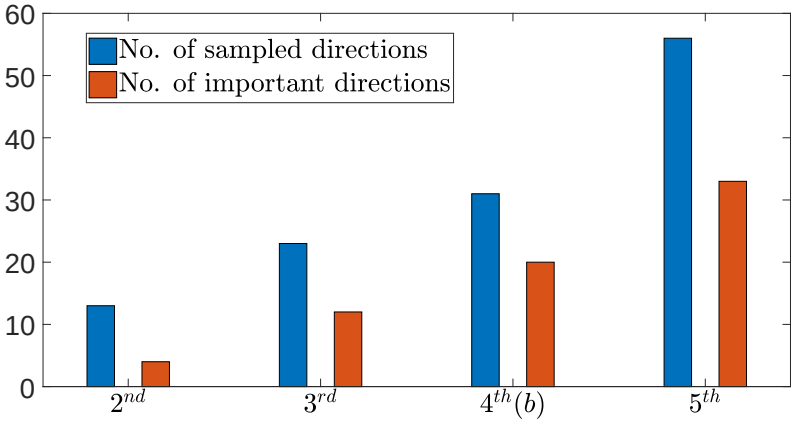

Figure 4.25: Comparison of No. of directions for the shear beam cases.

higher compared to larger number of important directions, if each of them take only 2−3 iterations to satisfy the tol criterion.

The relative influences that the input random variables in the standard normal space have on the reliability outcome are assessed by comparing the direction cosines, called the influence coefficients (denoted by α), of the direction vector of the design point. Unlike FORM, the DARS algorithm does not try to find the design point. The λ_{min}, in Figure 4.22 and 4.23 for example, is only the smallest distance found among the directions sampled. The comparison of the α_i is presented in Figures 4.27, 4.28 and 4.29. The α_i of $4^{th}(a)$ case, where ϑ is not considered, is also included in Figure 4.29 for com-

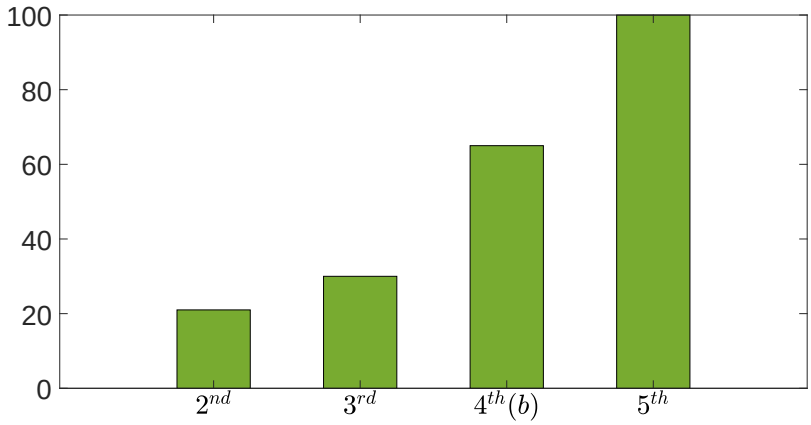

Figure 4.26: Comparison of No. of NLFEA for the shear beam cases.

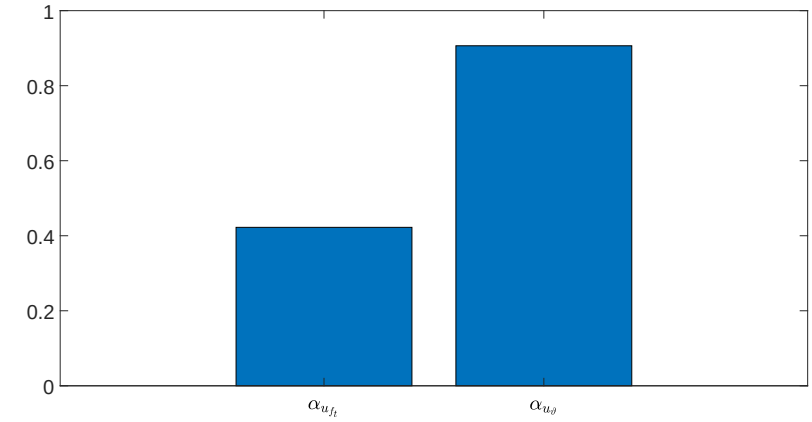

Figure 4.27: Influence coefficients for the shear beam 2^{nd} case.

parison. The influence coefficients were not investigated for the 5^{th} case, as it has no physical significance when the random variables are correlated. Because there exists no one to one correspondence between the correlated random variables in the original space (log-normal in this case) with transformed variables in the standard normal space. For all the three cases ϑ consistently has a significant influence in the reliability estimation. The reason follows directly from the way the limit state function is defined. The LSF $\frac{\vartheta R_{FEM}}{F} - 1$ is an explicit function of ϑ. So, unlike the other random variables whose effect on the LSF is expressed implicitly, ϑ effects the LSF directly, i.e. the variability of ϑ will be induced into the limit state function directly. As long as the cov_ϑ is high, it will certainly

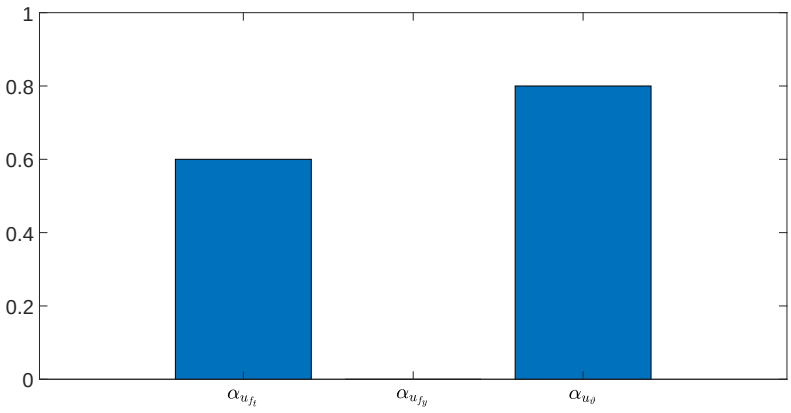

Figure 4.28: Influence coefficients for the shear beam 3^{rd} case

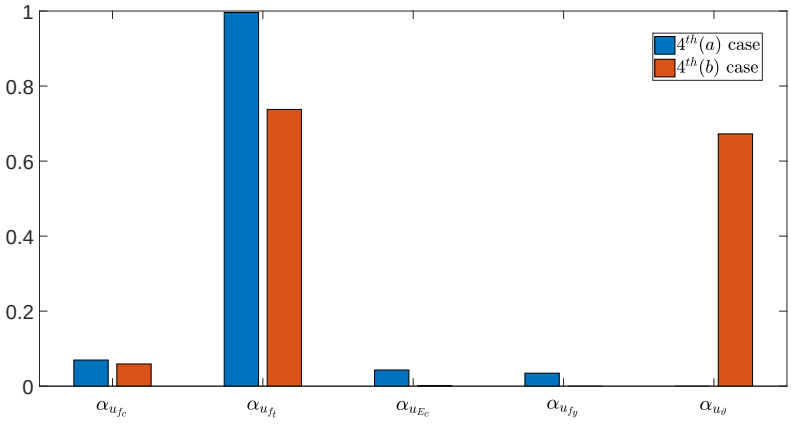

Figure 4.29: Influence coefficients for the shear beam $4^{th}(a)$ and $4^{th}(b)$ cases.

have a significant influence in the reliability analysis because of the way it enters the LSF. Implicit variables can only significantly influence if they have high sensitivity factor. The pattern of α for cases 2^{nd} to $4^{th}(b)$ in Figures 4.27, 4.28 and 4.29 is consistent with the notion of shear failure. $\alpha_{u_{f_t}}$ is quite high and for all other variables, except ϑ, $\alpha_i \leq 0.2$. For example, the α_i values for the 2^{nd} and 3^{rd} case are almost identical. Because f_y in the 3^{rd} case does not influence the LSF at all. It is important to note that FORM analysis on the final response surface $\hat{G} = 0$ produces an approximate design point. Because $\hat{G} = 0$ is best fit around the most important region of the limit state surface, there will be small inaccuracies in α values. As long as the available points to obtain a fit for $\hat{G} = 0$ is

sufficiently high, the error would be negligible however.

4.4. CONCLUDING REMARKS FOR THE FOURTH CHAPTER

This Chapter illustrated the full probabilistic reliability analysis of an RC beam by DARS. The use of the model uncertainty in the full probabilistic format is a novel addition to the RC structure reliability literature. The specific implementation of DARS has been validated against single element test cases first.

From the test cases, as well as the RC beam case without model uncertainty, it was demonstrated that the efficiency of the DARS analysis depends on the value used for λ_{add}. Low values of λ_{add} generally result into better efficiency, however there can be exceptions. $\lambda_{add} = 3$ has been used to ensure accuracy disregarding the economic concern.

It is revealed that for RC structures with a brittle failure mode, NLFEA predictions of the loading capacity during the line search in DARS could produce large scatter. In such circumstance, the line search algorithm does not help much in guiding the process to locate an important sample on the failure surface. The present implementation circumvents this problem by using a relaxed line search tolerance $tol = 0.1$, which results in low NLFEA consumption. Comparison with the result of $tol = 0.01$ suggests there is no big difference in the final prediction of the reliability index β, while the number of NLFEA is significantly low for $tol = 0.1$.

Along with the modeling uncertainty ϑ several combination of random variables are studied in four cases. Among the four cases, the β value varies within the range 3.06 – 3.72. However, the reliability index β is completely out of this range ($\beta = 5.63$) when compared with the case where ϑ is not considered an input random variable.

The modeling uncertainty in this work is obtained by combining the results of shear failure and bending failure cases. Had they been calculated distinctly, corresponding to the failure modes, the resulting modeling uncertainty of shear failure mode would have had much larger variance. Considering different modeling uncertainties for shear and bending failure modes would have significantly influenced the result of reliability analysis. It is quite likely that considering different modeling uncertainty for different failure modes will improve the reliability estimate even further. But in order to make such implementation possible, it is necessary to be able to quantitatively determine the failure mode, during a reliability analysis. The ductility index introduced by Engen *et al.* [17] can be useful in this regard, to quantitatively distinguish between the brittle and ductile failure modes during a reliability analysis.

The sensitivity analysis of all the four cases reaffirms the notion that concrete tensile strength f_t plays a more important role in shear failure compared to other physical parameters. However, it is also found that the significance of ϑ can be comparable to f_t. It is apparent that both cov_ϑ and cov_{f_t} are important for shear failure case. This underscores the importance of having a good estimate of cov_ϑ and cov_{f_t}. The cov_{f_t} followed from the mean of f_t provided by Yang *et al.* [64] and the standard deviation of f_t provided by Wiśniewski *et al.* [65]. The cov_ϑ followed from the Equation 3.4, based on 53 RC beam cases. In this work it is assumed that the statistical uncertainty of ϑ is independent of f_t. However, if the experiments are repeated, the loading capacities R_{EXP} are likely to vary for each case, primarily due to the statistical uncertainty of f_t. In that sense, the cov_ϑ

depends indirectly on the cov_{f_t}.
Several such case studies will provide an idea of the range of α_i for each variables. From this the appropriate values of α_i can be inferred and used in semi probabilistic reliability methods.

5

IMPROVEMENTS IN DARS ALGORITHM FOR NOISY CASES

5.1. INTRODUCTION

ONE crucial observation in the previous chapter was that the prominent numerical noise in the limit state function of the shear beam made DARS quite inefficient, in terms of number of NLFEA based limit state function evaluations. The source of this inefficiency was found to be the interpolation based line search method employed by DARS. Eventually the line search tolerance had to be relaxed in order to reduce the number of limit state function evaluations. Such compromise can have serious consequence on the accuracy of the reliability estimate. But more importantly, such measure may not even always work. Impact of numerical noise associated with nonlinear finite element predictions in structural reliability methods is underappreciated in the structural reliability literature. The uni-variate line search strategy used in adaptive directional importance sampling is particularly susceptible to such noise, which effects the overall performance of the algorithm. Other reliability algorithms, like first order reliability method, also struggle against noisy limit state function. This chapter highlights the performance aspect of the surrogate-based adaptive directional importance sampling, or directional adaptive response surface (DARS) method, when applied to nonlinear finite element based noisy limit state functions. As will be shown later in this chapter, DARS shows reduced performance due to the reduced performance in finding the root of a noisy uni-variate function in each direction. To overcome this, several alternate line search strategies are explored in this chapter. The alternative strategies are centered around the key theme that the surrogate function, or response surface, is used not just for distinguishing the important region, but also to assist the line search itself. A stochastic non-parametric Bayesian approach to regression, Gaussian process regression (GPR), is used to construct the response surface instead of a polynomial response surface typically associated with DARS. The GPR works on the principle that the regression errors associated with nearby locations are strongly correlated. This allows GPR to sense obvious

trends or patterns in the data and make better predictions with small sample learning, which helps the line search and contributes to the overall efficiency.

5.2. MINOR ADJUSTMENT TO THE EXISTING DARS METHOD

The DARS method used in the previous chapter (4) lacked in two aspects, which impeded the efficiency of DARS. Firstly, the line search in each direction started with an initial guess $\lambda = 3$. Waarts [14] discussed that if this initial guess is set at the λ corresponding to G^*_{RS} for that direction, the line search iteration becomes more efficient. This adjustment is made in the basic DARS method in this chapter. Secondly, in the previous chapter a constant λ_{add} is used through out the entire process. It was discussed in the previous chapter that a large λ_{add} improves the possibility of finding an important direction by relaxing the criterion of deciding whether a direction is important or not. This is particularly useful when the limit state surface is noisy. But a too large λ_{add} would mean that a larger number of directions would be deemed as important, thereby increasing the total number of NLFEAs. While Waarts [14] kept λ_{add} as constant, Grooteman [46] introduced a method to update λ_{add} in each successive iteration. This increases the efficiency of the overall procedure in terms of the number of function calls, without compromising the accuracy. This strategy of adaptive λ_{add} is incorporated in the DARS algorithm in this chapter. The procedure to find the adaptive λ_{add} is based on the principle that as the DARS process progresses, the total contribution of the unimportant directions to the failure probability increases. In this method the total failure probability due to all the unimportant directions are calculated. An already existing important direction is looked for whose associated λ is such that its contribution to the failure probability just surpasses the total failure probability by all the unimportant directions. This specific λ is termed as λ_{thres}. The value of λ_{add} is then found by subtracting λ_{min} from the λ_{thres}. Needless to say, as the DARS procedure proceeds, the value of λ_{thres} reduces, and consequently the value of λ_{add} also reduces. The algorithm can be summarized as follows: after the completion of an iteration, the individual failure probabilities are ranked in the ascending order in an array. The particular value of the probability in that array, for which the cumulative sum of probabilities till that value exceeds the total probability due to unimportant directions, is obtained. The corresponding distance to the limit state surface is termed as λ_{thres}. The value of λ_{add} at the beginning of the next DARS iteration then becomes $\lambda_{add} = \lambda_{thres} - \lambda_{min}$. Following Grooteman's recommendation, the adaptive λ_{add} starts with an initial value $\lambda_{add} = 0.1$.

The DARS algorithm starts off with line searches for a few chosen directions. A quadratic response surface is fitted based on those available samples. Then the actual DARS iteration starts. Based on this primitive response surface it is judged whether a direction is important or not, until the response surface is updated in the next iteration. In structural reliability applications, it is useful to do the initial exact line searches along the 'axis'directions in the standard normal space. These axes are defined by the transformed random variables in the standard normal space. Waarts [14] termed these initial line searches as 'axis directional line searches'or ADI. This strategy is adopted in this work.

5.3. DARS: PROPOSED IMPROVEMENT

As illustrated in Chapter 2, during a line search the G^*_{NLFEA} point is sought by progressively improving the polynomial describing the G function with each newly available point on the search direction. The hope is that this procedure would guide the line search to locate the G^*_{NLFEA} point for a given direction. For a smooth and well behaving G function this takes about $3-4$ iterations to locate the important sample near/on the limit state surface $G = 0$ depending on the tol. But in presence of noise in the NLFEA prediction of G function, it might be unrealistic to expect that the polynomial is consistently indicating any trend. In such circumstance, the line search might consume a large number of NLFEAs to obtain a G^*_{NLFEA}, or might even fail to obtain one.

Other alternative root location schemes, like Brent's method [89] might stand a better chance of finding the uni-variate root instead of polynomial interpolation. Brent's method is an improvement of the Bisection method, which has the robustness of bracketing methods (like Bisection) and the convergence rate of open methods (like Secant). Similar to the Bisection method, Brent's algorithm assumes the root can be bracketed in an interval of sign change. Brent's algorithm first attempts to find the root using the inverse interpolation scheme. If the estimate of the root falls outside the interval, then Bisection is used to narrow the interval and the process is repeated. Eventually, either the interpolation scheme will directly locate the root, or it will narrow the interval sufficiently such that the Bisection scheme will locate the root. The advantage of Brent's method over polynomial interpolation for noisy limit state cases is that the inverse quadratic interpolation will only help to guide the line search iterations to a narrow interval of sign change. Once the interval is narrow enough, the Bisection method, which is faster in a narrow interval compared to interpolation, will locate the root. Brent's algorithm fits an inverse quadratic interpolation based on the three latest iterates. For noisy equations the trend indicated by this interpolation is only weak (or even wrong) when the iteration is close to the root, where the effect of noise is most severe. This switching to the Bisection method in a narrow interval of sign change mitigates the possibility of the interpolation step to be entangled in the noise of the uni-variate equation. However, while otherwise reliable and fast, Brent's method might also be inefficient in case of an irregular limit state function if the line search starts far off from the root. The inverse quadratic interpolation steps can be slow to guide the iteration to the narrow interval in that case. Only in the case of excessively noisy limit state function the interpolation step would be completely erroneous Because in presence of noise the inverse quadratic interpolation step may produce bad estimates for next possible roots. This would virtually turn Brent method into simple Bisection method which has only linear rate of convergence. But such degree of noisy limit state function would only occur in case of poorly conceived nonlinear finite element model.

The limitation of one dimensional line search is that for every direction, the line search is done independently. A new direction starts the line search with no other information about the limit state surface other than the value of G function at the origin. In other words, such a procedure does not make use of the neighboring directions for which line searches have already been carried out. There exists examples in the literature where the λ obtained from the adjacent important direction is used as an initial guess to increase the efficiency of line search in a new direction [54].

The fact that for neighboring important directions the G^*_{NLFEA} samples on the limit state surface $G = 0$ are close to each other is utilized in this chapter to make the subsequent line search processes more efficient. In fact the strategy of using the λ corresponding to G^*_{RS} as the initial guess discussed in the previous section works on the same philosophy. As the surrogate function a Gaussian process regression based response surface is used. It is preferred because GPR makes direct use of closely located samples to make prediction for a nearby location. If a couple of line searches are already completed, then the initial guess for λ obtained from the response surface for a new direction will already be quite close to the actual uni-variate root along that direction. So when coupled with Brent's method, the line search will not have to entirely depend on the interpolation to bring the iteration to a narrow interval. The DARS algorithm with this new line search strategy will be called BDARS in this chapter, as opposed to DARS for the existing method.

The GPR based response surface can be so accurate in the important region that it is contemplated whether the response surface itself can be used to conduct the line search, instead of doing it in the uni-variate manner. In contrast with the traditional line search scheme, where the next prediction depends only on the earlier predicted points on a direction, the GPR based response surface guided line search makes use of the G^*_{NLFEA} and G_{NLFEA} samples of the surrounding directions through correlation to make the next prediction. In surrogate function based important sampling the surrogate function is improved progressively to obtain samples around the design point. The line search will work on the same principle. Along a direction the response surface would improve progressively, getting closer to the eventual G^*_{NLFEA} point. This method will be addressed as GDARS in this chapter. All the three methods are summarized in Table 5.1.

Table 5.1: Summary of the methods

Method	DARS	BDARS	GDARS
RS	Quadratic	GPR	GPR
Line search	Interpolation	Brent	RS

5.3.1. GAUSSIAN PROCESS REGRESSION BASED SURROGATE FUNCTION

In principle, a quadratic response surface, which is usually used in DARS, can be used to guide the line search as well. The regression problem like this has the general form,

$$\boldsymbol{g}(\mathbf{x}) = \boldsymbol{f}(\mathbf{x})^T \boldsymbol{\zeta} + \boldsymbol{Z}(\mathbf{x}) \tag{5.1}$$

where $\boldsymbol{f}(\mathbf{x})^T = [f_1(\mathbf{x}), .., f_m(\mathbf{x})]^T$ is the vector of basis functions of variables $\mathbf{x}$, $\boldsymbol{\zeta} = [\zeta_1, .., \zeta_m]^T$ is the vector of regression coefficients and m denotes the number of basis functions. $\boldsymbol{Z}(\mathbf{x})$ is the error of the regression model.

Applying regression to a reliability problem has the practical limitation that the functional form of the objective function is unknown. Hence quadratic only regression terms may not be sufficient. Of course, one can consider using a flexible functional form that assumes different shapes via different parameter settings. But flexible functional forms,

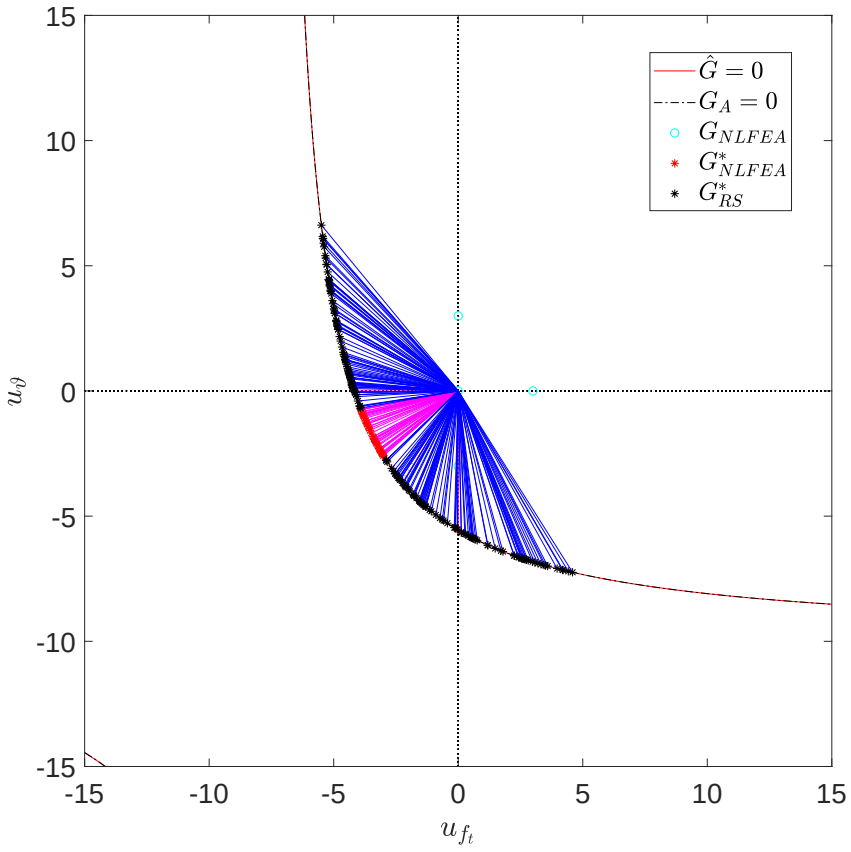

Figure 5.1: First test case with DARS. Random f_c,ϑ. $cov_{P_f} = 0.1$, adaptive λ_{add} and $tol = 0.01$

by their very nature, have many parameters, and so it would require many function evaluations to estimate these parameters, making the process inefficient. There is also a conceptual problem with regression. It is assumed that the regression errors $\boldsymbol{Z}(\mathbf{x}_i)$ and $\boldsymbol{Z}(\mathbf{x}_j)$ associated with two locations $\mathbf{x}_i$ and $\mathbf{x}_j$ are independent. But this assumption of independent errors is unjustified when using a deterministic computer code. Since a deterministic computer code produces reproducible result, any lack of fit can be entirely ascribed to regression error (incomplete set of regression terms), not measurement error or noise. If the points $\mathbf{x}_i$ and $\mathbf{x}_j$ are close, then the associated errors $\boldsymbol{Z}(\mathbf{x}_i)$ and $\boldsymbol{Z}(\mathbf{x}_j)$ should also be close. It is more reasonable to assume that these error terms are related or correlated and that this correlation is high when $\mathbf{x}_i$ and $\mathbf{x}_j$ are close. Similarly, when the distance between the points is large, the correlation will approach zero.

In the stochastic process approach the independence of error assumption is dis-

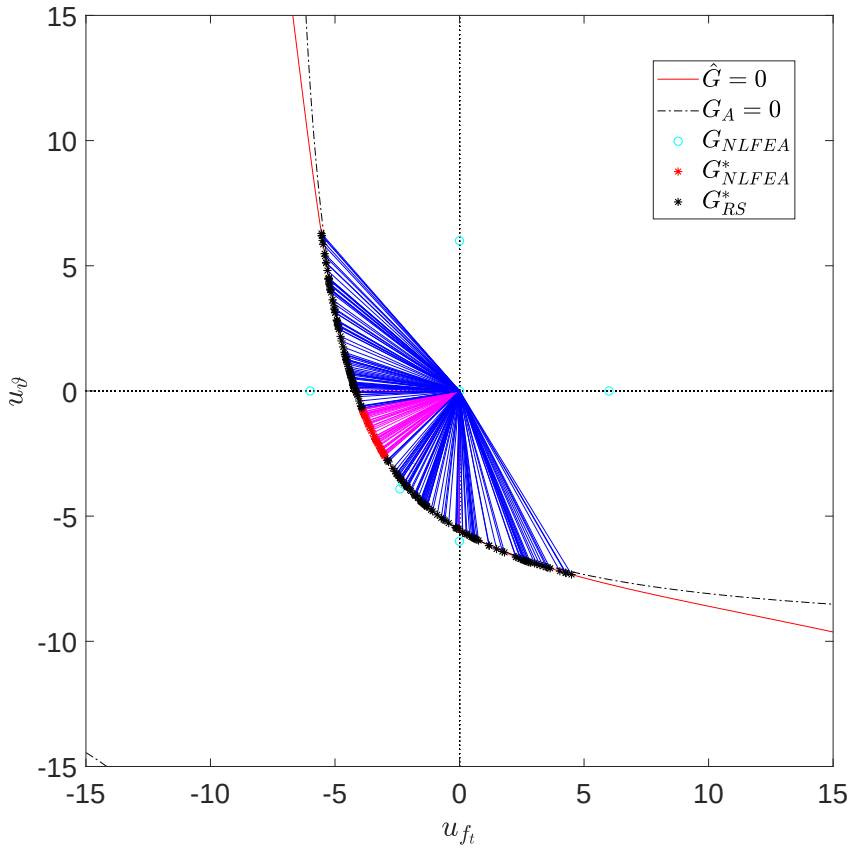

Figure 5.2: First test case with BDARS. Random f_c,ϑ. $cov_{P_f} = 0.25$, adaptive λ_{add} and $tol = 0.01$

carded. The error instead is assumed as a Gaussian process with zero mean, like the following,

$$\text{cov}[Z(\mathbf{x}_i), Z(\mathbf{x}_j)] = \sigma^2 \boldsymbol{R}(\mathbf{x}_i, \mathbf{x}_j) \tag{5.2}$$

where N is the number of samples. σ^2 is the process variance, $\boldsymbol{R}$ is the correlation function. The covariance is defined such that the correlation between errors is related to the distance between the corresponding points. A weighted distance formula is used in the correlation function, as defined below,

$$\boldsymbol{R}(\mathbf{x}_i, \mathbf{x}_j) = \exp(-\sum_{l=1}^{n} \theta_l |\mathbf{x}_{il} - \mathbf{x}_{jl}|^{pl}) \tag{5.3}$$

here n is the dimension of the space spanned by $\mathbf{x}$, the exponent pl determines the

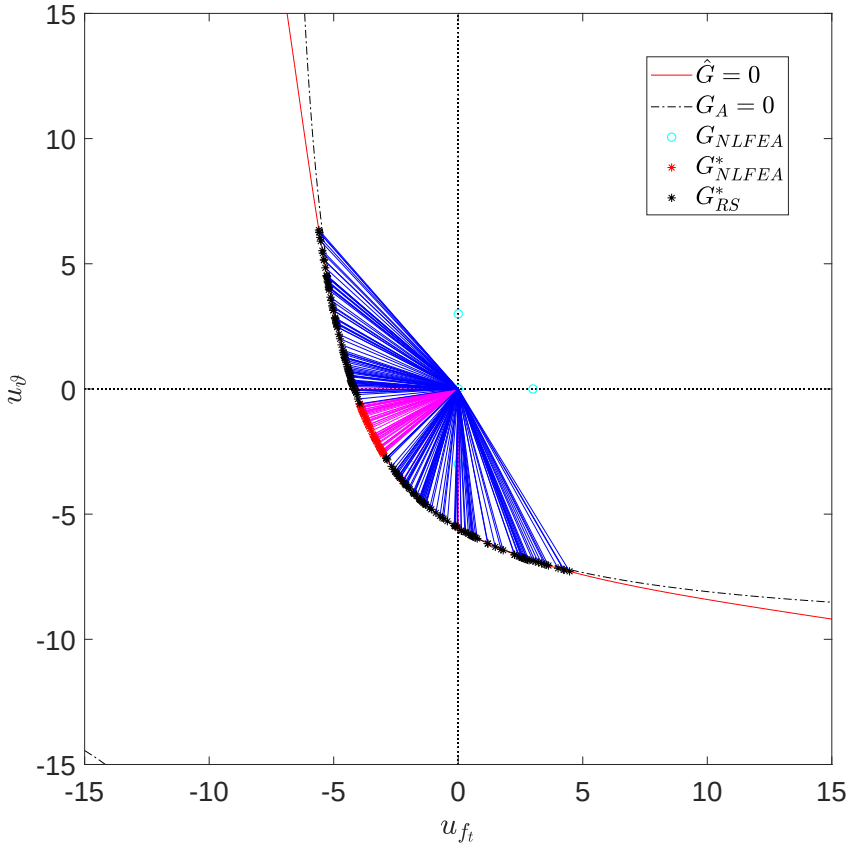

Figure 5.3: First test case with GDARS. Random f_c,ϑ. $cov_{P_f} = 0.1$, adaptive λ_{add} and $tol = 0.01$

smoothness of the function in the l^{th} coordinate direction. $pl = 2$ is widely used since it leads to a smooth function. θ_l is the correlation parameter, $\mathbf{x}_{il}$ and $\mathbf{x}_{jl}$ are the l^{th} component of position vector $\mathbf{x}_i$ and $\mathbf{x}_j$ respectively. θ_l can be interpreted as measuring the importance of the l^{th} input variable. Saying that l^{th} input variable is important means that even small values of $|\mathbf{x}_{il} - \mathbf{x}_{jl}|$ may lead to a large difference in the function values in those respective locations. In statistical terms, this implies that even small values of $|\mathbf{x}_{il} - \mathbf{x}_{jl}|$ lead to low correlation between the errors $\boldsymbol{Z}(\mathbf{x}_i)$ and $\boldsymbol{Z}(\mathbf{x}_i)$.
Now if a set of N training samples $[\mathbf{x}_1, \mathbf{x}_2, .., \mathbf{x}_N]$ is used and corresponding response set $\boldsymbol{g} = [\boldsymbol{g}(\mathbf{x}_1), \boldsymbol{g}(\mathbf{x}_2), ..., \boldsymbol{g}(\mathbf{x}_N)]$ is obtained from Eq.5.1, then the unknown parameters σ^2 and ζ can be obtained as,

$$\hat{\zeta} = (\boldsymbol{F}^T \boldsymbol{R}^{-1} \boldsymbol{F})^{-1} \boldsymbol{F}^T \boldsymbol{R}^{-1} \boldsymbol{g} \tag{5.4}$$

$$\hat{\sigma}^2 = \frac{1}{N}(\boldsymbol{g} - \boldsymbol{F}\hat{\zeta})^T \boldsymbol{R}^{-1}(\boldsymbol{g} - \boldsymbol{F}\hat{\zeta}) \tag{5.5}$$

Here $\boldsymbol{F} = [\boldsymbol{f}(\mathbf{x}_1), \boldsymbol{f}(\mathbf{x}_2), ..., \boldsymbol{f}(\mathbf{x}_N)]$ and the correlation matrix $\boldsymbol{R}$ based on these N training samples can be explicitly written as,

$$\boldsymbol{R} = \begin{bmatrix} R(\mathbf{x}_1, \mathbf{x}_1) & \cdots & R(\mathbf{x}_1, \mathbf{x}_N) \\ \vdots & \ddots & \vdots \\ R(\mathbf{x}_N, \mathbf{x}_1) & \cdots & R(\mathbf{x}_N, \mathbf{x}_N) \end{bmatrix} \tag{5.6}$$

It can be noted that the unknown parameters σ^2 and $\boldsymbol{\zeta}$ are the implicit functions of the correlation function parameters θ_l (Eq.5.3). In order to calculate σ^2 and ζ, the values of θ_l needs to be determined first. This is done by minimization of the likelihood function, $\frac{1}{2}(2N \ln \hat{\sigma} + \ln |\boldsymbol{R}|)$. The details behind the selection of this likelihood function can be found from [90]. Once the parameters θ_l are obtained, the regression coefficients $\boldsymbol{\zeta}$ and the process variance σ^2 are estimated from Eq.5.4 and Eq.5.5 respectively.

If $\boldsymbol{r}(\mathbf{x})^T = [R(\mathbf{x}, \mathbf{x}_1), .., R(\mathbf{x}, \mathbf{x}_N)]^T$ is the correlation vector between a point $\mathbf{x}$ and other sample points $(\mathbf{x}_1, ...\mathbf{x}_N)$, then the best unbiased predictor $\mu_{\hat{G}}$ of the Gaussian process regression model prediction at a point $\mathbf{x}$ is,

$$\mu_{\hat{G}}(\mathbf{x}) = \boldsymbol{f}(\mathbf{x})^T \boldsymbol{\zeta} + \boldsymbol{r}(\mathbf{x})^T \mathbf{R}^{-1}(\boldsymbol{g} - \boldsymbol{F}\hat{\zeta}) \tag{5.7}$$

and the variance $\sigma^2_{\hat{G}}$ of the prediction at that point is,

$$\sigma^2_{\hat{G}}(\mathbf{x}) = \sigma^2 - \begin{bmatrix} \boldsymbol{f}(\mathbf{x})^T & \boldsymbol{r}(\mathbf{x})^T \end{bmatrix} \begin{bmatrix} \mathbf{0} & \boldsymbol{F}^T \\ \boldsymbol{F} & \boldsymbol{R} \end{bmatrix}^{-1} \begin{bmatrix} \boldsymbol{f}(\mathbf{x}) \\ \boldsymbol{r}(\mathbf{x}) \end{bmatrix} \tag{5.8}$$

From the above expression for the prediction $\mu_{\hat{G}}(\mathbf{x})$ at a location $\mathbf{x}$ it is apparent that the predicted value is effected by the neighboring sampled points, through correlations. The variance associated with the prediction (and hence, the confidence interval) also depends on the closely located sampled points.

In this work only the constant function is used as the basis function. As covariance function of the error model a squared exponential function is used. This is the most commonly used covariance function which uses same characteristic lengths θ_l (Eq.5.3) for all predictor variables. GPR in this work has been implemented through MATLAB's Gaussian process regression function.

5.3.2. SUMMARY OF THE PROPOSED ALGORITHMS

The outline of the DARS, BDARS and GDARS is summarized in the sequel.

1. *The axis directional integration*: For ADI the traditional one dimensional adaptive polynomial based line search (DARS, GDARS) or Brent's method (BDARS) is used. Based on the available samples after ADI, a Gaussian process regression is carried out to fit a response surface.

2. *Search for important directions*: From the set of sampled directions it is searched which of them are important. Based on the distance to the response surface from the origin along a direction, it is decided whether a direction is important or not.

3. *NLFEA based line search for important directions*: For a direction deemed as important, the NLFEA based line search is initiated. The λ corresponding to G^*_{RS} is used as initial guess. During the iteration, with each available sample the response surface is updated for GDARS. Line search stops when the value of G falls below a prescribed line search tolerance tol.

4. *Checking the convergence*: Whenever the coefficient of variation of failure probability cov_{P_f} is below a prescribed value, go back to step two.

5. *Final round*: When no new important direction emerges, the algorithm stops. Compute the final failure probability by Eq.(2.75) using the last updated parameters.

5.4. VERIFICATION OF THE IMPLEMENTATION BASED ON TEST CASES

The specific implementation of BDARS and GDARS have been verified based on three test cases. The performance is compared against DARS. The directions are generated using random seed for the three test cases. The reliability analysis are repeated for these test cases in order to have an estimate of the standard error of the reliability results. For the each test case, the reliability analysis is repeated 20 times. If the resulting βs and the number of limit state function evaluations (LSFE) are considered to be Normally distributed, then the standard error $\hat{\sigma}$ associated with the estimate (mean) of β and LSFE can be approximated from the expression $\hat{\sigma} \approx \frac{S}{\sqrt{2n(n-1)}}$. Here n is the number of reliability analysis. This expression is valid as long as $n > 10$. Also note that, the reliability calculations are not done in the space of original random variables. The random variables are transformed into independent standard normal variables. In due consideration of accuracy and computational effort choices of $cov_{P_f} = 0.1$ and $tol = 0.01$ have been made for all the test cases.

For the first and the last test cases the limit state functions are also available in analytical form. This makes reliability analysis by means of Monte Carlo simulation possible, which is used as benchmark for comparison.

As the first test case, a single element concrete model (Figure 4.2) described in Chapter 2 has been chosen. The details of the stochastic parameters are already given in Table 4.2.

Table 5.2: Summary of reliability results for the first test case

Method	MCS	DARS	BDARS	GDARS
β	3.8402	3.8238	3.8180	3.8128
$\hat{\sigma}_\beta$	-	0.0008	0.0011	0.0008
NLFEA	10^7	67.65	60.95	59.60
$\hat{\sigma}_{NLFEA}$	-	0.5595	0.4074	0.3269

The reliability results are summarized in the Table 5.2. The β is defined as $\beta = \Phi^{-1}(P_f)$, where P_f is the failure probability from Eq.(2.75). The β_{ref} denotes the reference value found by Monte Carlo, by $\beta_{ref} = \Phi^{-1}(P_{ref})$. The failure probability by Monte Carlo is denoted by P_{ref}. The reference results have been generated by Monte Carlo simulation on the analytical limit state functions. The number of samples for the Monte Carlo is selected based on the criterion, $N \geq \frac{1}{cov^2_{P_f}}(\frac{1}{P_f} - 1)$. A target $cov_{P_f} = 0.1$ and an expected P_f in the order of 10^{-5} is used in this criterion to determine the minimum number of required Monte Carlo samples (10^7). This produced a value of $\beta_{ref} = 3.84$. The results of the reliability analysis for the first test case is summarized in the Table 5.2. The reference analytical limit state surface $G_A = 0$ and the final $\hat{G} = 0$ are plotted along with directions (important or otherwise) in Figures 5.1 to 5.3.

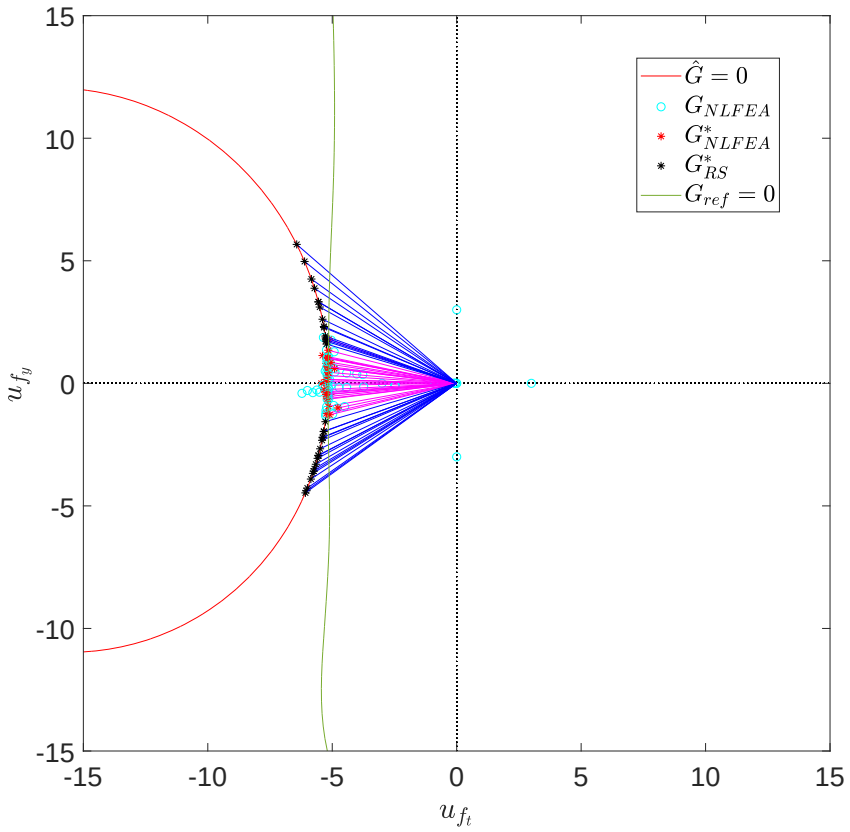

Figure 5.4: Shear beam 1^{st} case with DARS. Random f_t,f_y. $cov_{P_f} = 0.25$, adaptive λ_{add} and $tol = 0.01$.

As the second test case a slender steel beam with distributed load is considered (Figure

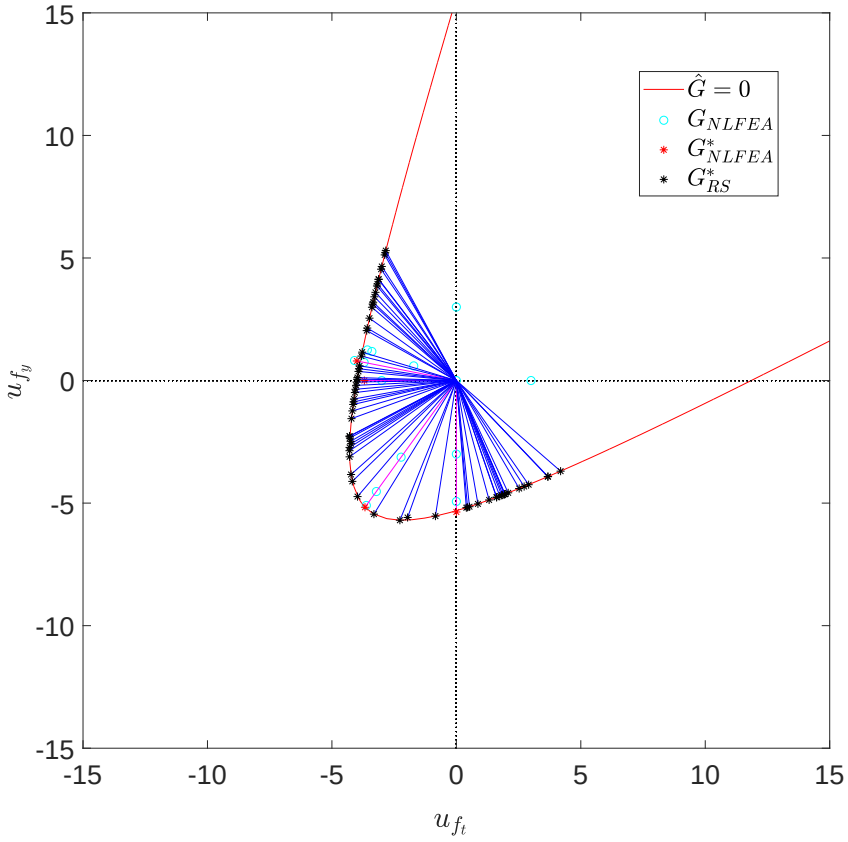

Figure 5.5: Mixed beam 2^{nd} case with DARS. Random f_t,f_y. cov_{P_f} = 0.25, adaptive λ_{add} and tol = 0.01.

2.3), simulated with linear finite element analysis (FEA). The length, breadth and depth of the beam is 10 m, 0.16 m and 0.5 m respectively. A distributed load of 1000 N/m is applied on the beam. 10 beam elements are used, with two degrees of freedom for each node. The Young's modulus (E) of the steel beam is considered as a Log normally distributed stationary random field with a mean 2.1 GPa and coefficient of variation 0.1. The characteristic length of the random field is assumed to be half the length of the beam. Optimal linear expansion (OLE) [50] is used to discretize the random field. 8 OLE discretization nodes are used, which means 8 input random variables. Nataf's transformation [20] is used to maintain the target correlation structure of the random field. The limit state function is described in the Eq.(5.9).

$$G(E(\mathbf{x})) = 1 - \frac{y_{midpoint}}{y_{ref}} \tag{5.9}$$

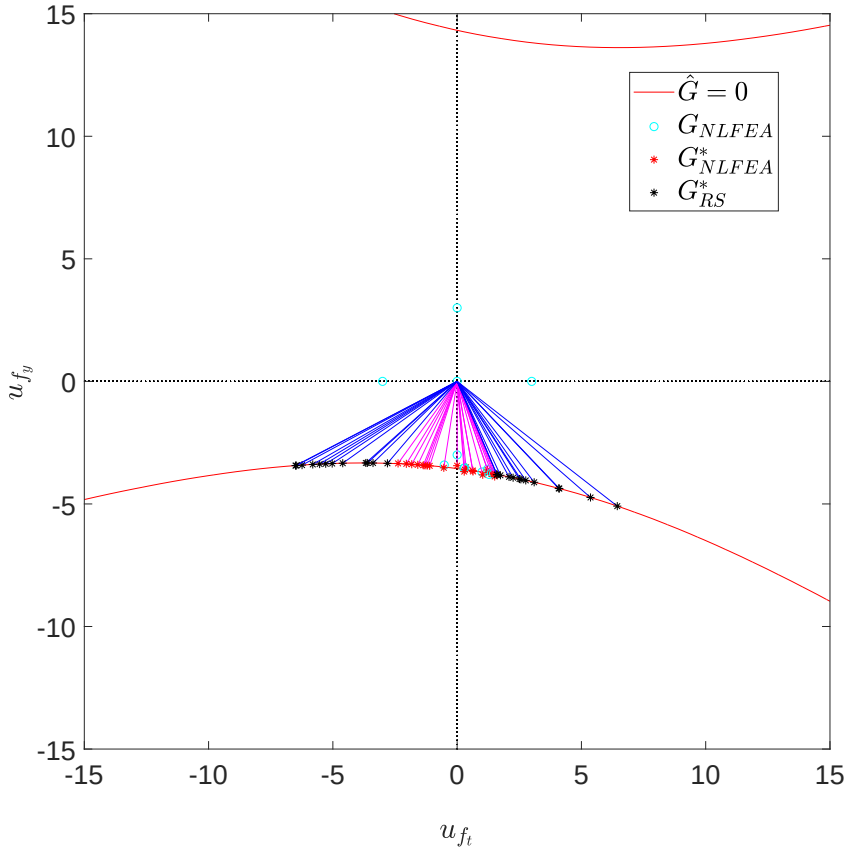

Figure 5.6: Bending beam 3^{rd} case with DARS. Random f_t,f_y. $cov_{P_f} = 0.25$, adaptive λ_{add} and $tol = 0.01$.

Here **x** denotes the spacial variable, $y_{midpoint}$ is the downward deflection at the mid point of the beam and $y_{ref} = 0.00055$ is the examination value for the same. The reliability results are presented in Table 5.3.

Table 5.3: Summary of reliability results for the second test case

Method	FORM	DARS	BDARS	GDARS
β	3.8821	3.8754	3.8824	3.8834
$\hat{\sigma}_\beta$	-	0.0008	0.0008	0.0008
FEA	51	43.90	43.67	45.35
$\hat{\sigma}_{FEA}$	-	0.3267	0.3372	0.3036

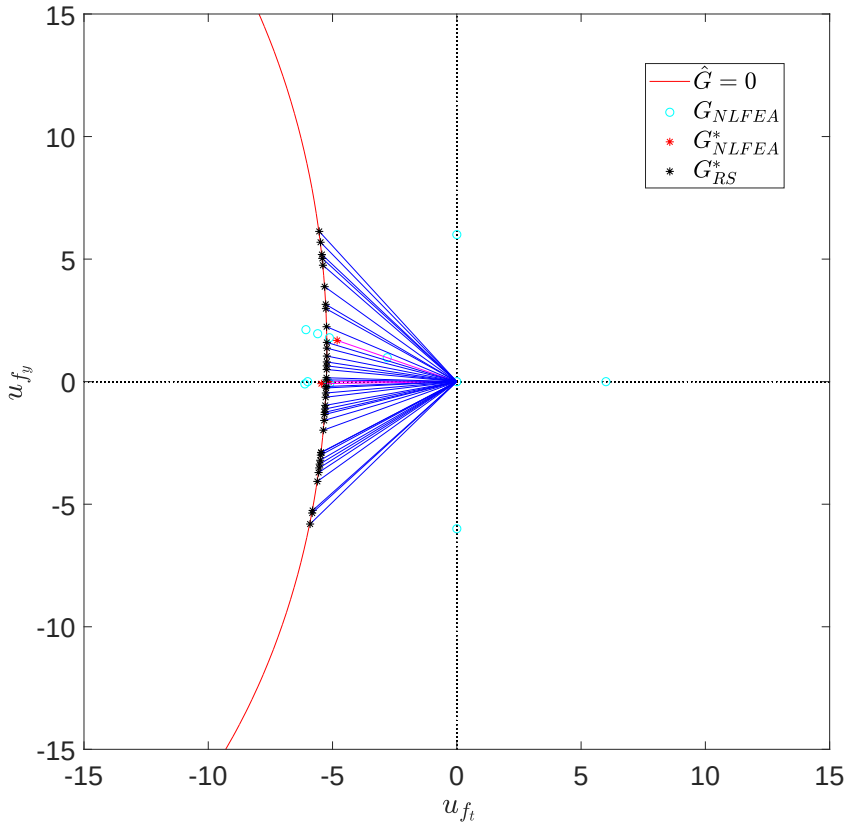

Figure 5.7: Shear beam 1^{st} case with BDARS. Random f_t,f_y. cov_{P_f} = 0.25, adaptive λ_{add} and tol = 0.01.

$$G(x_1,\cdots,x_6) = x_1+2x_2+2x_3+x_4-5x_5-5x_6 + 0.001\sum_{i=1}^{6}\sin(100x_i) \tag{5.10}$$

The third test case is a noisy limit state function described in the Eq.5.10 [91]. The six Log normally distributed independent random variables $x_1,\cdots,x_6$. x_1 to x_4 have mean 120 and standard deviation 12. x_5 has a mean 50 and a standard deviation 15. x_6 has a mean 40 and a standard deviation 12. cov_{P_f} = 0.1 and adaptive λ_{add} are used. The LSF in Eq.5.10 is not non-dimensionalized, unlike Eq.4.4 or Eq.5.9. So a line search tolerance tol = 0.01 is a stricter condition compared to the other three test cases. The results for the third test case are summarized in the Table 5.4. The Monte Carlo results for the third

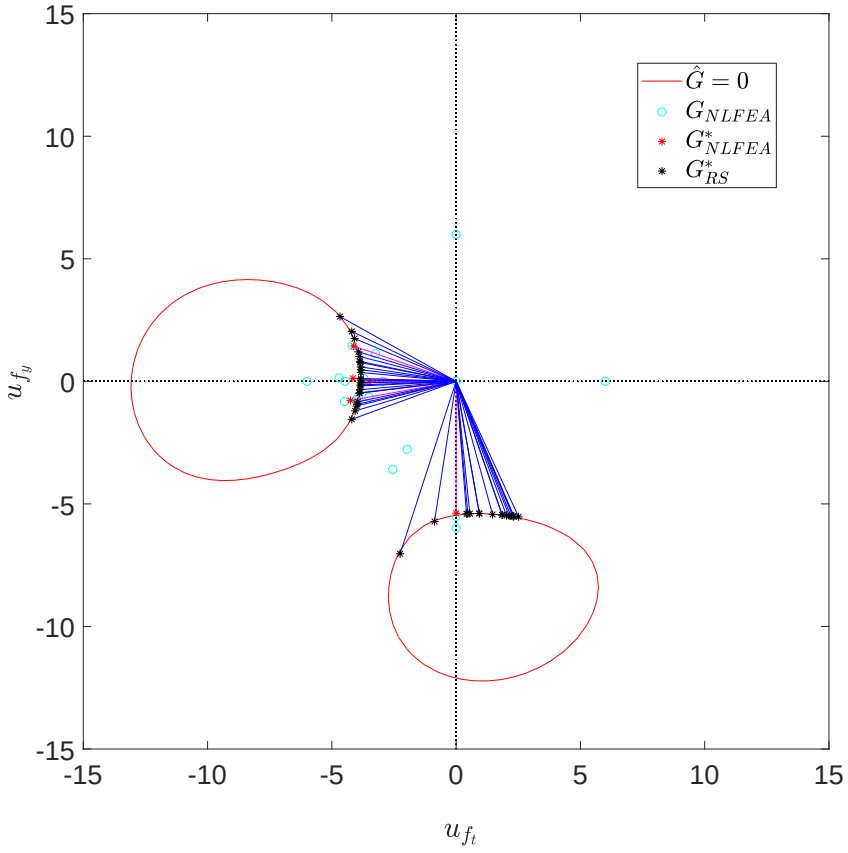

Figure 5.8: Mixed beam 2^{nd} case with BDARS. Random f_t,f_y. $cov_{P_f} = 0.25$, adaptive λ_{add} and $tol = 0.01$.

test case is obtained from Grooteman [46].

Table 5.4: Summary of reliability results for the third test case

Method	MCS	DARS	BDARS	GDARS
β	2.2507	2.2334	2.2512	2.2346
$\hat{\sigma}_\beta$	-	0.0019	0.0010	0.0013
LSFEs	7655	84.4000	64.6667	95.4762
$\hat{\sigma}_{LSFE}$	-	1.0003	0.6083	0.8262

DARS, BDARS and GDARS, all the three methods are observed to predict accurate

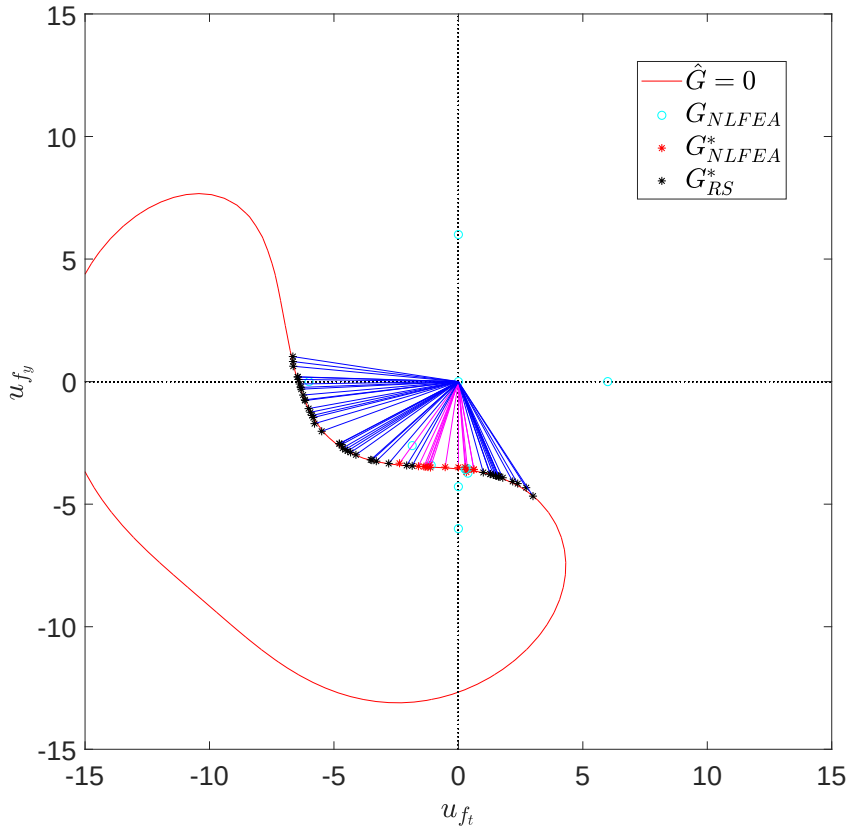

Figure 5.9: Bending beam 3^{rd} case with BDARS. Random f_t,f_y. $cov_{P_f} = 0.25$, adaptive λ_{add} and $tol = 0.01$.

estimate of β when compared to the reference results, with a similar standard error $\hat{\sigma}_\beta$. For the first two test cases with smooth limit state functions, the efficiency of the three methods are comparable, as measured by the average number of FEA (or LSFE) and their associated $\hat{\sigma}_{LSFE}$. DARS is observed to be only slightly less efficient compared to the other two. For the third case however, with noisy limit state function BDARS stands out from the other two, in terms of efficiency. Not only the average number of LSFE by BDARS is markedly lesser compared to DARS, its associated standard error $\hat{\sigma}_{LSFE}$ is also much lesser compared to DARS for the third case. For the test case the best performance for BDARS and GDARS is obtained by using a quadratic basis function in GPR instead of just the correlation function. The high value of limit state function around the mean implies that only the correlation function alone will not be sufficient to capture the global behavior of the limit state function. The performance of DARS, BDARS and GDARS are found to be comparable in terms of efficiency and accuracy for the first two

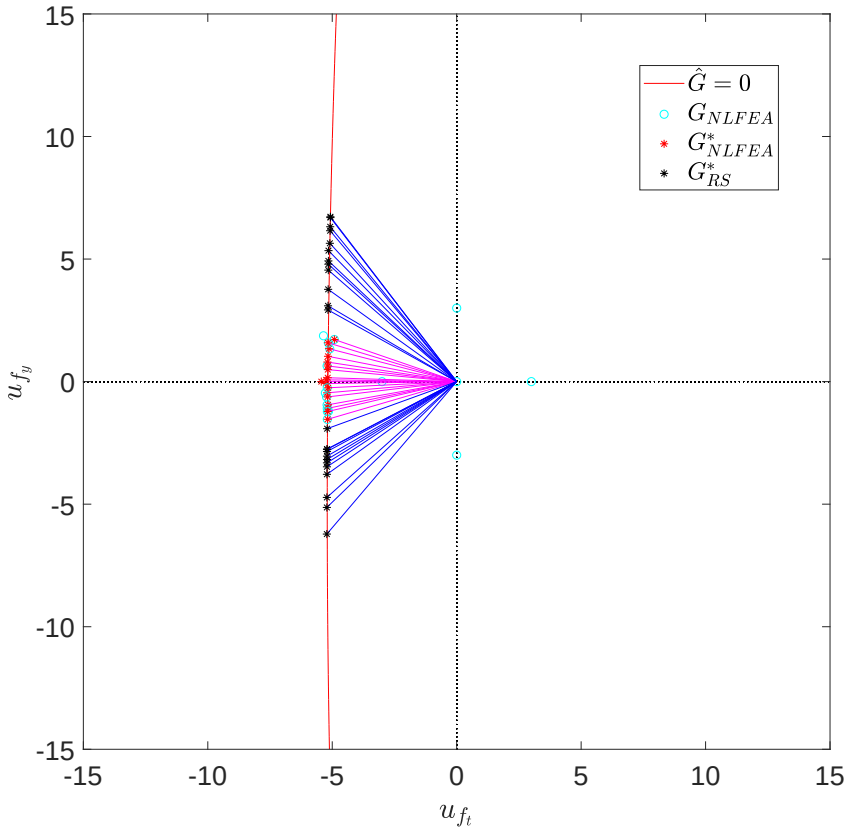

Figure 5.10: Shear beam 1^{st} case with GDARS. Random f_t,f_y. cov_{P_f} = 0.25, adaptive λ_{add} and tol = 0.01.

test cases. For the noisy limit state function in the third case GDARS is found to be least efficient compared to DARS and BDARS. It was found that stricter line search tolerance criterion made GDARS inefficient for this case, where as DARS or BDARS had faced no difficulty. The reason is that for GDARS the line search is done based on the response surface, which is fitted through regression. After a stage the response surface does not change much. This might be an impediment to achieve a stricter tolerance with GDARS, because after a while the estimate for λ will change only in third decimal place or beyond. Despite the limit state function being a noisy one, the performance of DARS is not found to be far worse compared to BDARS. The reason is that the contribution of the noisy terms (Eq.5.10) to G in terms of absolute value is quite low compared to the non-noisy terms. It is lower even compared to the line search tolerance tol = 0.01 for this case. As a consequence the polynomial interpolation based line search strategy of DARS had little difficulty in locating the root. If the contribution of noise were substantial, as is

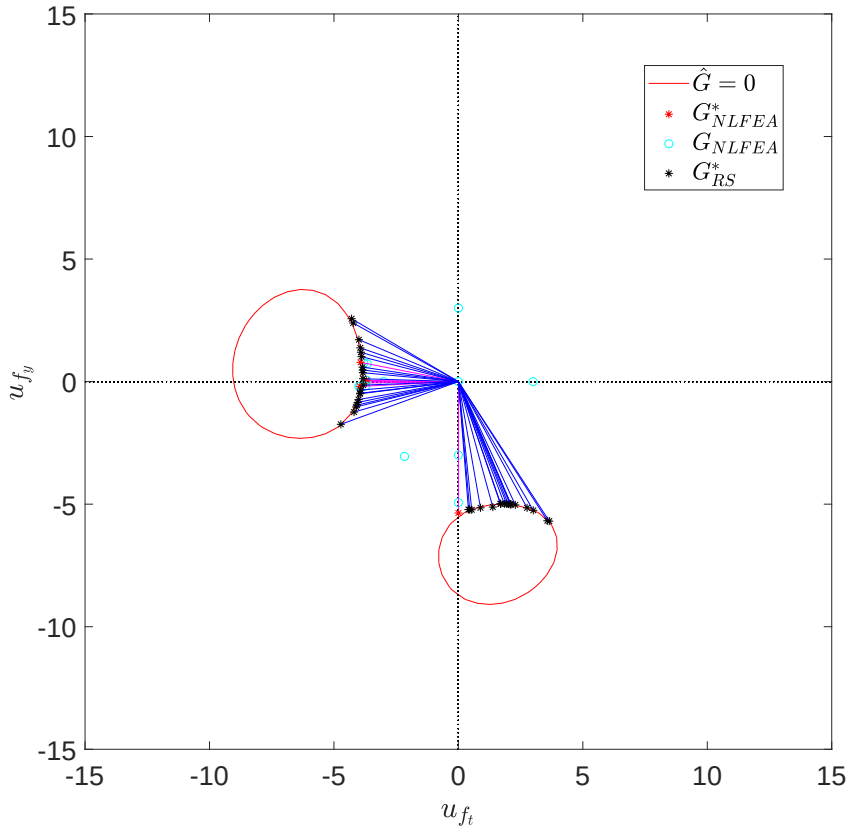

Figure 5.11: Mixed beam 2^{nd} case with GDARS. Random f_t,f_y. $cov_{P_f} = 0.25$, adaptive λ_{add} and $tol = 0.01$.

the case in Figure 3.5, polynomial based interpolation would have struggled to find the root in a line search. Such cases will be demonstrated in the subsequent section.

5.5. CASE STUDY: DEMONSTRATIVE EXAMPLES WITH RC BEAM CASES

Waarts [14] applied DARS on a number of different structures. He compared those results with other methods for accuracy and efficiency. But those structures were so chosen such that the finite element part was relatively simple and the limit state functions were relatively well behaved. When it comes to DARS reliability analysis of RC structures based on simulating failure of the structure by means of NLFEA, there is a paucity of demonstrative examples in literature. NLFEA based reliability analysis of RC structures

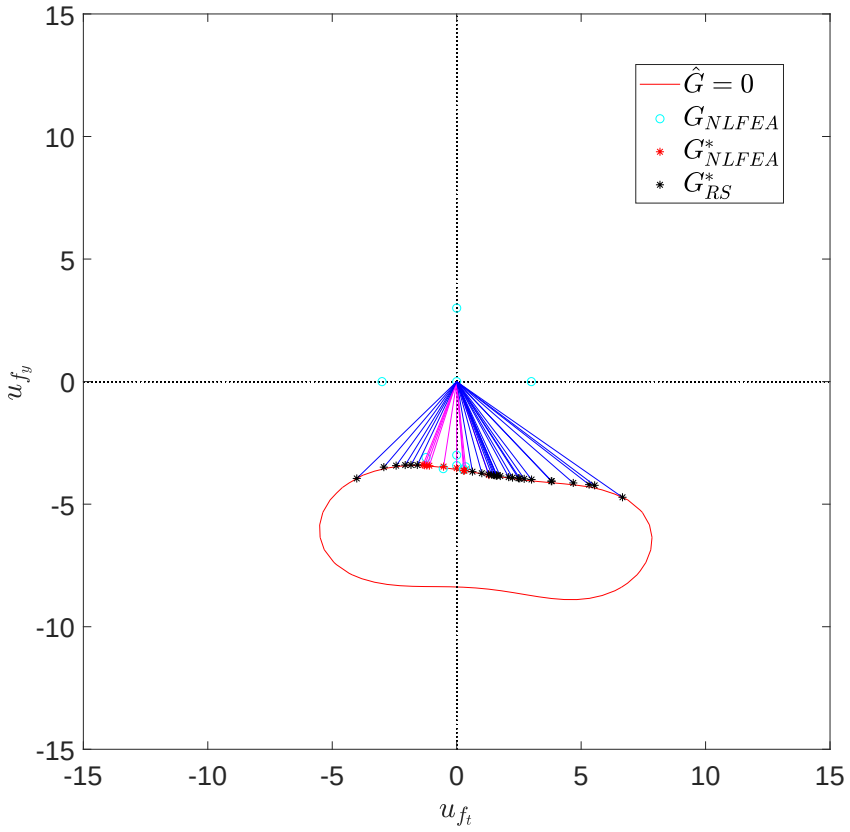

Figure 5.12: Bending beam 3^{rd} case with GDARS. Random f_t,f_y. $cov_{P_f} = 0.25$, adaptive λ_{add} and $tol = 0.01$.

with DARS has several critical elements of its own, which merits detailed study of its own. The three RC beam cases introduced in the Chapter 3 are selected in this chapter as demonstrative examples. In total six cases have been considered based on these three beams. The cases are summarized in Table 5.5.

The correlations between the random variables can have substantial effect on the outcome of reliability analysis. However, the information on correlation between all the concrete properties is relatively scarce in literature, as discussed in the previous chapter. In this chapter it is assumed that the stochastic properties are mutually independent. Only the concrete tensile strength f_t and tensile fracture energy G_F are considered to be fully correlated. Also, the concrete compressive strength f_c and compressive fracture energy G_c are considered to be fully correlated.

A $cov_{P_f} = 0.57$ has been considered as a convergence criterion in Chapter 4 for the shear beam, following the work of Waarts [14]. This was done in order to avoid exces-

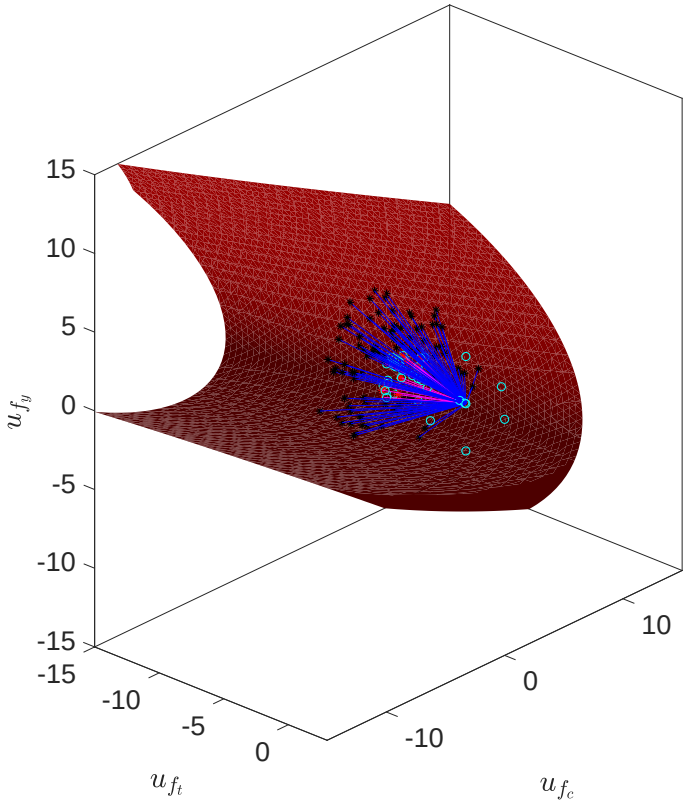

Figure 5.13: Shear beam 4^{th} case with DARS. Random f_t,f_c,f_y. $cov_{P_f} = 0.25$, adaptive λ_{add} and $tol = 0.01$

Table 5.5: Standard deviations of stochastic properties for various cases considered

Case	Beam type	f_c [MPa]	G_c [MPa]	f_t [MPa]	G_F [N/mm]	f_y [MPa]
1^{st}	Shear beam	-	-	0.8503	0.0309	30
2^{nd}	Mixed beam	-	-	0.8503	0.0309	55
3^{rd}	Bending beam	-	-	0.8503	0.0309	65
4^{th}	Shear beam	9.645	31.64	0.8503	0.0309	30
5^{th}	Mixed beam	9.645	31.45	0.8503	0.0309	55
6^{th}	Bending beam	9.645	31.73	0.8503	0.0309	65

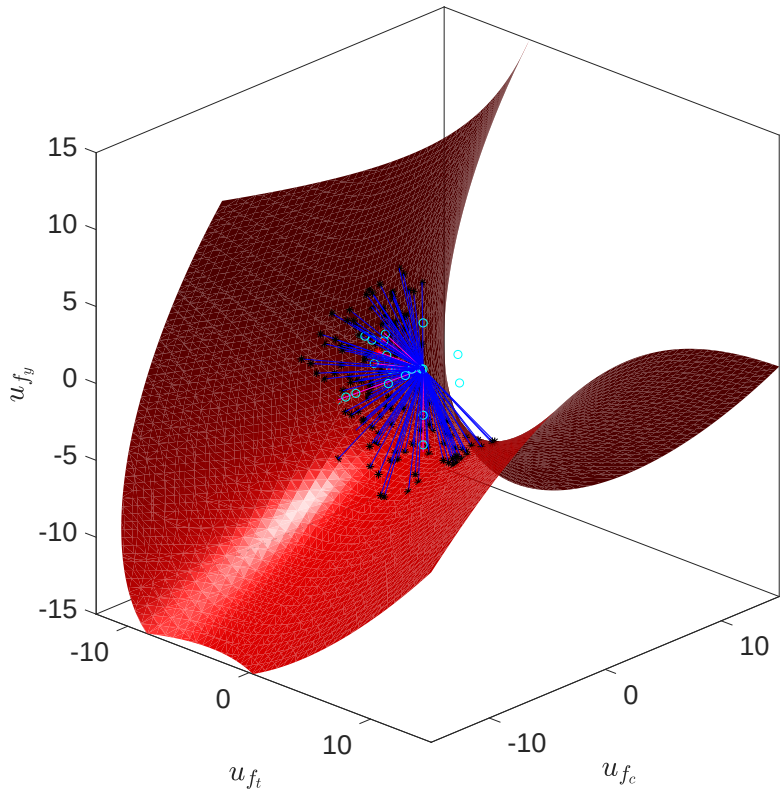

Figure 5.14: Mixed beam 5^{th} case with DARS. Random f_t,f_c,f_y. $cov_{P_f} = 0.25$, adaptive λ_{add} and $tol = 0.01$.

sive number of NLFEAs. But since the goal is to compare different methods in terms of efficiency, in this chapter a convergence criterion $cov_{P_f} = 0.25$ is used. For line search a relatively strict criterion of $tol = 0.01$ is used.

To enhance the chance of finding the G^*_{NLFEA} the width of the interval of sign change is looked at [14]. For the computationally intensive RC beam cases, when the interval is narrower, a secant step is carried out in that interval to locate the G^*_{NLFEA} point, without doing an additional NLFEA. However, while this way around increases efficiency, it still may not be sufficient against irregular NLFEA predictions, as will be shown later in the examples.

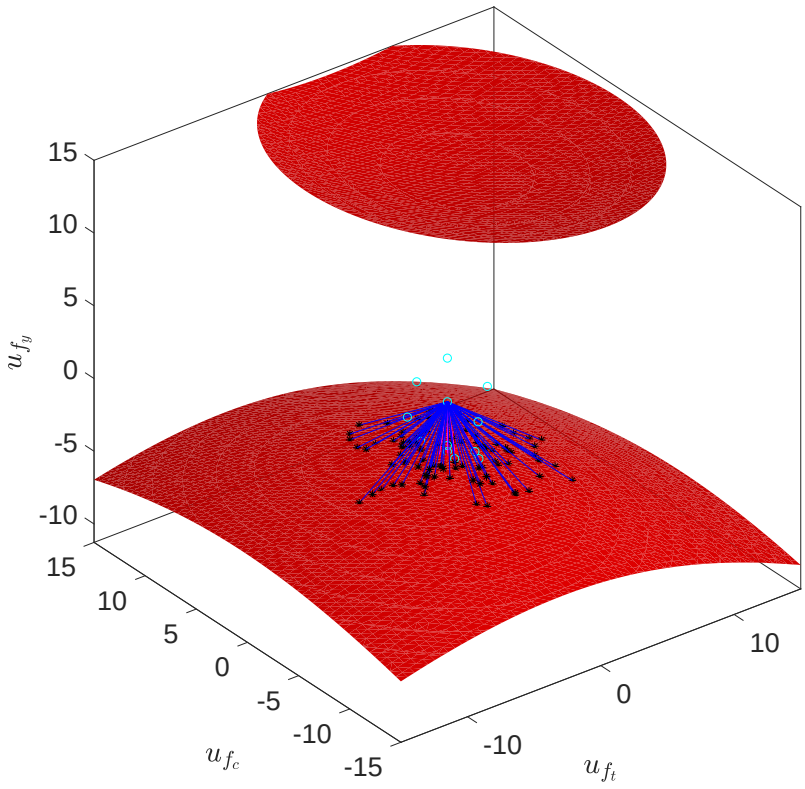

Figure 5.15: Bending beam 6^{th} case with DARS. Random f_t,f_c,f_y. cov_{P_f} = 0.25, adaptive λ_{add} and tol = 0.01.

5.6. RESULTS AND DISCUSSIONS

The proposed BDARS and GDARS algorithm are tested for efficiency and accuracy against DARS. The six cases described in Table 5.5 served as the benchmark for this comparison. Except for the 1^{st} case, the results are not verified with any other independent method. It can be argued that the different types of DARS algorithms used in this chapter count as independent methods by themselves, so their results can be seen viewed as corroborative evidence. Since each reliability evaluation for the RC beams are time consuming multiple runs with random seeds are not attempted. The reliability assessments are done using fixed seed only.

The reliability results are summarized in Table 5.6, indicating the β value and number of NLFEAs in the bracket. The β estimates by all three methods are in close proximity to each other for all the cases. For the 1^{st}case alone an independent verification has been

Table 5.6: Summary of reliability results for all the RC beam cases. The β values are given with associated number of NLFEAs indicated in the bracket.

Case	1^{st}	2^{nd}	3^{rd}	4^{th}	5^{th}	6^{th}
DARS	5.12(94)	3.88(18)	3.60(35)	5.15(66)	3.86(34)	3.59(20)
BDARS	5.17(15)	3.82(23)	3.63(26)	5.12(22)	3.82(29)	3.61(26)
GDARS	5.13(36)	3.80(20)	3.62(19)	5.11(18)	3.82(45)	3.62(19)

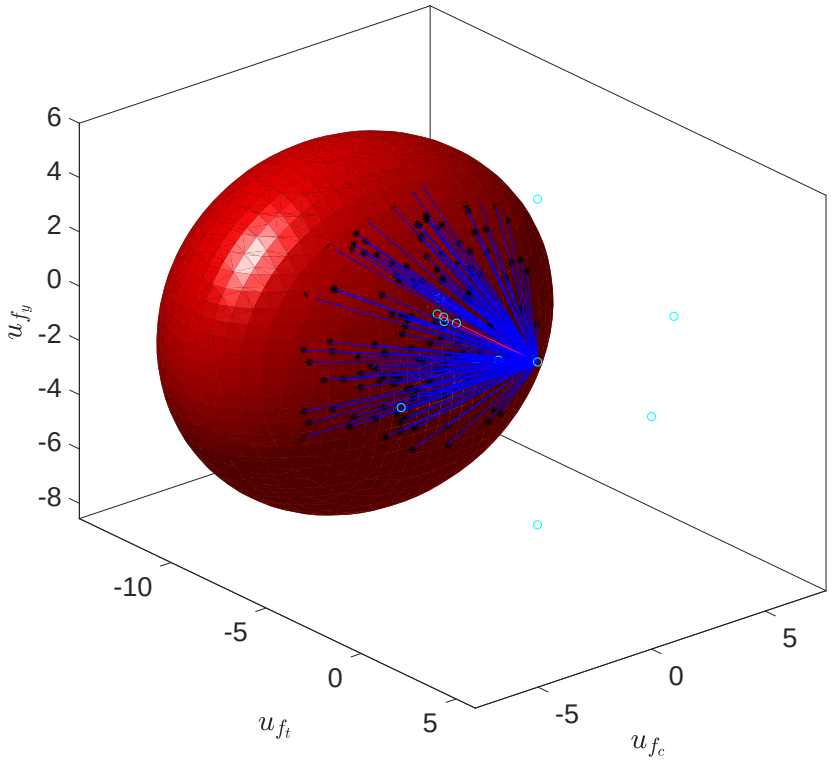

Figure 5.16: Shear beam 4^{th} case with BDARS. Random f_t,f_c,f_y. cov_{P_f} = 0.25, adaptive λ_{add} and tol = 0.01

performed. In order to verify the reliability result $12^2 = 144$ roots of a 12^{th} order Hermite polynomial is generated as samples. Inspiration is drawn from the paper of Berveiller *et al.* [38], where a subset of the roots is used as samples in regression problem. How-

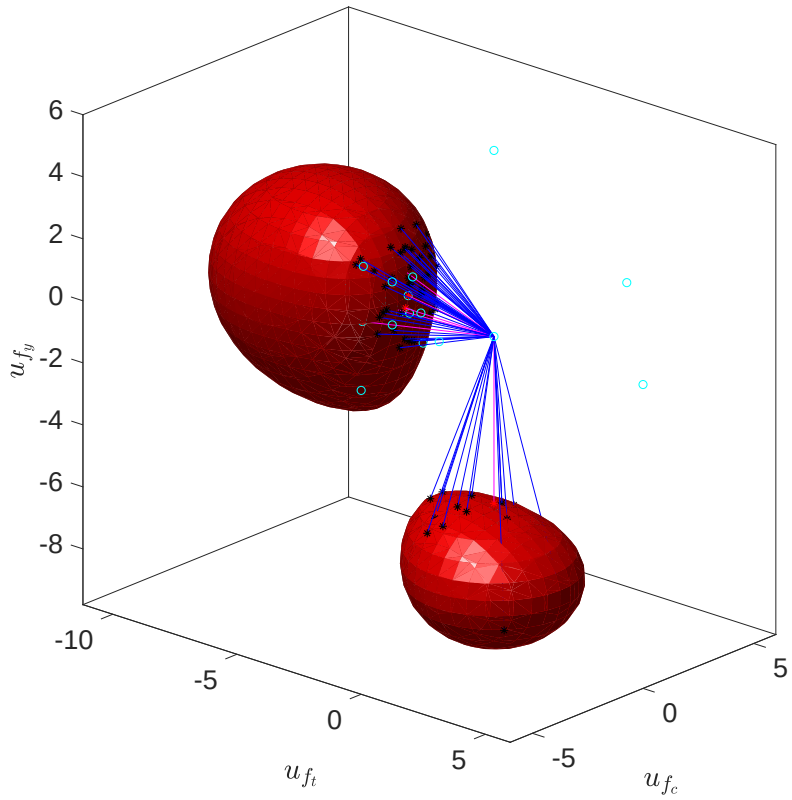

Figure 5.17: Mixed beam 5^{th} case with BDARS. Random f_t,f_c,f_y. $cov_{P_f} = 0.25$, adaptive λ_{add} and $tol = 0.01$.

ever, here all 144 samples are used. The order of the Hermite polynomial is deliberately selected to be high to capture the irregularity of the response surface. A feed forward neural network based response surface is fitted. Only single hidden layer is chosen. To avoid over fitting, regularization is used. Number of neurons in the hidden layer is optimized based on cross validation error. From Figure 5.4 it can be seen that the resulting response surface $G_{ref} = 0$ in the standard normal space of u_{f_t} and u_{f_y} is almost a vertical line. The line is located at a distance -5.15 from the u_{f_y} axis. So, it can be stipulated that the failure probability for the 1^{st} case is $P(u_{f_t} \leq -5.15)$. This is equivalent to a $\beta = 5.15$, which is quite close to the result obtained by all three methods.

The important samples G^*_{NLFEA}, intermediate line search iteration points G_{NLFEA}, unimportant samples G^*_{RS} and the final response surface $\hat{G} = 0$ for all cases are plotted in the transformed space of standard normal variables (Figures 5.4 to 5.21).

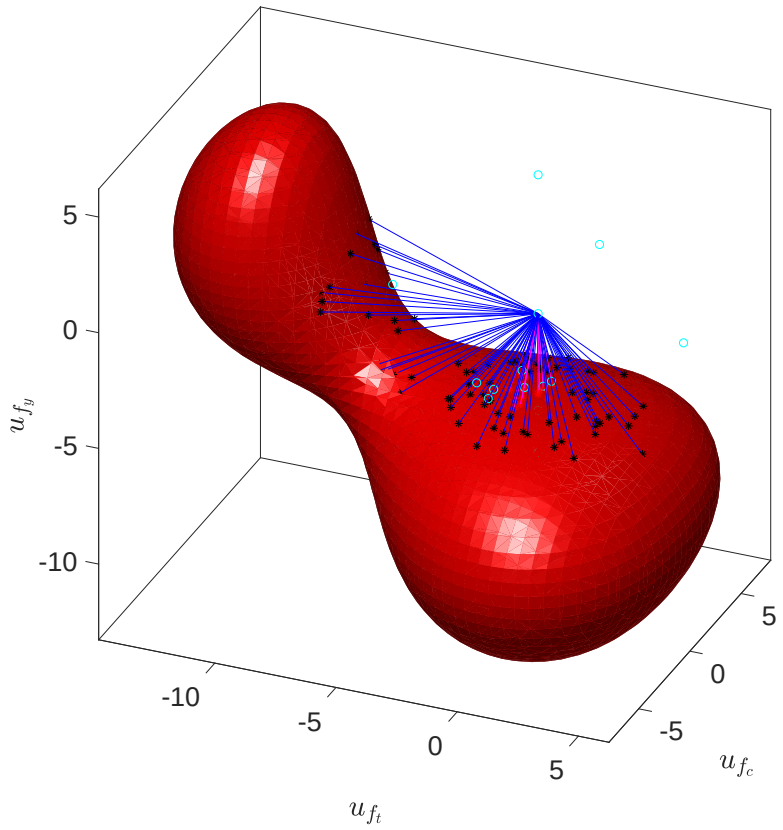

Figure 5.18: Bending beam 6^{th} case with BDARS. Random f_t,f_c,f_y. cov_{P_f} = 0.25, adaptive λ_{add} and tol = 0.01.

In terms of efficiency it is observed from the Figure 5.22 and Table 5.6 that except for the 1^{st} and 4^{th} cases the number of function evaluations are comparable for all three methods. The number of function evaluations depend on variety of factors, such as the failure probability, shape of the limit state function. Given the simple shape of the limit state surface in 1^{st} and 4^{th} cases there is good reason to suspect that the significantly larger number of function calls for DARS is solely due to the noisy limit state function of the shear beam. The pronounced noise for the shear dominated cases render the usual line search mechanism ineffective.

This fact is corroborated in the Figure 5.4 (1^{st} case). It is observed that for DARS there are some line search directions, which took lot of iterations to locate the G^*_{NLFEA}. Even though there are closely located neighboring important directions. This is precisely the reason why DARS took more NLFEAs than the other two methods. BDARS for this case

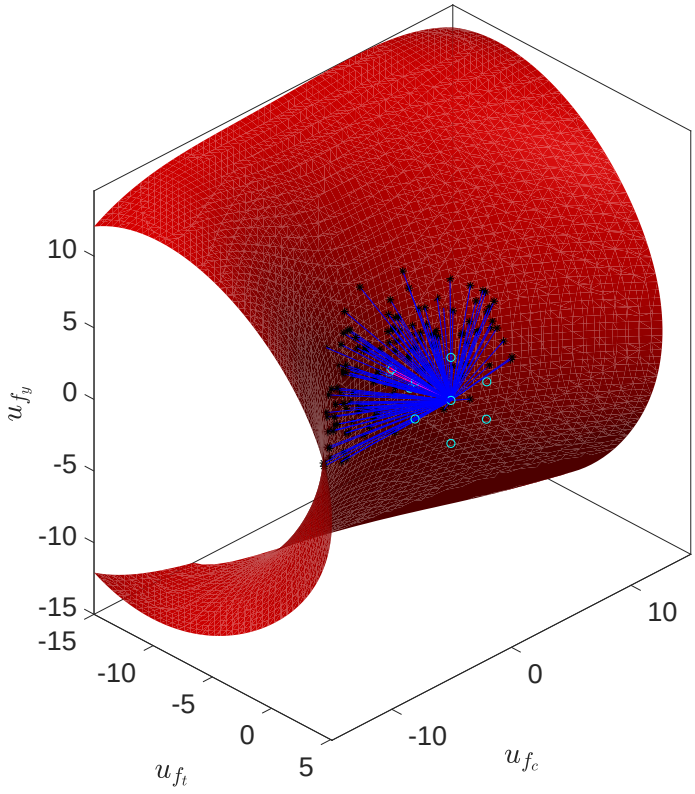

Figure 5.19: Shear beam 4^{th} case with GDARS. Random f_t, f_c, f_y. $cov_{P_f} = 0.25$, adaptive λ_{add} and $tol = 0.01$

consumed much fewer function evaluations. However, that fact can be primarily attributed to the extremely low number of important directions (Figure 5.7). For the 4^{th} case also BDARS had fewer function evaluations because of low number of important directions (Figure 5.16). In order to depict a fair comparison of the line search performances between DARS and BDARS the 1^{st} case is re-attempted with DARS and BDARS. But this time the λ_{min} is not updated immediately after each exact line search. Instead it is updated at the end of each loop. Also, instead of using adaptive Λ_{add} a fixed value of $\Lambda_{add} = 1.1$ is used. These two strategies increase the number of exact line searches. The results are depicted in Figure 5.23. The comparison of Figures 5.23a and 5.23b clearly establishes the superior performance of BDARS over DARS, when it comes to line search. The total number of function call is 62 by DARS, where as it is 26 by BDARS. Majority of directions for BDARS converged in $2-3$ iterations, where as it took as many as $5-7$ iterations for some directions with the polynomial interpolation based line search of DARS.

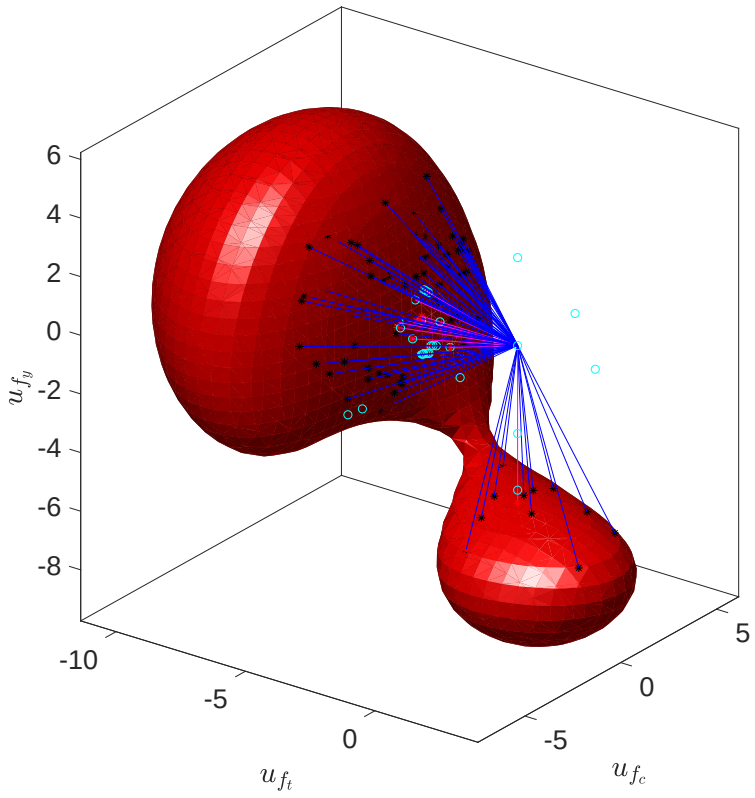

Figure 5.20: Mixed beam 5^{th} case with GDARS. Random f_t,f_c,f_y. $cov_{P_f} = 0.25$, adaptive λ_{add} and $tol = 0.01$.

The effectiveness of BDARS over DARS in noisy case is also visible in the 2^{nd} case. DARS is the most efficient for this case, however the efficiency is primarily due to low number of important directions. In Chapter 3 it was shown that for the mixed beam there is pronounced noise along the u_{f_t} axis (Figure 3.6). In Figure 5.5 it can be seen that around the important region there is one direction which did not converge to a G^*_{NLFEA} after couple of iterations. The non convergence can be attributed to the failure of polynomial interpolation scheme due to noisy limit state function. The Brent method employed by BDARS however had no difficulty in obtaining a convergence for the same direction (Figure 5.17). The bracketing method in Brent makes sure that any bad estimate provided by the inverse interpolation is ignored. After couple of line searches the shape of the GPR based response surface is stable.In that case the initial guess provided by the response surface may even converge just in one shot. Many such instances are observed in Figures 5.9 for the 3^{rd} case with smooth limit state surface. But if convergence is not

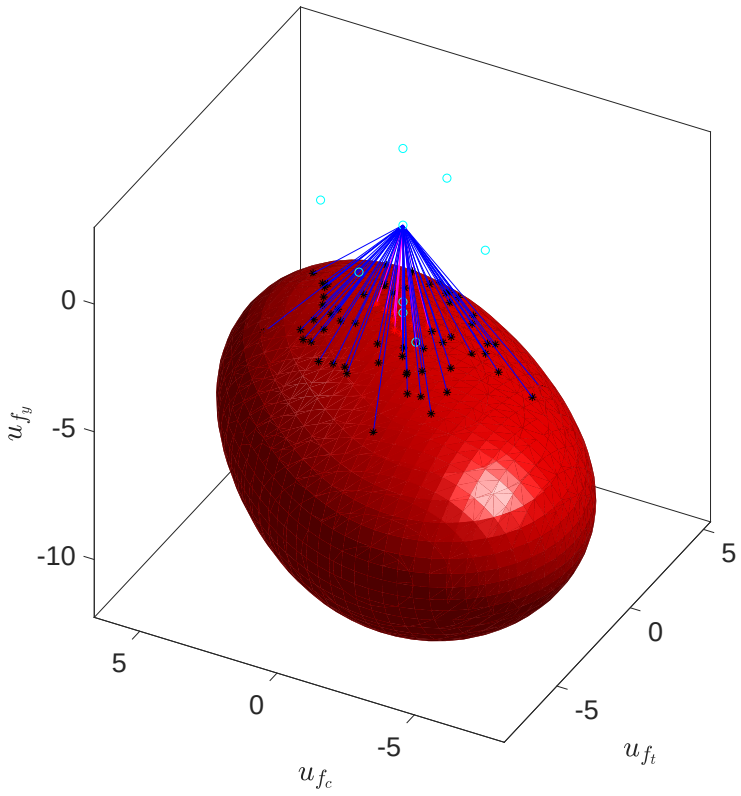

Figure 5.21: Bending beam 6^{th} case with GDARS. Random f_t,f_c,f_y. cov_{P_f} = 0.25, adaptive λ_{add} and tol = 0.01.

obtained at the initial guess then it is checked whether the initial guess and the origin bracket the root. If the root is not bracketed then another NLFEA is done at a λ, which is obtained by a linear interpolation between the origin and the initial guess. If no interval of sign change can be found between this third point and the initial guess, then it is decided that the limit state surface is too far away along that direction and the line search is abandoned for that direction. It can be questioned however, whether a linear interpolation is a safe choice in this context, when the limit state function has pronounced numerical noise.

What happens when the initial guess for the line search provided by the response surface is far off from the actual root, a glimpse of that can be found for one direction in Figure 5.16. It took 5 iterations to locate the root for that direction. Interpolation steps were slow to bring the iteration from a bad initial guess to a narrow interval. Such cases

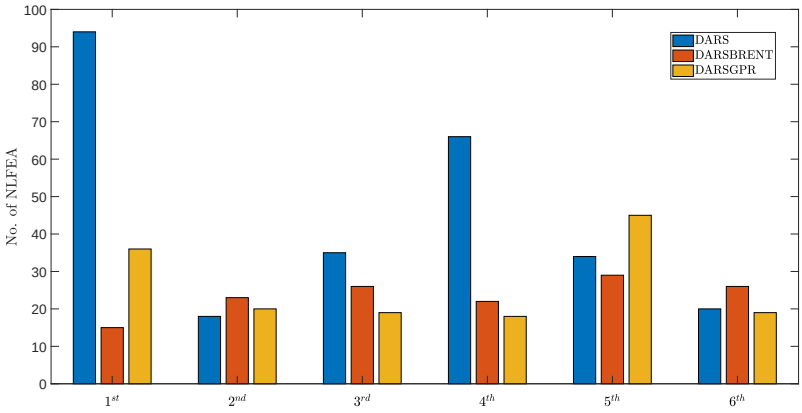

Figure 5.22: Comparison of the number of NLFEAs for all six RC beam cases.

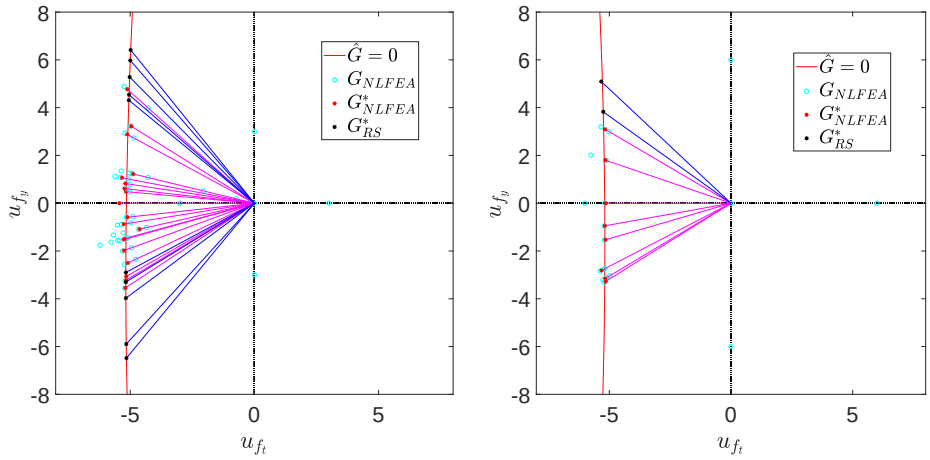

(a) DARS (b) BDARS

Figure 5.23: comparison of line search between performances DARS and BDARS for the shear beam 1^{st} case. cov_{P_f} = 0.57, λ_{add} = 1.1 and tol = 0.01. BDARS clearly outperforms DARS

might occur immediately after ADI, when the sample set of learning for GPR is relatively low. As more exact line searches take place GPR based response surface becomes a better surrogate function for the limit state function in the important region.

The benefit of GPR based response surface can be particularly evident for GDARS in the 1^{st} case. It follows from Figure 5.19 that for a good number of directions the line search converged at the initial guess provided by the response surface itself. Figure 5.24 brings deeper insight into the line search process with GPR for the 1^{st} case. After ADI

is over, GPR based line search takes over. For all directions line search starts with the λ corresponding to G^*_{RS}. Based on all the available NLFEA based samples GPR then makes the initial prediction about the location (λ value) of G^*_{NLFEA} along a direction. According to the response surface, value of G is 0 at this λ value. The confidence interval (blue vertical lines in Figure 5.24) around the GPR predicted value of G is constructed based on Eq.5.8. Then NLFEA calculation finds the actual value of G at this λ value. With the addition of each new sample during a line search, the response surface is updated. At G^*_{NLFEA} the GPR prediction and NLFEA prediction coincides. For each direction finding the G^*_{NLFEA} takes about $2-4$ iterations. Some times due to irregularity of NLFEA prediction the actual value of G does not seem the coincide with the GPR prediction even after $3-4$ iteration. If the interval of sign change of G is quite narrow, a secant step is carried out to locate the G^*_{NLFEA} without an additional NLFEA. The variance associated with the GPR prediction (Eq.(5.8)) and hence the confidence interval, depends on the availability of samples in the neighboring locations and the noise associated with NLFEA prediction of G.

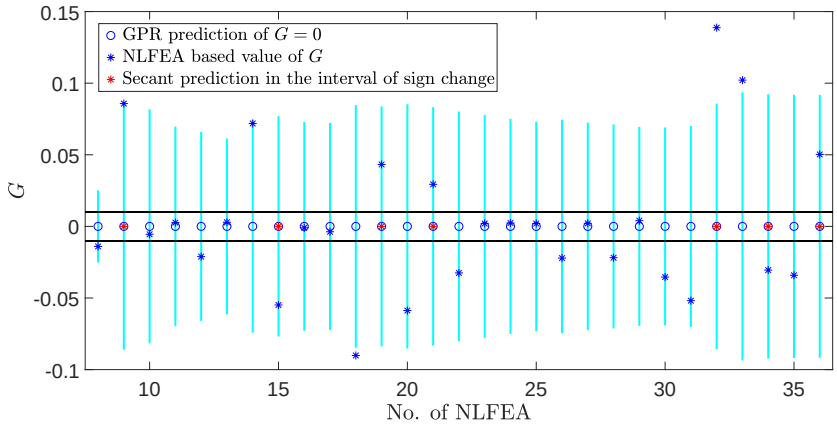

Figure 5.24: Confidence intervals for GPR predictions in the shear beam 1^{st} case. All the NLFEA based estimates of G fall within the confidence interval produced by GPR.

The GPR based response surface is seen to form a close shape in many of the cases (Figures 5.8, 5.11, 5.17, 5.20 for example). This is an unexpected behavior. This gives rise to an implication that the structure is exhibiting a physically impossible behavior. For example in the 2^{nd} case, with the mixed beam, the GPR based response surface in BDARS and GDARS separated the failure boundaries corresponding to the two different failure modes (Figure 5.8). This creates the impression that the structure is safe at the point $u_{f_t} = -5, u_{f_y} = -5$, which is impossible. The explanation is that the GPR based response surface is only an accurate predictor close to the G^*_{NLFEA} points (based on which the response surface is constructed), where the Gaussian process error correlation is stronger. But away from the G^*_{NLFEA} points, or the important region of the limit state function, the correlation is weak. As a result the response surface is not an accurate predictor away

from the important region.

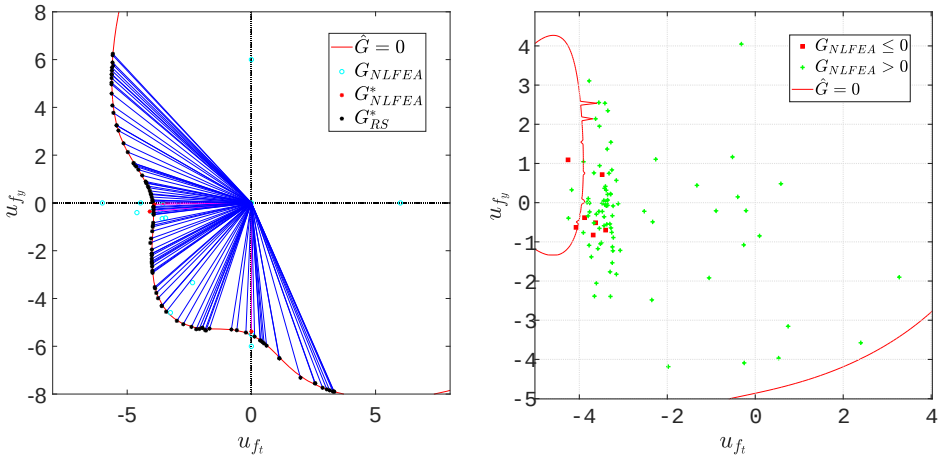

(a) BDARS (b) AK-MCS

Figure 5.25: Mixed beam 2^{nd} case with BDARS. Random f_t,f_y. cov_{P_f} = 0.25, adaptive λ_{add} and tol = 0.01. This time a quadratic basis function is considered instead of constant basis function. The resulting β = 3.91 and Number of NLFEA is 20. For comparison the result by AK-MCS, with polynomial chaos Kriging Meta model is also given.

The GPR model considered in this Chapter has only constant basis function. So the response surface is entirely constructed by the error correlation function in GPR. It has been attested by Echard *et al.* [48] that the correlation function is good at capturing the local behavior, around the experimental design (the samples used for fitting), but it is not good at capturing the global behavior of the limit state function. In the Figure 5.8 the failure boundaries separated because the samples (G^*_{NLFEA} and G_{NLFEA}) based on which the response surface is constructed cluster around two separate failure modes. Because the Gaussian process error correlation is good at capturing local behavior of the limit state function, but it is not good at capturing the global behavior. Echard *et al.* advocated using a non constant basis function in order to better predict the behavior of the limit state function. Such an example is shown in the Figure 5.25a for the 2^{nd} case. An incomplete quadratic basis function for GPR is considered in this example. Here in the Figure 5.25a it can be observed that the response surface is not separated any more. The two failure boundaries pertaining the two failure mechanisms appear to be almost orthogonal. This detailed behavior close to the important region has been captured quite well by the error correlation function. On the other hand, the quadratic basis function has ensured that away from the important region the behavior of the response surface is not absolutely wrong. As a reference , for the mixed beam 2^{nd} case, the result with AK-MCS is also provided 5.25b. It can be observed that the response surface by AK-MCS is also separated at the two failure modes. It should be mentioned at this place, that unlike AK-MCS, which samples in all parts close to the limit state surface, the DARS actively tries to sample close to the design point. This strategy implies that the response

surface from DARS will be only accurate close to the design point. The inaccuracy of response surface away from the important region is however not a concern for DARS method. Because even though the response surface directly contribute to the calculation of the failure probability, that contribution is only minor compared to the actual limit state surface.

GDARS is found to be reasonably efficient for many cases, for the 3^{rd} and 6^{th} cases for instance (Figures 5.12 and 5.21). However, conducting the line search solely based on the response surface can be risky, particularly for complicated limit state functions. Any flaw in the response surface will have severe consequence for the line search. A glimpse of such instance can be found in the Figure 5.20. Also, for the third test case in the Section 5.4 it was seen that the response surface based line search can be inefficient for tighter line search tolerances, because the response surface will evolve slowly after a while. Uni-variate root finding scheme of BDARS is more reliable and robust in that regard.

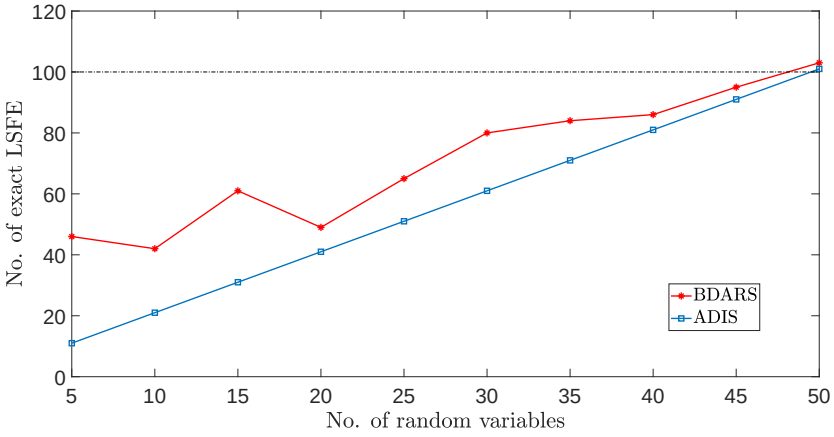

Figure 5.26: Number of exact LSFE versus the number of problem dimension for BDARS. An incomplete quadratic basis function is used in GPR. A $cov_{P_f} = 0.1$ is used.

$$G(x_1, ...x_n) = 3\sqrt{n} - \sum_{i=1}^{n} x_i \tag{5.11}$$

The basic principle of BDARS discussed in this Chapter is the same that of DARS, so it is expected that BDARS will behave in a similar way to DARS, when dealing with problems of higher dimension. For DARS Grooteman [46] showed based on a linear hyper-plane limit state surface (Eq.5.11) that the number of exact limit state function evaluations does not shoot up with the increase in the number of input random variables, as long as linear or incomplete quadratic response surfaces are used. Waarts [14] came to a similar conclusion based on number of different limit state surfaces, while using an incomplete quadratic response surface. However, when full quadratic response

surface is used, Grooteman showed that the number of exact limit state function evaluations increases considerably. Since BDARS uses a fundamentally different nature of response surface compared to DARS, it is important to investigate its efficiency for cases with higher number of random variables. This is done using the linear hyper-plane limit state problem, following Grooteman.

The linear hyper-plane limit state in Eq.5.11 is at a distance $\beta = 3$ from the origin. x_i are standard Normally distributed. The total number of exact limit state function evaluations (LSFE) with BDARS for this case are plotted against the number of random variables in the Figure 5.26. The number of LSFE for the ADI process is also marked in the same Figure. It follows from the Figure 5.26 that the number of LSFE for ADI increases linearly with the number of random variables. The total number of LSFE for BDARS also exhibit a linear behavior for increasing dimension. The difference between the number of exact LSFE for ADI with BDARS diminishes as the problem dimension increases.

5.7. CONCLUDING REMARKS FOR THE FIFTH CHAPTER

In this Chapter it is demonstrated that the polynomial interpolation based line search method employed in DARS suffers from inefficiency when dealing with noisy limit state functions. To reduce the number of function calls a novel improvement is proposed in this work where a Gaussian process regression based surrogate function is used to distinguish the important region of the failure boundary and the line search is done with Brent's algorithm. Three computationally intensive examples of RC beams have been chosen as demonstrative examples. Based on these beams six cases with different set of random variables have been studied. To make a clear assessment how much the GPR based response surface by itself contributes to the overall efficiency an additional method is also conceived where the response surface is directly used to conduct the line search. It is observed that the GPR based response surface is so good near the important region of the limit state surface that the initial guess provided by the response surface for the uni-variate root often converges in just one shot. This trait, combined with the bracketing method of Brent's algorithm worked well in cases of noisy limit state functions. It is because Brent's method does not rely on interpolation method alone to locate the root. Interpolation only helps to steer the iteration in a narrow interval, from where Bisection method takes over. If the initial guess provided by the GPR is already close to convergence, the role of interpolation diminishes even further. It is observed that the proposed method is substantially more efficient for the cases where shear is the dominant mode of failure. For bending failure cases, which have relatively smoother limit state functions, the performance of the proposed method (BDARS) is comparable to DARS.

DARS's ability to distinguish the different parts of the limit state surface, in the case of strong system effect has been investigated by Grooteman [46]. It was remarked that unless the different parts of the limit state functions are described with distinct limit state functions, DARS will produce erroneous result. DARS has the propensity to concentrate the exact directional sampling around the most vulnerable part of the limit state function. This attribute makes it difficult for it to identify all different parts of the failure surface, when there is system effect. For the multi-modal mixed failure RC beam cases in this Chapter the proposed method managed to distinguish the different failure modes. But that was mostly because the failure surfaces could be reached along the axes

directions (in the standard normal space). If the failure surfaces do not intersect the axes directions, then DARS (also BDARS and GDARS) can be inefficient. One possible way to ensure that all the different parts of the limit state surface is identified is to start with a Latin Hypercube sampling. This suggestion is inspired from the AK-MCS algorithm, which also starts off with Latin Hypercube sampling. The BDARS method can also benefit significantly in this regard, if a more advanced GPR meta model is used, which can learn from relatively small sample set.

For a linear hyper-plane limit state surface it is shown that the number of exact LSFE for the BDARS increases almost linearly with increasing dimension. This exercise provides some evidence that BDARS could be efficient for problems with higher dimension as well.

One disadvantage of BDARS is that the interval of sign change needs to be found first for any direction, before the actual of the line search starts, unless the initial guess provided by the GPR based response surface is already an accurate estimate of the univariate root for that direction. However, if the initial guess does not manage to converge, or close the bracket of sign change, a linear interpolation is used in the current development of BDARS. It can be questioned however, whether linear interpolation is an ideal choice, particularly for noisy limit state functions. In such situations updating the response surface immediately and using this updated response surface to predict the next iteration could be a better choice. This is in principle what GDARS does.

6

RELIABILITY ANALYSIS WITH ADAPTIVE KRIGING MONTE CARLO SIMULATION

6.1. INTRODUCTION

THE focus of the previous chapter was the performance issues of traditional the DARS algorithm when dealing with noisy limit state functions. An upgrade in the DARS algorithm has been forwarded, which was found to work quite well for different kind of problems, even for noisy limit state functions. Gaussian process regression played a key role in that upgrade. In this chapter the focus will be on another response surface based reliability method, which builds the surrogate function using Gaussian process regression or Kriging. Adaptive Kriging Monte Carlo simulation (AK-MCS) has been introduced and described in the Chapter 2. To the author's knowledge, the performance of AK-MCS method for computationally intensive RC structure cases have not been reported in the literature except the work of Rózsás *et al.* [16]. That specific work compared the performance of traditional DARS, with cubic order polynomial response surface, with AK-MCS. The comparison was made based on the examples of an RC deep beam and an RC continuous girder. The result was inconclusive with regards to the comparison of the efficiency for DARS and AK-MCS. Also, the effect of numerical noise on the efficiency of DARS and AK-MCS was not addressed in that work. In this chapter the RC beam cases introduced in the previous chapter will be examined with AK-MCS, in order to illustrate AK-MCS's performance in detail for RC structure cases. Of particular interest will be the performance of AK-MCS for the RC beam cases whose limit state functions evince pronounced numerical noise. The AK-MCS module developed by UQLab is used in this work [92].

6.2. DISCUSSION ON THE CONVERGENCE CRITERION USED IN AK-MCS

AK-MCS uses the two convergence criterion outlined in Eq.2.78 and Eq.2.80. These convergence criterion are given here again for reference. The first convergence criterion has been proposed by Echard *et al.* [48],

$$\min[U(\mathbf{x})] \geq 2 \tag{6.1}$$

where $\mathbf{x}$ is vector of random variables. The second convergence criteria is proposed by Schöbi *et al.* [49],

$$\frac{\hat{P}_f^+ - \hat{P}_f^-}{\hat{P}_f^0} \leq \varepsilon_{\hat{P}_f} \tag{6.2}$$

here $\hat{P}_f^{\pm} = P[\mu_{\hat{G}}(\mathbf{X}) \pm k\sigma_{\hat{G}}(\mathbf{X}) \leq 0]$ are the upper and lower bound failure probabilities and $\hat{P}_f^0 = P[\mu_{\hat{G}}(\mathbf{X}) \leq 0]$. $\mathbf{X}$ is the set of all the samples considered for the Monte Carlo simulation.

It is important to understand how the convergence criterion given in the Eq.2.78 and Eq.2.80 works in order to understand how AK-MCS works. AK-MCS builds response surface (or meta model) based on actual limit state function evaluations. Instead of the actual limit state function this response surface is used in a Monte Carlo simulation to determine the failure probability (P_f). Based on the current response surface new candidate sample is selected by a learning function. Based on the current state of the response surface this sample is the closest to the limit state function, according to the learning function. The response surface is updated with the addition of each new candidate samples (this process is termed as design enrichment by Schöbi *et al.* [49]), making the response surface adaptive. This selection of new candidate samples for the improvement of the response surface continues till all the samples (from the set $\mathbf{X}$) located in the close proximity of the limit state function are added for design enrichment. The convergence criterion given in the Eq.2.78(or Eq.2.80) sets the maximum limit within which a sample can be considered close to the limit state function. Once the convergence is achieved, the algorithm stops adding new samples any further and the response surface is considered to be in its final state. The Monte Carlo simulation with this final response surface (based on the set of all samples $\mathbf{X}$) gives the failure probability (P_f), along with the coefficient of variation of P_f, cov_{P_f}. It can be remarked that there is no relationship between cov_{P_f} and the convergence criterion given in Eq.2.78 or Eq.2.80, because these convergence criteria are strictly a quantitative measure of how good a surrogate function the response surface is to the actual limit state function. These two convergence criteria will be referred to as cv1 and cv2 throughout this chapter.

6.3. DEMONSTRATIVE EXAMPLES WITH SIMPLE TEST CASES

Before testing the RC beam cases with AK-MCS, the three test cases (with computationally inexpensive limit state functions) introduced in the Section 5.4 of the previous chapter have been attempted with AK-MCS. Both ordinary AK-MCS and polynomial chaos Kriging AK-MCS have been used for the test cases.

Table 6.1: Summary of reliability results for the first test case. For cv2 $\varepsilon_{\hat{P}_f} = 0.05$ is considered.

Method	AK-MCS, cv1	AK-MCS, cv2	PC-AK-MCS, cv1	PC-AK-MCS, cv2
β	3.8381	3.8381	3.8330	3.8330
LSFEs	29	29	21	17

Table 6.2: Summary of reliability results for the second test case. For cv2 $\varepsilon_{\hat{P}_f} = 0.05$ is considered.

Method	AK-MCS, cv1	AK-MCS, cv2	PC-AK-MCS, cv1	PC-AK-MCS, cv2
β	3.8906	3.8906	3.8461	3.8461
LSFEs	36	36	25	25

Table 6.3: Summary of reliability results for the third test case. For cv2 $\varepsilon_{\hat{P}_f} = 0.05$ is considered.

Method	AK-MCS, cv1	AK-MCS, cv2	PC-AK-MCS, cv1	PC-AK-MCS, cv2
β	2.2524	2.2524	2.2530	2.2724
LSFEs	113	85	47	21

The results for the three test cases are summarized in Tables 6.1, 6.2 and 6.3. The results are fairly close to the reference results for these cases in the Chapter 5 (Section 5.4). For the first two test cases AK-MCS is observed to be less efficient compared to PC-AK-MCS. For third test case, with noisy limit state function, the contrast among performances the AK-MCS and PC-AK-MCS becomes really prominent. The convergence plots for the AK-MCS and PC-AK-MCS are plotted in Figure 6.1 for comparison.

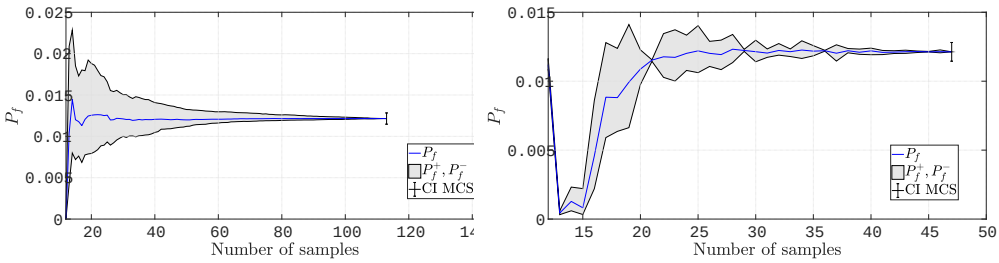

(a) Convergence for AK-MCS (b) Convergence for PC-AK-MCS

Figure 6.1: comparison of the convergence between AK-MCS and PC-AK-MCS for the third test case. cv1 is used as convergence criterion

Polynomial chaos Kriging is better compared to simple Kriging at capturing the global and local behavior of the limit state function. PC-AK-MCS owes its efficiency to this particular feature of PC-Kriging.

6.4. DEMONSTRATIVE EXAMPLES WITH RC BEAM CASES

The RC beam cases (based on the shear, mixed and bending beams) discussed in the previous chapters are examined with PC-AK-MCS. Ordinary AK-MCS is not used for the RC beam cases, so PC-AK-MCS will be generally addressed as AK-MCS from here onwards. The beam cases are selected such that their $\beta < 4$. This ensures that the resulting $cov_{P_f} \leq 0.40$ within 10^5 Monte Carlo simulations with the response surface. The RC beam cases are summarized in the Table 6.4 for reference. The beam cases will be addressed with the names introduced in the previous chapter for the sake of consistency. An additional beam case, refereed by the name 7^{th} case is introduced in this chapter. This case is based on the shear beam. It has the random variables f_t (with fully correlated G_F) and model uncertainty ϑ. This case was analyzed previously in the Chapter 4 with DARS. The limit state function for this case was given in the Eq.4.12. The mean value of ϑ is 0.971 (refer Table 4.5). This case will serve as the example of limit state function with numerical noise in this chapter.

Table 6.4: Standard deviations of stochastic properties for various RC beam cases considered

Case	f_c [MPa]	G_c [MPa]	f_t [MPa]	G_F [N/mm]	f_y [MPa]	ϑ [-]
2^{nd}	-	-	0.8503	0.0309	55	-
3^{rd}	-	-	0.8503	0.0309	65	-
5^{th}	9.645	31.45	0.8503	0.0309	55	-
6^{th}	9.645	31.73	0.8503	0.0309	65	-
7^{th}	-	-	0.8503	0.0309	-	0.1327

The results are summarized in the Table. 6.5.

Table 6.5: Summary of reliability results for all the RC beam cases with AK-MCS. The β values are given with associated number of NLFEAs indicated in the bracket. For cv2 $\varepsilon_{\hat{P}_f} = 0.30$ is considered.

RC Beam cases	Mixed 2^{nd}	Bending 3^{rd}	Mixed 5^{th}	Bending 6^{th}	Shear 7^{th}
PC Kriging, cv1	3.85(92)	3.58(44)	3.89(125)	3.53(61)	3.23(310)
PC Kriging, cv2	3.81(97)	3.56(31)	3.85(107)	3.52(58)	3.29(310)

6.5. DISCUSSION ON THE RESULTS FOR THE RC BEAM CASES

The results in the Table 6.5 for the RC beam cases pretty much fall into the consistent pattern seen in the previous chapter. The bending beam is found to be easiest for the reliability analysis. The smooth limit state surface for the 3^{nd} case (Figure 6.3) makes it easier for the PC kriging meta model to predict the behavior of the limit state function around the limit state surface, even with smaller sample learning. This helps the U-function (learning function) to select candidate samples close to the limit state sur-

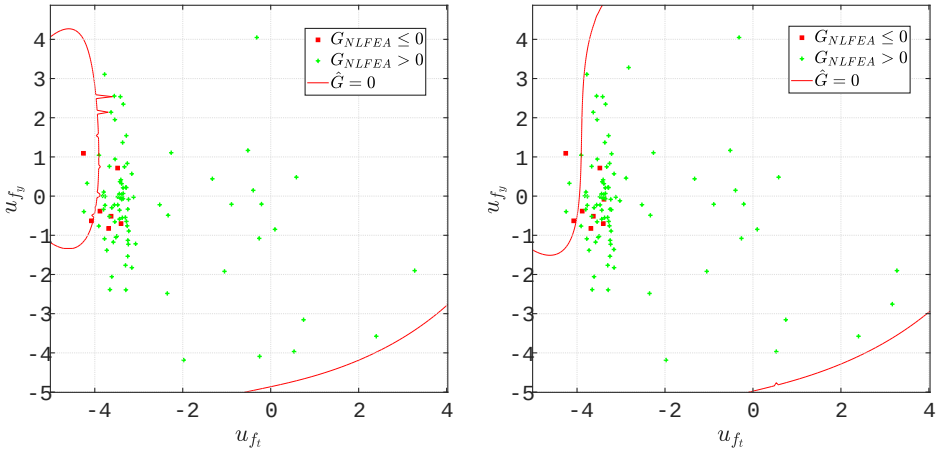

(a) Mixed beam 2^{nd} case, for cv1 (b) Mixed beam 2^{nd} case, for cv2

Figure 6.2: Mixed beam 2^{nd} case with the mixed beam for convergence criterion cv1 and cv2.

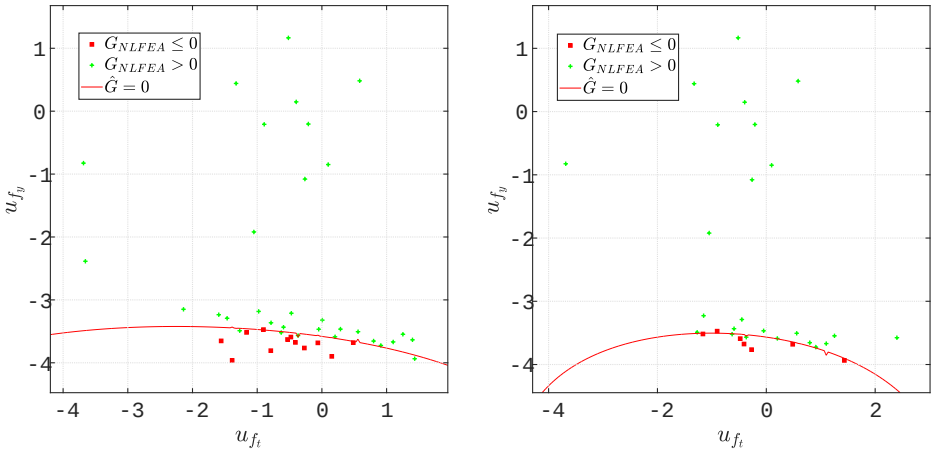

(a) Bending beam 3^{rd} case, for cv1 (b) Bending beam 3^{rd} case, for cv2

Figure 6.3: Bending beam 3^{rd} case with the bending beam for convergence criterion cv1 and cv2.

face. The PC-Kriging based meta model in turn progressively gets improved around the limit state surface, till the convergence is achieved. For the mixed beam 3^{rd} case it took many more NLFEA. The reason could be partially attributed to the fact that there are two branches of failure boundary for this particular case. However, Schöbi *et al.* [49] demonstrated that AK-MCS has no trouble dealing with system effect in the limit state function. Figures 6.3a and 6.3b reveal that most of the samples are concentrated around the shear

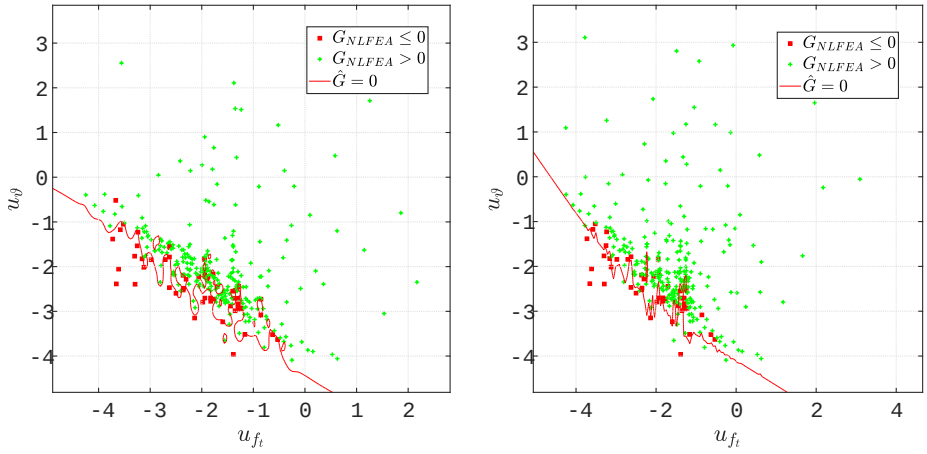

(a) Shear beam 7^{th} case, for cv1

(b) Shear beam 7^{th} case, for cv2

Figure 6.4: Shear beam 7^{th} case, with the shear beam. No convergence is obtained after 310 NLFEA.

6

dominated failure boundary for this case. So the noisy limit state surface at the shear dominated failure boundary can be possible reason for high number of NLFEA.

The role of noisy limit state function in the inefficiency of AK-MCS is particularly evident for the 7^{th} case. AK-MCS could not manage to get a convergence even after 310 NLFEA The effect of noise is vividly depicted in the Figure 6.4 for this case. From the Figure it follows that around the failure boundary no clear distinction could be found between the region with samples $G_{NLFEA} \leq 0$ and $G_{NLFEA} > 0$ and the response surface is extremely irregular.

Why this is such an impediment for convergence is illustrated in light of the convergence criterion cv1 in Eq.6.1. For a candidate sample $\mathbf{x}$ the learning function $U(\mathbf{x}) = -\frac{|\mu_{\hat{G}}(\mathbf{x})|}{\sigma_{\hat{G}}(\mathbf{x})}$ judges whether it is close to the limit state surface or not. This $\mu_{\hat{G}}(\mathbf{x})$ is the mean value found by the Kriging meta model with the associated noise variance $\sigma_{\hat{G}}(\mathbf{x})$. For a candidate sample located extremely close to the limit state surface the quantity $\frac{|\mu_{\hat{G}}(\mathbf{x})|}{\sigma_{\hat{G}}(\mathbf{x})}$ should be close to zero. The method converges when no more such candidate samples can be found in the close proximity of the limit state surface, or in other words, all the possible samples which are closer to limit state surface have already been added for the enrichment of the meta model. If the noise variance $\sigma_{\hat{G}}(\mathbf{x})$ is high that means that $\frac{|\mu_{\hat{G}}(\mathbf{x})|}{\sigma_{\hat{G}}(\mathbf{x})}$ can still be close to zero, even when $\mathbf{x}$ is not absolutely close to the limit state surface. Thus because of the noise candidate samples which are not the closest to the limit state surface often times get misidentified for design enrichment, which in turn delays the convergence.

The β estimate for the 7^{th} case by AK-MCS (3.23 with cv1) is found to be quite close to the estimate by BDARS (3.21) (Figure 6.5), even though AK-MCS did not converge for this case. If the convergence criterion were based on the statistics of interest (fail-

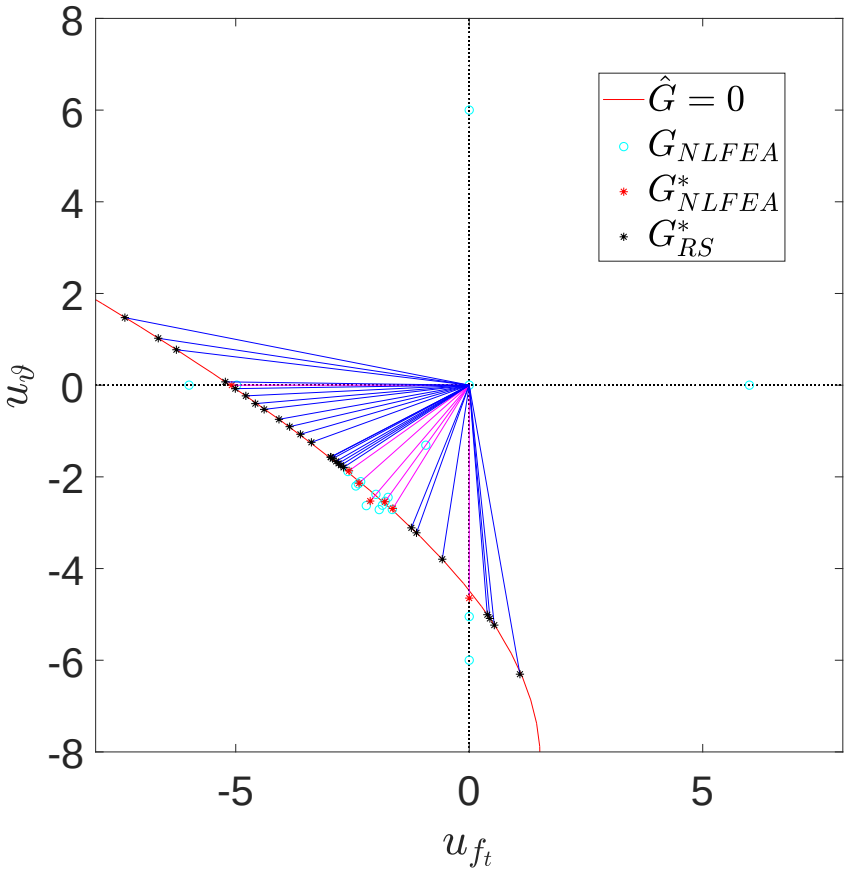

Figure 6.5: Shear beam 7^{th} case with BDARS. cov_{P_f} = 0.25, adaptive λ_{add} and tol = 0.01. The β = 3.21 with 26 NLFEA.

ure probability), AK-MCS would have converged with greater ease, it seems. However, following the discussion in section6.2 it can be said that unlike DARS it is difficult to consider a convergence criterion based on the coefficient of variation of failure probability (cov_{P_f}) in AK-MCS. Because AK-MCS executes the Monte Carlo simulation based on the response surface. So when the response surface is at its initial stage, a low cov_{P_f} will be of no indication whatsoever for the accuracy of the failure probability estimate. DARS could use the convergence criterion based on cov_{P_f} because the failure probability for the most part is estimated based on the actual limit state function. Response surface's role in DARS is mostly limited in discerning the important region from unimportant one. Its contribution in calculating the failure probability is only minor. One ad hoc way around can be to use less number of samples (i.e. total number of samples in

the set **X**) in AK-MCS. This however runs the risk of not obtaining the β at all when β for the problem in reality is high ($\beta > 4$ for examples). Because if the β is large, that means the failure boundary in the space of standard normal variables is located far away from the mean values. Small sample size may not even be able to generate sufficient number (or any) of samples close to the failure boundary in that case, rendering the Monte Carlo simulation ineffective. Another possibility is that a relaxed convergence criterion of the sort $\min[U(\mathbf{x})] \geq 1$ is considered. Meaning that only the samples extremely close to the actual limit state surface be considered for design enrichment. This could however compromise the accuracy of the meta model, or the response surface, resulting in a poor failure probability estimate.

The convergence criterion cv2 (Eq.(6.2)) is less conservative compared to cv1 [49], although it works with the same philosophy as cv1. This criterion necessitates that the confidence bound (obtained from the Kriging process) around the response surface is sufficiently low. That can only happen when the samples close to the limit state surface are added for the design enrichment. So as far as the selection of the close samples for enrichment is concerned, cv2 pretty much faces the same problem for the noisy limit state function as the cv1. It is observed for the noisy cases 2^{nd}, 5^{th} and 7^{th} that even a relatively high value of $\varepsilon_{\hat{P}_f} = 0.30$ could not make the reliability analysis substantially more efficient. The confidence interval around the response surface would be wider for cases with heavy numerical noise (this was observed in the Figure 5.24 also in the Chapter 5), so setting a high value of $\varepsilon_{\hat{P}_f}$ might make it easier to obtain a convergence. On the other hand, a higher value of $\varepsilon_{\hat{P}_f}$ would mean a premature termination of the reliability analysis for smooth limit state functions, even when the response surface is far from its final stage. The failure probability estimate with such a response surface would not be the most accurate.

6.5.1. IMPLICATION OF THE FAILURE BOUNDARY FOR THE BENDING BEAM

In the Figures 5.9 and 5.12 from the previous chapter, it is observed that the failure boundary is not a horizontal line for the bending case. The Figure 6.3 in this chapter shows the same thing. This is counter intuitive because bending is solely dominated by the reinforcement yield strength, with the concrete tensile strength (f_t) playing no important role. The design point for the 3^{rd} case is $(0, -4.13)$. To investigate the possible nature of the limit state function far from the design point, the displacement verses load graph is plotted at $\lambda = 8$ along a direction $(1, -1)$ (Figure 6.6). If it is found out that at this point the value of limit state function is positive (i.e. $G > 0$) then that will be a sufficient evidence that the failure boundary is indeed not horizontal. From Figure 6.6 it follows that the load capacity is greater than the examination load $F = 50\,\text{kN}$. This implies that $G > 0$ at this point (also, a horizontal plateau after the peak load clearly indicates reinforcement yield failure). Evidently, for high values of f_t failure boundary is indeed not horizontal. It must be noted though, that the response surface far away from the important region is of no interest for DARS or AK-MCS, it matters little if the response surface is inaccurate elsewhere, other than the important region.

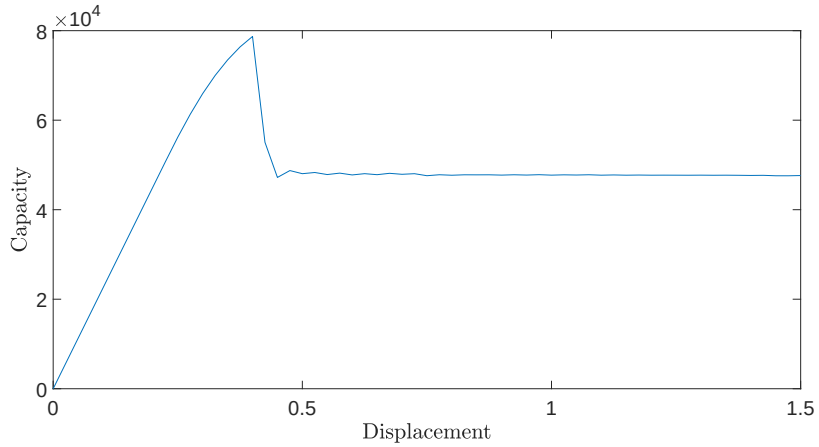

Figure 6.6: Displacement verses load plot for the bending beam 3^{rd} case, at $\lambda = 8$ along the direction $(1,-1)$. The plot clearly suggests that the peak load is more than the examination load $F = 50\,\text{kN}$.

6.6. CONCLUDING REMARKS FOR THE SIXTH CHAPTER

For the test cases with computationally inexpensive analytical limit state functions or linear finite element based limit state function, it was seen that AK-MCS's performance is often better compared to DARS (and BDARS). For the RC beams however the opposite is found to be the case. The performance of AK-MCS is observed to be comparable to DARS only for the smooth limit state functions of the bending beams. For the shear dominated cases the performance of AK-MCS is found to be inferior compared to DARS. It is stipulated that the samples which do not lie in the closest proximity to the actual limit state surface often get misidentified for design enrichment by the learning function. This unnecessarily increases the overall NLFEA, delaying the convergence.

One important distinction between AK-MCS and DARS is the nature of convergence criterion in these two algorithms. The convergence criterion in AK-MCS is essentially a quantitative measure of how good a surrogate function the response surface is to the actual limit state function. Unlike DARS, it is difficult to consider a convergence criterion based on the coefficient of variation of failure probability in AK-MCS. Because AK-MCS executes the Monte Carlo simulation based on the response surface. So when the response surface is yet to converge to its final stage, a low coefficient of variation of failure probability will not be a meaningful measure of the accuracy of the failure probability estimate. DARS could use the convergence criterion based on coefficient of variation of failure probability because the failure probability is chiefly estimated based on the actual limit state function in DARS. Nevertheless, it should be stressed that the comparison of the performances of AK-MCS and DARS should be interpreted with caution. Because the results by these two methods are effected by their respective stopping criterion, and these criteria are potentially difficult to compare.

Some ad hoc remedies for the convergence issue were discussed in this chapter. However, they may not universally work in all cases. It is stipulated that only adding the

samples extremely close to the actual limit state surface for design enrichment, by relaxing the convergence criterion, can make the process more efficient. However it might compromise the accuracy of the meta model and which will result into a poor failure probability estimate. Perhaps the learning function employed to select the candidate samples is not ideally suited for limit state functions with pronounced numerical noise. It could be that an additional stopping criterion needs to be considered. Detailed investigations are necessary to come up with a solution which works for all cases.

7

CONCLUSION

IN this thesis accurate and efficient methods have been developed for the reliability assessment for structures analyzed with Non-Linear Finite Element Analysis (NLFEA) where the presence of numerical noise plays an important role. It has been shown that the numerical noise in the ultimate load bearing capacity, predicted by the NLFEA, is closely associated with the shear failure mechanism. Whereas for the bending failure mechanism NLFEA solution strategy produces a much more smooth capacity prediction. It is shown in this thesis that slight variation in the convergence criterion in the Quasi-Newton equilibrium iteration procedure for the solution of the system of nonlinear equations can significantly alter the ultimate load bearing capacity predictions for a beam failing in shear. Why shear governed failure mechanisms are more sensitive to the choices adopted in the solution strategy has not been investigated in this thesis. This remains an interesting research question for the future.

The uncertainty arising due to the idealizations and assumptions in the NLFEA solution strategy, called the modeling uncertainty, has been accounted for in this thesis in the reliability analysis of RC structures. Modeling uncertainty has been quantified based on the ratio of experimentally obtained and NLFEA predicted ultimate load bearing capacity. Since the modeling uncertainty term is multiplied with the ultimate load bearing capacity term in the limit state function, this makes the limit state function an explicit function of the modeling uncertainty. So the variance of the modeling uncertainty will directly influence the outcome of the reliability analysis. Inclusion of the modeling uncertainty in the reliability analysis is observed to have a profound impact in the outcome of the reliability estimate. It is shown for the RC beam failing in shear that without accounting for the modeling uncertainty the reliability index is 5.6 whereas with the modeling uncertainty the reliability index varies in the range $3.0 - 3.7$ for different combinations of random variables. This difference underscores the importance of accounting for the modeling uncertainty in a NLFEA based reliability analysis. In this thesis no distinction is made in the modeling uncertainty corresponding to the failure mode. Given the significant influence that modeling uncertainty has on the result of reliability analysis, it is quite likely that considering different modeling uncertainty for different failure modes

will improve the reliability estimate even further. But in order to make such implementation possible, it is necessary to be able to quantitatively determine the failure mode, during a reliability analysis. The ductility index introduced by Engen *et al.* [17] can be useful in this regard, to quantitatively distinguish between the brittle and ductile failure modes during a reliability analysis.

The primary reliability algorithm examined in detail in this thesis is the Directional adaptive response surface method (DARS). This algorithm measures failure probability content along random directions, with a process called the line search. An adaptive response surface is used to distinguish the important directions for which the NLFEA based exact line searches are to be used. It is observed that in the absence of numerical noise in the limit state function, the number of exact function evaluations in DARS method primarily depends on the shape of the limit state surface, i.e. concave, convex, linear etc. It also depends on the target coefficient of variation of failure probability, line search tolerance and the added offset to the current minimum distance of the limit state surface. It is demonstrated that a strict line search tolerance criterion only marginally improves the reliability index, even though the number of exact function evaluation increases significantly with stricter tolerance. This is explained by the fact that DARS uses the distance to the limit state surface (from the origin) to calculate the failure probability. A strict line search tolerance will ensure that those distances are calculated (in an uni-variate root finding process, or line search) accurately up to third or even fourth decimal places, at a heavy computational expense (in terms of number of exact function evaluations). But measuring those distances in the standard normal space with an accuracy beyond the second decimal place will not be particularly rewarding in terms of the accuracy of the reliability index. A moderate value of the line search tolerance will be sufficient to efficiently obtain an accurate reliability index. It is because due to the law of large numbers the error in the probabilities from each direction tend to be independent random variables. As a result these errors tend to cancel each other when the probabilities are added up. The law of large numbers helps this. As for the influence of the added offset, it is found out that using a fixed value of the offset throughout the reliability analysis increases the number of exact limit state function evaluations. Using an adaptive offset instead of a constant offset value increased the efficiency of DARS.

While the adaptive offset and moderate line search tolerance criterion sufficiently ensures efficient reliability analysis with DARS for smooth limit state functions, such measures alone are found to be inadequate for the RC beam case which fail in shear. The pronounced numerical noise in the limit state function for this case made DARS quite inefficient. The polynomial interpolation based uni-variate line search scheme of DARS is identified to be the major source of inefficiency for this case. It is demonstrated that in the presence of pronounced noise the interpolation based scheme fails to consistently indicate the next best possible root, contributing to the inefficiency. The effect of numerical noise on such an interpolation scheme is particularly severe closer to the limit state surface, where the value of the limit state function is in the range of the noise variance. It is also found out that starting the line search from a fixed initial guess is less efficient. This limitations prompted the modifications in the uni-variate line search scheme. Instead of polynomial interpolation method Brent's method [89] is used. Brent's method uses inverse quadratic interpolation only when the interval of sign

change is wider. In narrower interval it switches to the Bisection method. The Bisection method is faster compared to interpolation in a narrow interval and it is not effected by numerical noise. Since interpolation is quite erroneous close to the limit state surface in noisy condition, switching to Bisection brings better outcome in terms of efficiency. The response surface in DARS provides an initial estimate of the possible root along a direction. Starting the exact line search from this initial guess profoundly reduces the number of exact limit state function evaluations. To better exploit this initial guess provided by the response surface a Gaussian process regression is used to construct the response surface instead of quadratic polynomial. This novel improvement in DARS is called BDARS in this thesis. It is shown that if the line search is done purely on the basis of this GPR based response surface alone, it is still more efficient compared to the interpolation based traditional line search scheme. One disadvantage of Brent's method is that the interval of sign change for the root needs to be established at the beginning. Currently, the line search procedure is abandoned for a particular direction if the interval is not found within two NLFEAs. This strategy runs the risk of erroneously abandoning the line search for an important direction, particularly for noisy limit state functions. A possible improvement could be to update the response surface immediately and using this updated response surface to guess the next iteration.

Another reliability method examined in this thesis is the Adaptive Kriging Monte Carlo simulation (AK-MCS). This method tries to obtain samples close to the limit state surface with help of a response surface. The samples are selected based on a learning function. With each such selected samples, the existing response surface is updated, making the process adaptive. Once the response surface has converged, it is used in a crude Monte Carlo simulation to determine the failure probability. The study of the performance of AK-MCS revealed that while this method performed equally well (or even better) for smooth limit state functions, it is found to be inefficient under the presence of pronounced numerical noise in the limit state functions of RC beams. The reason is that the pronounced noise, due to higher noise variance associated with candidate sample, can deceive the learning function employed by AK-MCS into selecting samples, which are not the closest to the limit state surface, for design enrichment (in other words, improvement of the response surface). This can increase the total number of function evaluations, making the process inefficient. If the convergence criterion were based on the failure probability, AK-MCS would have converged with greater ease. However, unlike DARS it is difficult to consider a convergence criterion based on the coefficient of variation of failure probability in AK-MCS. Because unlike DARS, it is the quality and accuracy of the response surface in AK-MCS which governs the accuracy of the failure probability estimate. The convergence criterion of AK-MCS is strictly a quantitative measure of how good a surrogate function the response surface is to the actual limit state function. Once the convergence is achieved, the algorithm stops adding new samples any further and the response surface is considered to be in its final state. AK-MCS executes the Monte Carlo simulation based on the response surface. So when the response surface is not at its final stage, a low coefficient of variation of failure probability will be of no indication whatsoever for the accuracy of the failure probability estimate. DARS could use the convergence criterion based on failure probability because the failure probability for the most part is estimated based on the actual limit state function in DARS. Response

surface's role in DARS is mostly limited in discerning the important region from unimportant one. Its contribution in calculating the failure probability is only minor. The current convergence criterion in AK-MCS is clearly not a practical choice for cases where numerical noise is involved. One possibility is that a relaxed convergence criterion for the design enrichment is used. Meaning that only the samples extremely close to the actual limit state surface be considered for design enrichment. This is not a general solution because such a measure can compromise the accuracy of the meta model, or the response surface, resulting in a poor failure probability estimate. Additional stopping criteria might also be useful in this regard.

AK-MCS provides an opportunity to exploit high performance computer architecture, by running the exact function evaluations in parallel (even though the candidate samples selection may not be the most optimal). This is an attractive prospect because most other efficient reliability algorithms, including DARS are inherently sequential. Being able to run multiple samples at a time can significantly reduce the computational time. However, this gain in computational time is of little use if AK-MCS takes a high number of function evaluations to converge.

The primary motivation behind the development of BDARS is to make it possible to efficiently evaluate the reliability for noisy limit state cases. However, for BDARS to be practically useful, it has to be efficient for problems with higher dimension as well. Some authors have shown in the literature, based on few examples, that DARS can achieve an efficiency in the same order of FORM when dealing with higher dimensionality. This efficiency however, is shown to be achieved only when linear or incomplete quadratic response surface is used in DARS. For a case with linear hyper-plane limit state surface it is shown the number of exact limit state function evaluations with BDARS increases almost in a linear fashion, for increasing dimensionality. So there is at least some evidence that BDARS, with its GPR based response surface, can retain its efficiency for higher stochastic dimension problems as well.

With the improvements forwarded in this thesis for DARS, together with the fact that only a moderate value of line search tolerance suffices to obtain a sufficiently accurate reliability estimate reliability estimate, makes the improved DARS (BDARS) method potentially suitable for the structural engineering community. The relevance of this contribution in terms of practical utility can be highlighted by the fact that the improved DARS has been demonstrated to consistently converge with around 20 NLFEA for RC beam problems (with failure probability in the range of $10^{-3}-10^{-4}$) examined in this thesis, irrespective of the presence of numerical noise or multiple failure mode in the limit state function. The RC beam examples used in this thesis are so chosen that they do not compromise in any aspect of computational challenges. The conclusions drawn in this thesis with regards to the RC beam examples are expected to be valid for more complex structures. This means that the structural engineering community will no longer have to remain content with NLFEA based safety check with semi probabilistic verification methods. The improved DARS method can be used directly to obtain an accurate estimate of failure probability for computationally intensive RC structures, including model uncertainty and notwithstanding considerable numerical noise, within a feasible number of NLFEA.

ACKNOWLEDGEMENTS

Foremost, I would like to express my sincere gratitude to my promoters Max Hendriks and Raphaël Steenbergen for the continuous support during my Ph.D study and research, with their patience, motivation, and vast experience. Their foresight and advise helped me at all the critical juncture of my Ph.D, starting from the formulation of the research question down to the writing of my thesis.
Besides my advisor, I am grateful to Rijkswaterstaat for providing the financial support for my PhD research. The project was initiated by Ane de Boer from Rijkswaterstaat and is now managed by Arjen van Maaren. I would also like to thank Árpád Rózsás and Arthur Slobbe from TNO. My collaboration with them resulted in the most productive part of my thesis. Their suggestion and critical assessment helped me refine the content of my thesis in the most significant parts. My sincere thanks also goes to Panagiotis Evangeliou from Diana FEA and Yuguang Yang from TU Delft for helping me to lay the ground work for my research.
A special commendation is also due for the administrative and technical stuff of the civil faculty, for making the research scholars' life way easier than it could have been otherwise.
I thank my fellow floor mates, Manimaran, Suman, Tao, Anupam, Sayeda for helping me in day to day affairs in times of need. If nothing else, the casual conversations at the coffee corner often took my mind off niggling concerns and anxiety. Also I thank my friend Sagar for keeping me company at Delft all this time.
Last but not the least, I would like to thank my family and my girlfriend, who have been a constant source of inspiration, encouragement and validation. The unbridled joy and pride they feel at my accomplishments made these grueling five years all the more worthwhile.

A

Model uncertainty Calculation

Table A.1: The summary of the ratios $\vartheta = \frac{R_{Exp}}{R_{FEM}}$ calculated based on the experiments by Yang *et al.* [64]

Name	a [mm]	d [mm]	f_c [MPa]	Rebar [mm]	R_{Exp} [kN]	R_{FEM} [kN]	ϑ
A121A1	1500	269.5	77.5	3Φ20	115.3	127.4	0.90
A121A2	1255	269.5	77.7	3Φ20	138.8	131.9	1.05
A121A3	1000	269.5	77.7	3Φ20	144.6	142.7	1.01
A121B1	1000	269.5	77.8	3Φ20	157.6	139.1	1.13
A122B1	1000	270.5	78.5	3Φ20	152.3	134.6	1.13
A123A1	1000	270.0	79.2	3Φ20	136.5	137.6	0.99
A122A1	750	270.5	78.2	3Φ20	194.7	151.1	1.29
A122B2	750	270.5	78.5	3Φ20	139.1	151.0	0.92
A123A2	800	270.0	80.1	3Φ20	139.0	148.2	0.94
A123B1	1250	270.0	79.3	3Φ20	134.9	134.9	0.97
A123B2	1150	270.0	79.3	3Φ20	151.4	144.6	1.05
A901A1	1250	274.0	78.5	1Φ12 + 2Φ20	105.6	120.0	0.88
A901A2	1000	274.0	78.5	1Φ12 + 2Φ20	123.9	138.6	0.89
A901A3	750	274.0	78.5	1Φ12 + 2Φ20	145.0	141.9	1.02
A901B2	750	274.0	78.5	1Φ12 + 2Φ20	124.2	141.9	0.87
A901B1	880	274.0	78.5	1Φ12 + 2Φ20	127.5	132.5	0.96
A902A1	995	276.0	78.5	1Φ12 + 2Φ20	120.7	130.3	0.93

A

A902A2	900	276.0	78.5	1Φ12 + 2Φ20	136.0	126.7	1.07
A902A3	800	276.0	78.5	1Φ12 + 2Φ20	149.4	137.5	1.09
A902B1	1100	276.0	78.5	1Φ12 + 2Φ20	121.5	128.3	0.95
A902B2	1000	276.0	78.5	1Φ12 + 2Φ20	124.2	130.8	0.95
A751A1	1000	274.5	78.5	3Φ16	97.1	116.2	0.83
A751A2	750	274.5	78.5	3Φ16	118.4	149.1	0.79
A751B1	800	274.5	78.5	3Φ16	106.7	116.4	0.92
A751B2	850	274.5	78.5	3Φ16	111.3	127.7	0.87
A752A1	900	273	78.5	3Φ16	108.7	126.6	0.86
A752A2	850	273	78.5	3Φ16	119.0	149.1	0.80
A752A3	850	273	78.5	3Φ16	121.6	149.1	0.82
A752B1	750	273	78.5	3Φ16	122.1	139.4	0.88
A752B2	700	273	78.5	3Φ16	142.0	126.4	1.12
A601A1	1000	275.5	78.5	1Φ10 + 2Φ16	80.3	93.7	0.86
A601A2	750	275.5	78.5	1Φ10 + 2Φ16	102.1	103.5	0.99
A602A1	750	275.5	78.5	1Φ10 + 2Φ16	98.9	103.5	0.96
A601B1	700	275.5	78.5	1Φ10 + 2Φ16	118.7	115.1	1.03
A601B2	600	275.5	78.5	1Φ10 + 2Φ16	114.2	105.1	1.09
A602A3	695	272.5	78.5	1Φ10 + 2Φ16	114.2	105.1	1.09
A602B2	650	272.5	78.5	1Φ10 + 2Φ16	117.5	126.7	0.92
B701A1	2250	471.5	81.0	3Φ20	175.5	200.6	0.87
B701A2	2000	471.5	81.0	3Φ20	179.5	206.1	0.87
B701A3	1750	471.5	81.0	3Φ20	185.7	201.7	0.92
B701B1	1700	471.5	81.1	3Φ20	193.6	211.0	0.92
B701B2	1500	471.5	81.1	3Φ20	202.4	217.3	0.93
B702A1	1250	471.5	81.7	3Φ20	183.2	143.3	1.28
B702B1	1450	471.5	81.7	3Φ20	164.9	181.9	0.91
C451A1	1250	272.5	23.7	3Φ12	41.4	49.4	0.83
C451A2	1000	272.5	23.7	3Φ12	52.9	57.1	0.93
C451A3	750	272.5	23.7	3Φ12	73.5	67.6	1.09
C451B1	850	272.5	23.7	3Φ12	58.5	63.7	0.92
C451B2	800	272.5	23.7	3Φ12	70.6	67.0	1.05
C451B4	700	272.5	23.7	3Φ12	77.2	70.5	1.09

C751A1	1250	270.0	23.7	3Φ16	76.5	71.9	1.06
C901A1	1250	271.5	23.7	1Φ12 + 2Φ20	101.7	76.7	1.33
C901A2	1000	271.5	23.7	1Φ12 + 2Φ20	103.4	88.4	1.17

REFERENCES

[1] A Muttoni and MF Ruiz. The levels-of-approximation approach in mc 2010: application to punching shear provisions. *Structural Concrete*, 13(1):32–41, 2012.

[2] M Pimentel, E Brühwiler, and J Figueiras. Safety examination of existing concrete structures using the global resistance safety factor concept. *Engineering Structures*, 70:130–143, 2014.

[3] EK Henriksen, MGB Bjerva, G Lindgren, and N Afzal. Reliability analysis of reinforced concrete using non-linear finite element analysis. Master's thesis, NTNU, 2016.

[4] R Lu, Y Luo, and JP Conte. Reliability evaluation of reinforced concrete beams. *structural safety*, 14(4):277–298, 1994.

[5] L Wang, Y Ma, J Zhang, X Zhang, and Y Liu. Uncertainty quantification and structural reliability estimation considering inspection data scarcity. *ASCE-ASME Journal of Risk and Uncertainty in Engineering Systems, Part A: Civil Engineering*, 1(2): 04015004, 2015.

[6] F Sangiorgio, J Silfwerbrand, and G Mancini. Scatter in the shear capacity of slender rc members without web reinforcement: an overview study. *Structural Concrete*, 17 (1):11–20, 2016.

[7] D Val, F Bljuger, and D Yankelevsky. Reliability evaluation in nonlinear analysis of reinforced concrete structures. *Structural Safety*, 19(2):203–217, 1997.

[8] F Biondini, F Bontempi, and DM Frangopol. Reliability of material and geometrically nonlinear reinforced and prestressed concrete structures. In *Computational Fluid and Solid Mechanics 2003*, pages 2208–2212. Elsevier, 2003.

[9] MS Darmawan and MG Stewart. Spatial time-dependent reliability analysis of corroding pretensioned prestressed concrete bridge girders. *Structural Safety*, 29(1): 16–31, 2007.

[10] J Delgado, M de Azeredo, and R Delgado. Probability of failure estimation of current reinforced structures using the latin hypercube sampling. *WIT Transactions on Ecology and the Environment*, 45, 2000.

[11] E Zio and N Pedroni. Subset simulation and line sampling for advanced monte carlo reliability analysis. In *Proceedings of the European Safety and RELiability (ESREL) 2009 Conference*, pages 687–694, 2009.

[12] J Cheng and QS Li. Artificial neural network-based response surface methods for reliability analysis of pre-stressed concrete bridges. *Structure and Infrastructure Engineering*, 8(2):171–184, 2012.

[13] Alf Harbitz. An efficient sampling method for probability of failure calculation. *Structural safety*, 3(2):109–115, 1986.

[14] PH Waarts. *Structural reliability using finite element methods. An appraisal for DARS: Directional Adaptive Response surface Sampling*. PhD thesis, TU Delft, Delft University of Technology, 2000.

[15] P Evangeliou. Probabilistic nonlinear finite element analysis of reinforced concrete beams without shear reinforcement. Master's thesis, TU Delft, 2016.

[16] R Caspeele, L Taerwe, and DM Frangopol. *Life Cycle Analysis and Assessment in Civil Engineering: Towards an Integrated Vision: Proceedings of the Sixth International Symposium on Life-Cycle Civil Engineering (IALCCE 2018), 28-31 October 2018, Ghent, Belgium*, volume 5. CRC Press, 2018.

[17] M Engen, MAN Hendriks, J Köhler, JA Øverli, and E Åldstedt. A quantification of the modelling uncertainty of non-linear finite element analyses of large concrete structures. *Structural Safety*, 64:1–8, 2017.

[18] MAN Hendriks, A De Boer, and B Belletti. Guidelines for nonlinear finite element analysis of concrete structures. *Rijkswaterstaat Centre for Infrastructure, RTD*, Report 1016-1:2017, 2017.

[19] B Sudret and A Der Kiureghian. *Stochastic finite element methods and reliability: a state-of-the-art report*. Department of Civil and Environmental Engineering, University of California Berkeley, 2000.

[20] A Der Kiureghian and PL Liu. Structural reliability under incomplete probability information. *Journal of Engineering Mechanics*, 112(1):85–104, 1986.

[21] I Elishakoff, YJ Ren, and M Shinozuka. Improved finite element method for stochastic problems. *Chaos, Solitons & Fractals*, 5(5):833–846, 1995.

[22] Y Zhang and A Der Kiureghian. Dynamic response sensitivity of inelastic structures. *Computer Methods in Applied Mechanics and Engineering*, 108(1-2):23–36, 1993.

[23] DA Tortorelli and P Michaleris. Design sensitivity analysis: overview and review. *Inverse problems in Engineering*, 1(1):71–105, 1994.

[24] HS Gopalakrishna. System reliability assessment with nonlinear finite element analysis. 1986.

[25] T Haukaas and A Der Kiureghian. Parameter sensitivity and importance measures in nonlinear finite element reliability analysis. *Journal of engineering mechanics*, 131(10):1013–1026, 2005.

[26] AM Hasofer and NC Lind. Exact and invariant second-moment code format. *Journal of the Engineering Mechanics division*, 100(1):111–121, 1974.

[27] PT Boggs and JW Tolle. Sequential quadratic programming. *Acta numerica*, 4:1–51, 1995.

[28] J B Rosen. The gradient projection method for nonlinear programming. part i. linear constraints. *Journal of the society for industrial and applied mathematics*, 8(1): 181–217, 1960.

[29] K Breitung. Asymptotic approximations for multinormal integrals. *Journal of Engineering Mechanics*, 110(3):357–366, 1984.

[30] A Der Kiureghian and MD Stefano. Efficient algorithm for second-order reliability analysis. *Journal of engineering mechanics*, 117(12):2904–2923, 1991.

[31] M Lemaire. Eléments finis et fiabilité: un mariage à la mode. *Fiabilité des Matériaux et des Structures*, pages 95–112, 1998.

[32] A H Elhewy, E Mesbahi, and Y Pu. Reliability analysis of structures using neural network method. *Probabilistic Engineering Mechanics*, 21(1):44–53, 2006.

[33] I Kaymaz. Application of kriging method to structural reliability problems. *Structural Safety*, 27(2):133–151, 2005.

[34] J Zhang, HW Huang, and KK Phoon. Application of the kriging-based response surface method to the system reliability of soil slopes. *Journal of Geotechnical and Geoenvironmental Engineering*, 139(4):651–655, 2012.

[35] V Dubourg, B Sudret, and F Deheeger. Metamodel-based importance sampling for structural reliability analysis. *Probabilistic Engineering Mechanics*, 33:47–57, 2013.

[36] G Su, L Peng, and L Hu. A gaussian process-based dynamic surrogate model for complex engineering structural reliability analysis. *Structural Safety*, 68:97–109, 2017.

[37] CG Bucher and U Bourgund. A fast and efficient response surface approach for structural reliability problems. *Structural safety*, 7(1):57–66, 1990.

[38] M Berveiller, B Sudret, and M Lemaire. Stochastic finite element: a non intrusive approach by regression. *European Journal of Computational Mechanics/Revue Européenne de Mécanique Numérique*, 15(1-3):81–92, 2006.

[39] R Ghanem. The nonlinear gaussian spectrum of log-normal stochastic processes and variables. *Journal of applied mechanics*, 66(4):964–973, 1999.

[40] M Berveiller, B Sudret, and M Lemaire. Stochastic finite element: a non intrusive approach by regression. *European Journal of Computational Mechanics/Revue Européenne de Mécanique Numérique*, 15(1-3):81–92, 2006.

[41] S Marelli, R Schöbi, and B Sudret. Uqlab user manual–structural reliability. Technical report, Technical report, Chair of Risk, Safety and Uncertainty Quantification, ETH . . . , 2017.

[42] G Stefanou. The stochastic finite element method: past, present and future. *Computer Methods in Applied Mechanics and Engineering*, 198(9-12):1031–1051, 2009.

[43] A Olsson, G Sandberg, and O Dahlblom. On latin hypercube sampling for structural reliability analysis. *Structural safety*, 25(1):47–68, 2003.

[44] RE Melchers. Radial importance sampling for structural reliability. *Journal of engineering mechanics*, 116(1):189–203, 1990.

[45] RE Melchers. Importance sampling in structural systems. *Structural safety*, 6(1): 3–10, 1989.

[46] F Grooteman. An adaptive directional importance sampling method for structural reliability. *Probabilistic Engineering Mechanics*, 26(2):134–141, 2011.

[47] J Nie and BR Ellingwood. A new directional simulation method for system reliability. part ii: application of neural networks. *Probabilistic Engineering Mechanics*, 19 (4):437–447, 2004.

[48] B Echard, N Gayton, and M Lemaire. Ak-mcs: an active learning reliability method combining kriging and monte carlo simulation. *Structural Safety*, 33(2):145–154, 2011.

[49] R Schöbi, B Sudret, and S Marelli. Rare event estimation using polynomial-chaos kriging. *ASCE-ASME Journal of Risk and Uncertainty in Engineering Systems, Part A: Civil Engineering*, 3(2):D4016002, 2016.

[50] CC Li and A Der Kiureghian. Optimal discretization of random fields. *Journal of engineering mechanics*, 119(6):1136–1154, 1993.

[51] Zurich Joint Committee on Structural Safety, 12th Draft. Jcss-probabilistic model code, 2001.

[52] N Impollonia and G Muscolino. Static and dynamic analysis of non-linear uncertain structures. *Meccanica*, 37(1-2):179–192, 2002.

[53] A Der Kiureghian and T Dakessian. Multiple design points in first and second-order reliability. *Structural Safety*, 20(1):37–49, 1998.

[54] MA Shayanfar, MA Barkhordari, M Barkhori, and M Barkhori. An adaptive directional importance sampling method for structural reliability analysis. *Structural Safety*, 70:14–20, 2018.

[55] AI J. Forrester, AJ Keane, and NW Bressloff. Design and analysis of" noisy" computer experiments. *AIAA journal*, 44(10):2331–2339, 2006.

[56] FV Berghen and H Bersini. Condor, a new parallel, constrained extension of powell's uobyqa algorithm: Experimental results and comparison with the dfo algorithm. *Journal of computational and applied mathematics*, 181(1):157–175, 2005.

[57] CA Gilkeson, VV Toropov, HM Thompson, MCT Wilson, NA Foxley, and PH Gaskell. Dealing with numerical noise in cfd-based design optimization. *Computers & Fluids*, 94:84–97, 2014.

[58] B Belletti, C Damoni, and MAN Hendriks. Development of guidelines for nonlinear finite element analyses of existing reinforced and pre-stressed beams. *European Journal of Environmental and Civil Engineering*, 15(9):1361–1384, 2011.

[59] M Engen, MAN Hendriks, JA Øverli, and E Åldstedt. Solution strategy for non-linear finite element analyses of large reinforced concrete structures. *Structural Concrete*, 16(3):389–397, 2015.

[60] I Nilsen-Nygaard. Structural safety assessment of reinforced concrete structures with nonlinear finite element analyses and the significance of the modelling uncertainty-application to structural walls. Master's thesis, NTNU, 2015.

[61] DIANA FEA BV. Diana 10.2 user's manual, 2018.

[62] RG Selby and FJ Vecchio. A constitutive model for analysis of reinforced concrete solids. *Canadian journal of civil engineering*, 24(3):460–470, 1997.

[63] FJ Vecchio and MP Collins. The modified compression-field theory for reinforced concrete elements subjected to shear. *ACI J.*, 83(2):219–231, 1986.

[64] Y Yang and RT Koekkoek. Measurement report on the transition between flexural and shear failure on rc beams without shear reinforcement. *Delft University of Technology*, Report 25.5-16-04, 2016.

[65] DF Wiśniewski, PJS Cruz, AAR Henriques, and RAD Simões. Probabilistic models for mechanical properties of concrete, reinforcing steel and pre-stressing steel. *Structure and Infrastructure Engineering*, 8(2):111–123, 2012.

[66] H Nakamura and T Higai. Compressive fracture energy and fracture zone length of concrete. *Modeling of inelastic behavior of RC structures under seismic loads*, pages 471–487, 2001.

[67] H Schlune, M Plos, and K Gylltoft. Safety formats for non-linear analysis of concrete structures. *Magazine of Concrete Research*, 64(7):563–574, 2012.

[68] M Engen. Aspects of design of reinforced concrete structures using nonlinear finite element analyses. 2017.

[69] JGM Van Mier and JP Ulfkjœr. Round-robin analysis of over-reinforced concrete beams comparison of results. *Materials and Structures*, 33(6):381–390, 2000.

[70] MP Collins, FJ Vecchio, and G Mehlhorn. An international competition to predict the response of reinforced concrete panels. *Canadian Journal of Civil Engineering*, 12(3):624–644, 1985.

[71] T Jaeger and P Marti. Reinforced concrete slab shear prediction competition: Entries and discussion. *ACI Structural Journal*, 106(3):309, 2009.

[72] T Jaeger and P Marti. Reinforced concrete slab shear prediction competition: Experiments. *ACI Structural Journal*, 106(3):300, 2009.

[73] Workshop on the assessment of the shear strength of concrete structures, 2008.

[74] B Ellingwood and TV Galambos. Probability-based criteria for structural design. *Structural safety*, 1(1):15–26, 1982.

[75] H Schlune, M Plos, and K Gylltoft. Safety formats for non-linear analysis of concrete structures. *Magazine of Concrete Research*, 64(7):563–574, 2012.

[76] P Gardoni, A Der Kiureghian, and KM Mosalam. Probabilistic capacity models and fragility estimates for reinforced concrete columns based on experimental observations. *Journal of Engineering Mechanics*, 128(10):1024–1038, 2002.

[77] O Ditlevsen. Model uncertainty in structural reliability. *Structural safety*, 1(1):73–86, 1982.

[78] R Zhang and S Mahadevan. Model uncertainty and bayesian updating in reliability-based inspection. *Structural Safety*, 22(2):145–160, 2000.

[79] Eurocode—basis of structural design. *EN1990*, 2002.

[80] *fib* Bulletin No. 80. *Partial factor methods for existing concrete structures*. Ernst & Sohn, 2016.

[81] DL Allaix, VI Carbone, and G Mancini. Global safety format for non-linear analysis of reinforced concrete structures. *Structural Concrete*, 14(1):29–42, 2013.

[82] J Schneider. *Introduction to safety and reliability of structures*, volume 5. Iabse, 2006.

[83] V Cervenka. Reliability-based non-linear analysis according to fib model code 2010. *Structural Concrete*, 14(1):19–28, 2013.

[84] E Rosenblueth. Point estimates for probability moments. *Proceedings of the National Academy of Sciences*, 72(10):3812–3814, 1975.

[85] International Standard Organization. *General Principles on Reliability for Structures*. ISO/FDIS 2394, 1998.

[86] T Zimmermann, D Lehkỳ, and A Strauss. Correlation among selected fracture-mechanical parameters of concrete obtained from experiments and inverse analyses. *Structural Concrete*, 17(6):1094–1103, 2016.

[87] *fib*. fib. *Model code for concrete structures 2010*. Ernst & Sohn, 2013.

[88] MA Rashid, MA Mansur, and P Paramasivam. Correlations between mechanical properties of high-strength concrete. *Journal of Materials in Civil Engineering*, 14 (3):230–238, 2002.

[89] RP. Brent. An algorithm with guaranteed convergence for finding a zero of a function. *The Computer Journal*, 14(4):422–425, 1971.

[90] WJ Welch, RJ Buck, J Sacks, HP Wynn, TJ Mitchell, and MD Morris. Screening, predicting, and computer experiments. *Technometrics*, 34(1):15–25, 1992.

[91] A Harbitz. An efficient sampling method for probability of failure calculation. *Structural safety*, 3(2):109–115, 1986.

[92] S Marelli and B Sudret. Uqlab: A framework for uncertainty quantification in matlab. In *Vulnerability, Uncertainty, and Risk: Quantification, Mitigation, and Management*, pages 2554–2563. 2014.